

Stagnation point flows over a surface



By

Ansa Rafique

Department of Mathematics
Quaid-i-Azam University
Islamabad, Pakistan
2013

Stagnation point flows over a surface



By

Ansa Rafique

Department of Mathematics
Quaid-i-Azam University
Islamabad, Pakistan
2013

Stagnation point flows over a surface



By

Ansa Rafique

Supervised By

Dr. Malik M. Yousaf

Co-supervised By

Prof. Dr. Tasawar Hayat

Department of Mathematics
Quaid-i-Azam University
Islamabad, Pakistan
2013

Stagnation point flows over a surface



By

Ansa Rafique

A THESIS SUBMITTED IN THE PARTIAL FULFILLMENT OF THE REQUIREMENT

FOR THE DEGREE OF

DOCTOR OF PHILOSOPHY

IN

MATHEMATICS

Supervised By

Dr. Malik M. Yousaf

Co-supervised By

Prof. Dr. Tasawar Hayat

Department of Mathematics

Quaid-i-Azam University

Islamabad, Pakistan

2013

CERTIFICATE


Stagnation point flows over a surface


By


Ansa Rafique


A THESIS SUBMITTED IN THE PARTIAL FULFILLMENT OF THE
REQUIREMENTS FOR THE DEGREE OF THE DOCTOR OF
PHILOSOPHY

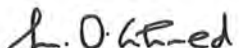
We accept this thesis as conforming to the required standard

1. 
Prof. Dr. Muhammad Ayub
(Chairman)

2. 
Dr. Malik M. Yousaf
(Supervisor)

3. 
Prof. Dr. Tasawar Hayat
(Co-supervisor)

4. 
Dr. M. Salahuddin
(External Examiner)

5. 
Prof. Dr. M. Ozair Ahmad
(External Examiner)

Department of Mathematics
Quaid-i-Azam University
Islamabad, Pakistan
2013

Dedicated to

*My loving
parents*

Acknowledgements

First of all, I am profoundly grateful to Almighty **ALLAH**, the most merciful and beneficent who bestowed me the proficiency to shape and polish my thinking. His blessings hold me through all the barriers of goal attainment. There is a great debt of gratitude which I cannot repay to my research supervisor **Dr. Malik Muhammad Yousaf** for imparting essential knowledge, criticism and constant encouragement. I would like to express my sincere thanks to my research co-supervisor **Prof. Dr Tasawar Hayat**. He plays a vital role and provides me such a great platform to accomplish my task. His professional skills and visions has always stimulated my mind and made me out the truly understand about the research.

I am grateful to the chairman of department of Mathematics **Prof. Dr. M. Ayub**, all faculty members and administrative staff for their kind behavior throughout my academic period. I cannot put aside the **Higher Education Commission (HEC) of Pakistan** for financial support during my PhD degree.

I would like to acknowledge my friends also for their moral support, attention and prayers. My many many thanks go to caring **Humaira, Rahila, Aini, Asma, Fehmi, Dr. Najma, Dr. Maryam javed, Dr. Saima and Dr. Sadia**. I always feel good comfort to be with them. We spend a memorable time and shared special moments. I would also thanks to my class fellows **Qumar and Tariq Hussain** and all members of Fluid mechanics group (FMG).

Last but not least I can't imagine my current position without constant source of love and support from my family. They gave me freedom to explore my own and at the same time the guidance to recover when my steps faltered. The generous support from my younger brothers **Tamoor, Waseem** and younger sisters **Shumaila**, little angel **Anam** and my grandfather (late) are always source of inspiration for me. I also wish to thank my uncle **Yousaf** oats for his encouragement and practical advice.

Ansa Rafique

Preface

Heat transport over a stretching surface in the expanse of stagnation point flows have wide applications in fiber sheet manufacturing, glass production, polymers, paper production, metal spinning, continuous casting and many others.

According to the opinion of researchers, various fluids are chemical engineering and biomedical sciences are in nature. One usually comes across the situations where the flow of non-Newtonian fluids occurs. These fluids have relevance particularly in cosmetic products, biological liquids, butter, toothpaste, certain oils, grease, shampoos etc. Such material cannot be described in general by the classical Newtonian's law of viscosity. Thus various mathematicians, engineers and computer scientists have devoted their attention to the modeling and simulation of such flows. At present, the non-Newtonian fluids are characterized under three cases namely the differential, the integral and the rate. Although numerous works have been reported for the differential type fluids but the rate type classes are not given proper attention. Especially, the boundary layer flows in rate type fluids are not much studied. Various investigators in the field examined the unidirectional flows of Maxwell and Oldroyd-B fluids. Besides these, the appealing feature of micropolar theory is that it can additionally predict the microrotation effects. Specifically, the micropolar fluid deals with the mathematical and behavior of

various fluids such as liquid crystals, exotic lubricants, animal blood and ferro-liquid etc.

In view of the above mentioned discussion, this thesis is structured in the following forms.

Chapter 2 deals with the incompressible and unsteady flow of viscous fluid. Mixed convection flow in the vicinity of stagnation-point flow near a stretching surface is analyzed in second chapter. Free stream velocity has occupied time-dependency. The conservation laws are reformed into ODEs after employing the appropriate transformations. Analytical technique(HAM) is used to solve the nonlinear problem. The numerical values of skin friction coefficient and local Nusselt number for various pertinent parameters are tabulated. It is noticed that the magnitude of skin friction coefficient decays with the increasing values of radiation parameter and mixed convection parameter. **Such observations are published in "International Journal of Numerical Methods and Fluids, 68 (2012) 483-493".**

Chapter 3 addresses the mixed convection flow of viscous fluid towards stagnation point over a linearly stretching surface when fluid is magnetohydrodynamic (MHD). Series solutions are constructed for assisting and opposing flow cases. Moreover the effects of velocity and thermal slip parameters are scrutinized carefully. Physical parameters involving in governing problem are plotted. **This**

research has been submitted for publication in the "Journal of Aerospace Engineering".

MHD stagnation-point flow of viscous fluid is discussed in chapter 3. The flow is generated by the linearly stretched surface. Suitable transformations are applied for partial differential equations to convert these in the coupled set of ordinary differential equations. The thermal radiation effect has been considered through the Rosseland approximation. Slip conditions are applied to model the problem. Influences of different physical parameters are obtained by graphical and tabular results. It is observed that skin friction coefficient becomes larger when Hartman number increases. The skin friction and local Nusselt number decrease for large values of velocity slip parameter. **Such results are submitted in "Zeitschrift Naturforschung A".**

Chapter 4 exposes the solution of non-Newtonian fluid near the stagnation-point. Second grade incompressible fluid invades on the wall orthogonally. The homotopy analysis method (HAM) is applied to solve nonlinear problems. The obtained convergent solutions have been equaled with numerical solutions. Admirable agreement is noticed between both solutions. **These results are published in "Communications in Theoretical Physics, 57 (2012) 290-294".**

Chapter 5 investigates two-dimensional mixed convection flow of Maxwell fluid. The phenomenon of variable thermal conductivity has been considered. The flow

is considered near the region of stagnation-point. Analysis of heat transfer with thermal radiation and source/sink is also carried out. The solutions of transformed differential equations are obtained by homotopy analysis method. Discussion is provided for the velocity and temperature profiles. Convergence of series solution is examined. Results are compared with the previous limiting studies. **This research is submitted in “International Journal of Heat and Mass Transfer”.**

Chapter 6 provides the analysis of laminar flow for Maxwell fluid. Magnetic field effects for the stagnation-point flow near linear stretching sheet are also considered. Heat transfer with thermal radiation effect is addressed carefully. Convergence of the developed solutions is checked carefully. Appreciable change has been noticed for involved physical parameters for velocity and temperature. Comparison for local Nusselt number is presented with previous results in limiting case. **Such observations are published in “Heat Transfer; Asian Research”.**

The flow of an Oldroyd-B fluid with variable thermal conductivity is analyzed in chapter 7. The governing equations are modeled and then transformed into the ordinary differential equations. Deborah number and thermal radiation effects are attended in this chapter. It is found that the stretching parameter assists the velocity profile and resists the temperature profile. **This work is submitted for publication in “Thermal Science”.**

Chapter 8 examines the micropolar fluid near stagnation-point towards a stretching

sheet. Attention is given to the behavior of various emerging parameters via graphs. Numerical values of dimensionless skin friction coefficient and local Nusselt number are calculated. In limiting cases, appreciable agreement is made known with numerical solutions. Further, it is noted that temperature profile decreases by increasing microrotation parameter. **The results of this problem are submitted in "International Journal of Numerical Methods for Heat and Fluid Flow".**

Contents

1	Introduction	4
1.1	Fundamental expressions	7
1.1.1	Law of conservation of mass	7
1.1.2	Law of conservation of linear momentum	8
1.1.3	Law of conservation of energy	8
1.1.4	Fick's law	8
1.1.5	Maxwell's equations	9
1.2	Two-dimensional boundary layer equations	9
1.2.1	Boundary layer equations for second grade fluid	9
1.3	Boundary layer equation for upper-convected Maxwell (UCM) fluid	12
1.4	Boundary layer equation for micropolar fluid	14
1.5	Basic idea of homotopy analysis method (HAM)	15
2	Unsteady stagnation point flow over a stretching surface with mixed convection	17
2.1	Mathematical description	17
2.2	Solutions by homotopy analysis method	19
2.3	Convergence criteria	22
2.4	Graphical results and discussion	31
2.5	Conclusions	32

3	Slip effect in stagnation-point flow with thermal radiation	33
3.1	Development of the problems	33
3.2	Series solutions	36
3.3	Convergence of the homotopy solutions	38
3.4	Discussion	53
4	MHD mixed convection flow near a stagnation-point towards a stretching sheet	55
4.1	Mathematical description	55
4.2	Homotopy analysis solutions	58
4.3	Homotopy solutions	60
4.4	Results and discussion	74
4.5	Concluding remarks	76
5	Series solution for stagnation-point flow of second grade fluid	77
5.1	Mathematical analysis	77
5.2	Orthogonal flow	80
5.3	Oblique flow	81
5.4	Series solutions	82
5.5	Analysis of solutions	85
5.6	Discussion	92
6	Stagnation-point flow of Maxwell fluid with thermal radiation and source/sink	94
6.1	Mathematical model	94
6.2	Homotopy analysis solutions	97
6.3	Analysis of solutions	99
6.4	Discussion	108
7	MHD stagnation point flow of Maxwell fluid with radiation effects	110

7.1	Problem Statement	110
7.2	Solution by Homotopy Analysis Method	112
7.3	Analysis of solutions	115
7.4	Graphical results and discussion	123
8	Stagnation point flow of an Oldroyd-B fluid with variable thermal conductivity	125
8.1	Governing problems	126
8.2	Homotopy analysis solutions	128
8.3	Convergence of homotopy solutions	131
8.4	Graphical results and discussion	139
9	Effect of heat transfer on stagnation point flow of micropolar fluid with variable thermal conductivity and heat source/sink	141
9.1	Mathematical model	142
9.2	Analysis of solutions	146
9.3	Results and discussion	160
9.4	Conclusions	161

Chapter 1

Introduction

The dynamics of viscous fluid with stagnation-point flow specially near stretching surfaces has recently attracted the attention of mathematicians, engineers and numerical simulators. It is because of the fact that such flows appear extensively in several industrial and engineering processes. Such flows specifically occurs in the processes like extrusion, glass fiber, metal spinning, insulating materials etc. The steady stagnation point flow was initially discussed by Hiemenz [1]. The study of stagnation point flow over a linearly stretched sheet is considered by Chiam [2]. He concluded that boundary layer does not exist near the surface when plate stretching rate and constant rate of stagnation point flow are equal. Such layer depends upon the ratio of stretching and free stream rates. Although the relevant literature for such flows under different physical conditions is quite extensive but we here refer the readers to few very recent studies by Mahapatra and Gupta [3], Lok et al. [4], Ishak [5], Nadeem et al. [6] and Bachok [7]. The study of boundary layer flow combined with heat transport phenomenon has applications in technological process including metal and polymer extrusion, drawing of plastic sheets, cable coating, continuous casting, drawing of plastic sheets. The quality of final product in the manufacturing processes is highly dependent upon the rate of cooling. Such cooling rate can be controlled by considering thermal radiation with magnetic field. Further, consideration of boundary layer flow in presence of applied magnetic field is significant especially in metallurgy. Although ample investigations are presented for steady and unsteady flows on this topic

but Chiam [8] made an interesting study for the stagnation-point flow of viscous fluid in the region of stretching sheet. The thermal conductivity in this attempt is taken variable. Stagnation-point flow with heat transfer for both steady and unsteady cases has been studied by Mahapatra and Gupta [9], Pop et al. [10], Sharma and G. Singh [11], Abbas and Hayat [12] etc. A numerical scheme is applied on the stagnation-point flow over melting stretched surface by Bachok et al. [13]. The analysis of heat radiation is investigated over a porous stretching sheet with the existence of unique and dual solutions by Bhattacharyya and Layek [14], Fang et al. [15] discussed incompressible and unsteady stagnation point flow with mass transfer. Dual solutions are constructed under the assumption of chemical reaction and mass transfer by Bhattacharyya [16].

The topic of heat transfer in mixed convection process is the focus of several recent investigations during the last few years. This is due to its vast applications in the design of cooling systems for electronic devices, in field of solar energy collection etc. Further, the convection flow problems in context of magnetohydrodynamics are of great value due to its industrial applications such as geothermal reservoirs, cooling of nuclear reactors, petroleum reservoirs, thermal insulation etc. Such problems normally appear in electronic packages and microelectronic devices during their operations. Few attempts regarding such flows for the time-dependent and time-independent cases with stagnation-point over stretching flows have been reported in the references [17 – 20]. In continuation, various investigations concerning the stagnation-point flows of Newtonian and non-Newtonian fluids have been also reported by Mahapatra and Gupta [21], Labropulu and Li [22], Mustafa et al. [23], Robert et al. [24], Gorder and Vajravelu [25], Mahapatra et al. [26] and Hayat et al. [27]).

There are many materials such as blood, dyes, shampoo, ketchup, certain oils and greases, mud, paints, clay coating which do not follow the Newton's law of viscosity. Different from the viscous fluids, a single constitutive equation is not sufficient to describe such types of fluid flows. The appearance of rheological parameters in constitutive equations differ these fluids from the viscous fluids. The corresponding expressions of Cauchy stress tensors in non-Newtonian fluids give rise to

complicated and higher order differential equations in comparison to the Navier-Stokes equations. Therefore, the study of non-Newtonian fluids is an active topic of research for the mathematicians, engineers, physicists, modelers and numerical simulators. Extensive previous researches are now available on this topic. Majority of the existing investigations in non-Newtonian fluid mechanics dealt with the flows of differential type fluids. Less attention is paid to the rate type non-Newtonian fluids. The rate type fluids are capable for the prediction of relaxation and retardation times effects. The rate type fluid (i.e. Maxwell model) is useful to examine the relaxation time variation. This type of flow configuration has promising applications in polymer processing, fiber industry and boundary layer along material handling conveyers, aerodynamics etc. Some relevant recent studies involving Maxwell fluid model include the works of refs. [28 – 39]. An electroosmotic and time periodic electroosmotic flows of generalized Maxwell are studied by Jian et al. [40] and Liu et al. [41]. Zheng et al. [42] discussed the heat transfer flow of generalized Maxwell fluid caused by accelerating plate. Bhatnagar et al. [43] has done the seminal work on boundary layer flow of an Oldroyd-B fluid with free stream velocity. They have obtained a perturbation solution valid for the small values of viscoelastic parameter. Hayat et al. [44, 45] discussed simple unidirectional flows and hydromagnetic rotating flow of Oldroyd-B fluid. Tan and Masuoka [46] obtained the exact solution of viscoelastic fluid for Rayleigh's problem. Husain et al. [47] looked at the analytical solutions for invariable and variable accelerated flows of an Oldroyd-B fluid. Sajid et al. [48] developed a mathematical model for the boundary layer stagnation-point flow past a stretching surface. An explicit finite difference scheme is implemented for the computation of numerical solutions of the resulting differential system. Some fundamental unidirectional flows of an Oldroyd-B fluid are analyzed by Fetecau and Fetecau [49], Vieru et al. [50] and Fetecau et al. [51].

The hypothesis of micropolar fluids was initially projected by Eringen [52]. This theory describes the microrotation effects of the microstructures. It also explains the flow of various complex fluid systems including the polymer fluids, colloidal solutions, animal blood, liquid crystals and fluids with additives. Salient features of this theory have been explained by Ariman et al. [53, 54] and in the

books by Lukaszewicz [55] and Eringen [56]. Micropolar fluids have also received great attention in the past. For example the flow of micropolar fluid over permeable stretching sheet has been examined by Kelson and Farrel [57]. Influence of viscous dissipation and internal heat generation in the flow of micropolar fluid over a stretching sheet has been reported by Mohammadein [58]. Nazar et al. [59] numerically analyzed the micropolar fluid near stagnation-point using Keller-box method. Analytic solutions for boundary layer flow of micropolar fluid bounded by nonlinearly stretching sheet have been obtained by Hayat et al. [60]. Stagnation-point flow of micropolar fluid towards a stretching/shrinking surface with convective boundary conditions is studied by Yacob and Ishak [61]. Yacob et al. [62] also described the influence of melting heat transfer in the stagnation-point flow towards a linearly stretching/shrinking sheet. Hayat et al. [63] considered the thermal radiation effects and chemical reaction in the mixed convection flow of micropolar fluid. Rashidi et al. [64] provided the homotopy solutions of micropolar fluid with heat transfer immersed in porous medium.

1.1 Fundamental expressions

The research presented in this thesis will be modelled through the laws mentioned below.

1.1.1 Law of conservation of mass

The continuity equation for unsteady flow is

$$\frac{\partial \rho}{\partial t} + \nabla \cdot (\rho \mathbf{V}) = 0. \quad (1.1)$$

Eq. (1.1) for incompressible flow reduces to

$$\nabla \cdot \mathbf{V} = 0, \quad (1.2)$$

where ρ , \mathbf{V} respectively denote the density and velocity of the fluid, t the time and ∇ the operator.

1.1.2 Law of conservation of linear momentum

The momentum equation in mathematical form is represented by the following expression

$$\rho \frac{d\mathbf{V}}{dt} = \nabla \cdot \boldsymbol{\tau} + \rho \mathbf{b}, \quad (1.3)$$

$$\boldsymbol{\tau} = -p\mathbf{I} + \bar{\mathbf{S}}, \quad (1.4)$$

where τ , \mathbf{b} , p , \mathbf{I} , d/dt and $\bar{\mathbf{S}}$ denote the fluid density, velocity of the fluid, the Cauchy stress tensor, the body force, the pressure, identity tensor, the material derivative and extra stress tensor respectively.

1.1.3 Law of conservation of energy

The energy equation with radiation effects is expressed as follows:

$$\rho c_p \frac{dT}{dt} = k \nabla^2 T + \boldsymbol{\tau} \cdot \mathbf{L} + \rho r, \quad (1.5)$$

in which c_p depicts the specific heat at constant volume, k the thermal conductivity, ρr the coefficient of mass diffusivity and T the temperature.

1.1.4 Fick's law

Mathematical form of Fick's law is given by

$$\frac{dC}{dt} = De \nabla^2 C - k_n C^m, \quad (1.6)$$

in which \mathbf{L} , C , De and k_n the velocity gradient, the radiant heating, the concentration, and the reaction rate.

1.1.5 Maxwell's equations

These equations includes the equations listed below.

(i) Gauss's law

$$\nabla \cdot \mathbf{E} = \frac{\rho_c}{\varepsilon_0}. \quad (1.7)$$

(ii) Gauss's law for magnetism

$$\nabla \cdot \mathbf{B} = 0. \quad (1.8)$$

(iii) Faraday's law

$$\nabla \times \mathbf{E} = -\frac{\partial \mathbf{B}}{\partial t}. \quad (1.9)$$

(iv) Ampere's law

$$\nabla \times \mathbf{B} = \mu_0 \mathbf{J} + \mu_0 \varepsilon_0 \frac{\partial \mathbf{E}}{\partial t}. \quad (1.10)$$

(v) Ohms' law

$$\mathbf{J} = \sigma(\mathbf{E} + \mathbf{V} \times \mathbf{B}), \quad (1.11)$$

with ρ_c , ε_0 , \mathbf{B} , \mathbf{E} , μ_0 , \mathbf{J} and σ the charge density, electric constant, magnetic field, electric field, magnetic constant, current density and conductivity of the fluid.

1.2 Two-dimensional boundary layer equations

The concept of boundary layer is attributed primarily to Ludwig Prandtl. The boundary layer flows in a region of stagnation-point are very important in engineering and industrial applications. Precise forms of related equations with stagnation-point in cases such as viscous, second grade, Maxwell, Oldroyd-B fluid and micropolar fluid are mentioned below.

1.2.1 Boundary layer equations for second grade fluid

Cauchy stress tensor (τ) and extra stress tensor ($\tilde{\mathbf{S}}$) in second grade fluid satisfy [81]:

$$\boldsymbol{\tau} = -p\mathbf{I} + \bar{\mathbf{S}}, \quad (1.12)$$

$$\bar{\mathbf{S}} = \mu\mathbf{A}_1 + \alpha_1\mathbf{A}_2 + \alpha_2\mathbf{A}_1^2, \quad (1.13)$$

where μ , \mathbf{A}_1 , \mathbf{A}_2 , α_1 and α_2 denote the dynamic viscosity, the first two Rivlin-Ericksen tensors and material parameters respectively. The thermodynamic constraints related to second grade fluid are [82]:

$$\mu \geq 0, \quad \alpha_1 \geq 0 \text{ and } \alpha_1 + \alpha_2 = 0. \quad (1.14)$$

The two Rivlin-Ericksen tensors are defined as [84]:

$$\mathbf{A}_1 = \mathbf{L} + \mathbf{L}^T \text{ and } \mathbf{A}_2 = \frac{d\mathbf{A}_1}{dt} + \mathbf{A}_1\mathbf{L} + \mathbf{L}^T\mathbf{A}_1, \quad (1.15)$$

in which $\mathbf{L} + \mathbf{L}^T = \text{grad } \mathbf{V} + (\text{grad } \mathbf{V})^T$. The velocity field in two-dimensional flow is

$$\mathbf{V} = (u(x, y, t), v(x, y, t), 0). \quad (1.16)$$

The expression of Cauchy stress tensor $\boldsymbol{\tau}$ is

$$\boldsymbol{\tau} = \begin{bmatrix} \tau_{xx} & \tau_{xy} \\ \tau_{yx} & \tau_{yy} \end{bmatrix}, \quad (1.17)$$

with

$$\begin{aligned} \tau_{xx} = & -p + 2\mu \left(\frac{\partial u}{\partial x} \right) + \alpha_1 \left[\begin{aligned} & 2 \left(\frac{\partial^2 u}{\partial x \partial t} + u \frac{\partial^2 u}{\partial x^2} + v \frac{\partial^2 u}{\partial x \partial y} \right) + \\ & 4 \left(\frac{\partial v}{\partial y} \right)^2 + 2 \left(\frac{\partial v}{\partial x} \right)^2 + 2 \frac{\partial u}{\partial y} \frac{\partial v}{\partial x} \end{aligned} \right] \\ & + \alpha_2 \left[4 \left(\frac{\partial u}{\partial x} \right)^2 + \left(\frac{\partial u}{\partial y} \right)^2 + \left(\frac{\partial v}{\partial x} \right)^2 + 2 \frac{\partial u}{\partial y} \frac{\partial v}{\partial x} \right], \end{aligned} \quad (1.18)$$

$$\begin{aligned} \tau_{yy} = & -p + 2\mu \left(\frac{\partial v}{\partial y} \right) + \alpha_1 \left[\begin{aligned} & 2 \left(\frac{\partial^2 v}{\partial y \partial t} + v \frac{\partial^2 v}{\partial y^2} + u \frac{\partial^2 v}{\partial x \partial y} \right) + \\ & 4 \left(\frac{\partial u}{\partial y} \right)^2 + 2 \left(\frac{\partial u}{\partial x} \right)^2 + 2 \frac{\partial u}{\partial y} \frac{\partial v}{\partial x} \end{aligned} \right] \\ & + \alpha_2 \left[4 \left(\frac{\partial v}{\partial y} \right)^2 + \left(\frac{\partial u}{\partial y} \right)^2 + \left(\frac{\partial v}{\partial x} \right)^2 + 2 \frac{\partial u}{\partial y} \frac{\partial v}{\partial x} \right], \end{aligned} \quad (1.19)$$

$$\begin{aligned} \tau_{xy} = \tau_{yx} = & \mu \left(\frac{\partial u}{\partial y} + \frac{\partial v}{\partial x} \right) + \alpha_1 \left[\begin{aligned} & \frac{\partial^2 u}{\partial y \partial t} + \frac{\partial^2 u}{\partial x \partial y} + v \frac{\partial^2 u}{\partial y^2} + \frac{\partial^2 v}{\partial x \partial t} + \\ & u \frac{\partial^2 v}{\partial x^2} + v \frac{\partial^2 v}{\partial x \partial y} + 3 \frac{\partial u}{\partial y} \frac{\partial v}{\partial x} + \\ & 3 \frac{\partial u}{\partial x} \frac{\partial v}{\partial y} + \frac{\partial u}{\partial x} \frac{\partial v}{\partial x} + \frac{\partial u}{\partial y} \frac{\partial v}{\partial y} \end{aligned} \right] \\ & + \alpha_2 \left[\frac{\partial u}{\partial x} \frac{\partial u}{\partial y} + \frac{\partial u}{\partial x} \frac{\partial v}{\partial y} + \frac{\partial u}{\partial y} \frac{\partial v}{\partial y} + \frac{\partial v}{\partial x} \frac{\partial v}{\partial y} \right], \end{aligned} \quad (1.20)$$

$$\tau_{zz} = -p, \quad \tau_{xz} = \tau_{yz} = 0. \quad (1.21)$$

The scalar forms of equation of motion are

$$\rho \frac{du}{dt} = \frac{\partial \tau_{xx}}{\partial x} + \frac{\partial \tau_{xy}}{\partial y} + \frac{\partial \tau_{xz}}{\partial z} + \rho b_x, \quad (1.22)$$

$$\rho \frac{dv}{dt} = \frac{\partial \tau_{yx}}{\partial x} + \frac{\partial \tau_{yy}}{\partial y} + \frac{\partial \tau_{yz}}{\partial z} + \rho b_y, \quad (1.23)$$

$$\rho \frac{dw}{dt} = \frac{\partial \tau_{zx}}{\partial x} + \frac{\partial \tau_{zy}}{\partial y} + \frac{\partial \tau_{zz}}{\partial z} + \rho b_z, \quad (1.24)$$

where b_x, b_y, b_z are the body forces in the x, y and z directions. Inserting Eqs. (1.18) to (1.21) into Eqs. (1.22) – (1.24) and then using the boundary layer approximations, we have

$$\frac{\partial u}{\partial t} + u \frac{\partial u}{\partial x} + v \frac{\partial u}{\partial y} = -\frac{1}{\rho} \frac{\partial p}{\partial x} + \nu \frac{\partial^2 u}{\partial y^2} + \frac{\alpha_1}{\rho} \left[\frac{\partial^3 u}{\partial y^2 \partial t} + u \frac{\partial^3 u}{\partial x \partial y^2} + \frac{\partial u}{\partial x} \frac{\partial^2 u}{\partial y^2} + v \frac{\partial^3 u}{\partial y^3} \right] - \frac{\sigma B_0^2 u}{\rho}, \quad (1.25)$$

$$0 = -\frac{1}{\rho} \frac{\partial p}{\partial y}, \quad (1.26)$$

where u and v are the velocity components in the x - and y -directions and body force has been employed in terms of magnetic force through constant applied magnetic field B_0 . Here σ denotes the magnetic permeability. From above equation we note that $p \neq p(y)$.

1.3 Boundary layer equation for upper-convected Maxwell (UCM) fluid

Expression of extra stress tensor in an upper-convected Maxwell (UCM) fluid is defined as

$$\tilde{\mathbf{S}} + \lambda_1 \frac{D\mathbf{S}}{Dt} = \mu \mathbf{A}_1, \quad (1.27)$$

in which λ_1 defines the relaxation time and D/Dt is the covariant differentiation. The first Rivlin-Ericksen tensor \mathbf{A}_1 is given below

$$\mathbf{A}_1 = \begin{bmatrix} 2\frac{\partial u}{\partial x} & \frac{\partial u}{\partial y} + \frac{\partial v}{\partial x} \\ \frac{\partial u}{\partial y} + \frac{\partial v}{\partial x} & 2\frac{\partial v}{\partial y} \end{bmatrix}. \quad (1.28)$$

The momentum equation in the absence of pressure gradient is

$$\rho \left(1 + \lambda_1 \frac{D}{Dt} \right) \left(\frac{d\mathbf{V}}{dt} \right) = \mu (\nabla \cdot \mathbf{A}_1)_i, \quad (1.29)$$

The general form of covariant derivative D/Dt is [67]

$$\frac{D}{Dt}(\alpha)_i = \frac{\partial}{\partial t}(\alpha)_i + \mathbf{V}_r(\alpha)_{i,r} - \mathbf{V}_{i,r}(\alpha)_r. \quad (1.30)$$

For $i = 1$, we have

$$\left(1 + \lambda_1 \frac{D}{Dt}\right) \left(\frac{d\mathbf{V}}{dt}\right)_1 = \nu(\nabla \cdot \mathbf{A}_1)_1, \quad (1.31)$$

$$\begin{aligned} \frac{D}{Dt} \left(\frac{d\mathbf{V}}{dt}\right)_1 &= \frac{\partial}{\partial t} \left(\frac{d\mathbf{V}}{dt}\right)_1 + \mathbf{V}_1 \left(\frac{d\mathbf{V}}{dt}\right)_{1,1} + \mathbf{V}_2 \left(\frac{d\mathbf{V}}{dt}\right)_{1,2} \\ &\quad - \mathbf{V}_{1,1} \left(\frac{d\mathbf{V}}{dt}\right)_1 - \mathbf{V}_{1,2} \left(\frac{d\mathbf{V}}{dt}\right)_2, \end{aligned} \quad (1.32)$$

with

$$\left(\frac{d\mathbf{V}}{dt}\right)_1 = \frac{du}{dt} = u \frac{\partial u}{\partial x} + v \frac{\partial u}{\partial y}, \quad (1.33)$$

$$\left(\frac{d\mathbf{V}}{dt}\right)_2 = \frac{dv}{dt} = u \frac{\partial v}{\partial x} + v \frac{\partial v}{\partial y}. \quad (1.34)$$

The above equations yield

$$\begin{aligned} u \frac{\partial u}{\partial x} + v \frac{\partial u}{\partial y} + \lambda_1 \left[u^2 \frac{\partial^2 u}{\partial x^2} + v^2 \frac{\partial^2 u}{\partial y^2} + 2uv \frac{\partial^2 u}{\partial x \partial y} \right] &= -\frac{1}{\rho} \frac{\partial p}{\partial x} - \frac{\lambda_1}{\rho} \left[u \frac{\partial^2 p}{\partial x^2} + v \frac{\partial^2 p}{\partial x \partial y} - \frac{\partial u}{\partial x} \frac{\partial p}{\partial x} \right] \\ &\quad + \nu \left[\frac{\partial^2 u}{\partial x^2} + \frac{\partial^2 u}{\partial y^2} \right] \end{aligned} \quad (1.35)$$

For $i = 2$, one has

$$\begin{aligned} u \frac{\partial v}{\partial x} + v \frac{\partial v}{\partial y} + \lambda_1 \left[u^2 \frac{\partial^2 v}{\partial x^2} + v^2 \frac{\partial^2 v}{\partial y^2} + 2uv \frac{\partial^2 v}{\partial x \partial y} \right] &= -\frac{1}{\rho} \frac{\partial p}{\partial y} - \frac{\lambda_1}{\rho} \left[v \frac{\partial^2 p}{\partial x^2} + u \frac{\partial^2 p}{\partial x \partial y} - \frac{\partial v}{\partial x} \frac{\partial p}{\partial x} - \frac{\partial v}{\partial y} \frac{\partial p}{\partial x} \right] \\ &\quad + \nu \left[\frac{\partial^2 v}{\partial x^2} + \frac{\partial^2 v}{\partial y^2} \right]. \end{aligned} \quad (1.36)$$

The boundary layer admits the order relationship

$$u, x, \lambda_1 \sim O(1), y, v \sim O(\delta). \quad (1.37)$$

Hence the boundary layer equation in absence of pressure gradient is

$$u \frac{\partial u}{\partial x} + v \frac{\partial u}{\partial y} + \lambda_1 \left[u^2 \frac{\partial^2 u}{\partial x^2} + v^2 \frac{\partial^2 u}{\partial y^2} + 2uv \frac{\partial^2 u}{\partial x \partial y} \right] = \nu \frac{\partial^2 u}{\partial y^2}. \quad (1.38)$$

1.4 Boundary layer equation for micropolar fluid

In absence of without body force and body couple fundamental equations are

$$\rho \frac{d\mathbf{V}}{dt} = -\nabla \tilde{p} + (\mu + \kappa) \nabla^2 \mathbf{V} + \kappa \nabla \times \mathbf{N}, \quad (1.39)$$

$$\rho j \frac{d\mathbf{N}}{dt} = \gamma^* \nabla (\nabla \cdot \mathbf{N}) - \gamma^* \nabla \times (\nabla \times \mathbf{N}) + \kappa \nabla \times \mathbf{N} - 2\kappa \mathbf{N}, \quad (1.40)$$

where \mathbf{V} , \mathbf{N} , j , γ^* and κ depicts the velocity, the microrotation vector, the gyration parameter of fluid, spin, the gradient viscosity and vortex viscosity. We write

$$\mathbf{N} = [0, 0, N(x, y)], \quad (1.41)$$

where N the microrotation parameter. The scalar forms of equations of motion are

The resulting scalar equations are given as

$$u \frac{\partial u}{\partial x} + v \frac{\partial u}{\partial y} = -\frac{1}{\rho} \frac{\partial \tilde{p}}{\partial x} + \frac{(\mu + \kappa)}{\rho} \left(\frac{\partial^2 u}{\partial x^2} + \frac{\partial^2 u}{\partial y^2} \right) + \frac{\kappa}{\rho} \frac{\partial N}{\partial y}, \quad (1.42)$$

$$u \frac{\partial v}{\partial x} + v \frac{\partial v}{\partial y} = -\frac{1}{\rho} \frac{\partial \tilde{p}}{\partial y} + \frac{(\mu + \kappa)}{\rho} \left(\frac{\partial^2 v}{\partial x^2} + \frac{\partial^2 v}{\partial y^2} \right) + \frac{\kappa}{\rho} \frac{\partial N}{\partial x}, \quad (1.43)$$

$$u \frac{\partial N}{\partial x} + v \frac{\partial N}{\partial y} = -\frac{\gamma_1}{\rho j} \left(\frac{\partial^2 N}{\partial x^2} + v \frac{\partial^2 N}{\partial y^2} \right) + \frac{\kappa}{\rho j} \left(\frac{\partial v}{\partial x} - \frac{\partial u}{\partial y} \right) - \frac{2\kappa}{\rho j} N. \quad (1.44)$$

The above equations subjected to boundary layer approximations are simplified to

$$u \frac{\partial u}{\partial x} + v \frac{\partial u}{\partial y} = -\frac{1}{\rho} \frac{\partial \bar{p}}{\partial x} + \left(\nu + \frac{\kappa}{\rho} \right) \frac{\partial^2 u}{\partial y^2} + \frac{\kappa}{\rho} \frac{\partial N}{\partial y}, \quad (1.45)$$

$$u \frac{\partial N}{\partial x} + v \frac{\partial N}{\partial y} = \frac{\gamma^*}{\rho j} \frac{\partial^2 N}{\partial y^2} - \frac{\kappa}{\rho j} \left(2N + \frac{\partial u}{\partial y} \right) \dots \quad (1.46)$$

1.5 Basic idea of homotopy analysis method (HAM)

In 1992, the trustworthy analytical technique named as the homotopy analysis method (HAM) was introduced by Liao [65]. This technique is quite useful in the development of series solutions for algebraic, ordinary and partial differential equations. The procedure holds for both weak and strong nonlinear problems [66 – 80]. Considering nonlinear equation

$$A(v) + f(x) = 0, \quad (1.47)$$

in which A is the nonlinear operator, $f(x)$ known function, v unknown function, the homotopic equation is expressed as

$$(1 - q)L[\tilde{v}(x, q) - v_0(x)] = p\hbar\{A[\tilde{v}(x, p) - v_0(x)]\}, \quad (1.48)$$

$v_0(x)$ the initial guess, L an auxiliary linear operator and \hbar is auxiliary parameter.

For $q = 0$ and $q = 1$, we have

$$\tilde{v}(x, 0) = v_0(x), \quad (1.49)$$

$$\tilde{v}(x, 1) = v(x). \quad (1.50)$$

Obviously when variation of q is accounted from 0 to 1 then $\tilde{v}(x, q)$ varies from the initial approxi-

mation to final solution. Taylor's series represents that

$$\bar{v}(x, q) = v_0(x) + \sum_{k=1}^{\infty} v_k(x)q^k, \quad (1.51)$$

$$v_k(x) = \frac{1}{k!} \frac{\partial^k \bar{v}(x, q)}{\partial q^k} \Big|_{q=0}, \quad (1.52)$$

and the subjected problems at k^{th} order are

$$L[v_k(x) - \chi_k v_{k-1}(x)] = \hbar R_k(x), \quad (1.53)$$

$$\chi_k = \begin{cases} 0, & k \leq 1, \\ 1, & k > 1, \end{cases} \quad (1.54)$$

with

$$R_k(x) = \frac{1}{(k-1)!} \left\{ \frac{d^{k-1}}{dq^{k-1}} A \left[v_0(x) + \sum_{k=1}^{\infty} v_k(x)q^k \right] \right\}_{q=0}. \quad (1.55)$$

Chapter 2

Unsteady stagnation point flow over a stretching surface with mixed convection

This chapter looks at the stagnation-point flow towards a stretching sheet with mixed convection. Analysis has been carried out for time-dependent free stream over a stretching sheet. The momentum and energy equations become the ordinary differential equations after applying similarity transformations. Series solution is first constructed and then analyzed for convergence. Physical quantities like skin friction coefficient and local Nusselt number are computed and examined.

2.1 Mathematical description

Here we consider two-dimensional, unsteady and incompressible flow of viscous fluid with mixed convection. The stagnation-point flow over a stretching sheet is modelled for time-dependent free stream. The stretching and free stream velocities are respectively defined by $u_w(x, t)$ and $U(x, t)$. The wall and surface temperature are denoted by T_w and T_∞ respectively. Note that the x -axis is taken along the sheet while y -axis normal to it. The gravitational force acts in the x -direction.

The boundary layer equations for the present flow are

The relevant governing equations of the flow are

$$\frac{\partial u}{\partial x} + \frac{\partial v}{\partial y} = 0, \quad (2.1)$$

$$\frac{\partial u}{\partial t} + u \frac{\partial u}{\partial x} + v \frac{\partial u}{\partial y} = U \frac{\partial U}{\partial x} + \frac{\partial U}{\partial t} + \nu \frac{\partial^2 v}{\partial y^2} + g\beta_T (T - T_\infty), \quad (2.2)$$

$$\rho c_p \frac{\partial T}{\partial t} + u \frac{\partial T}{\partial x} + v \frac{\partial T}{\partial y} = k \frac{\partial^2 T}{\partial y^2} - \frac{\partial q_r}{\partial y}, \quad (2.3)$$

where u and v are the velocity components, T , $\nu = (\mu/\rho)$, ρ and k represents the fluid temperature, the kinematic viscosity, the density of fluid and the thermal conductivity respectively.

The relevant boundary conditions are defined as follows

$$u = u_w(x, t) = \frac{cx}{1 - \alpha t}, \quad v = 0, \quad T = T_w \quad \text{at } y = 0, \quad (2.4)$$

$$u = U(x, t) = \frac{bx}{1 - \alpha t}, \quad T = T_\infty \quad \text{as } y \rightarrow \infty, \quad (2.5)$$

here α , b and c have dimensions of $(\text{time})^{-1}$.

If ψ is the stream function then setting

$$u = \frac{\partial \psi}{\partial y}, \quad v = -\frac{\partial \psi}{\partial x}, \quad (2.6)$$

$$\eta(y, t) = \left[\frac{c}{\nu(1 - \alpha t)} \right]^{1/2} y, \quad (2.7)$$

$$\psi(x, y, t) = \left[\frac{\nu c}{(1 - \alpha t)} \right]^{1/2} x f(\eta), \quad (2.8)$$

$$\theta = \frac{T - T_\infty}{T_w - T_\infty}, \quad (2.9)$$

with

$$T_w - T_\infty = \frac{1}{(1 - \alpha t)^2} \quad (2.10)$$

Incompressibility condition is automatically satisfied and the Eqs. (2.2 – 2.5) give

$$f''' + \left(f + \frac{1}{2}\eta\alpha^*\right) f'' + (\alpha^* - f') f' + \epsilon^2 - \epsilon\alpha^* + \lambda_1\theta = 0, \quad (2.11)$$

$$\left(1 + \frac{4}{3}R_d\right) \theta'' + \text{Pr} \left(f + \frac{1}{2}\eta\alpha^*\right) \theta' + 2\text{Pr}\alpha^*\theta = 0, \quad (2.12)$$

$$f = 0, \quad f' = 1, \quad \theta = 1 \quad \text{at } \eta = 0, \quad (2.13)$$

$$f' = \epsilon, \quad \theta = 0 \quad \text{at } \eta = \infty. \quad (2.14)$$

In above equations $\epsilon = \frac{b}{c}$, $\text{Pr} = \frac{\mu C_p}{\kappa}$, $\alpha^* = \frac{\alpha}{c}$, $\lambda_1 = \frac{Gr_x}{\text{Re}_x^2}$, $Gr_x = \frac{g\beta(T_w - T_\infty)x^3/v^2}{u_w^2 x^2/v^2}$, $\text{Re}_x = \frac{u_w x}{\nu}$ and $R_d = \frac{4\sigma^* T_\infty^3}{\kappa\kappa^*}$ define the ratio of constants, the Prandtl number, the parameter, the mixed convection parameter, the local Grashof number, the local Reynolds number and the thermal radiation parameter respectively.

2.2 Solutions by homotopy analysis method

f and θ (which represents dimensionless velocity and temperature respectively) in the set of base functions

$$\{\eta^k \exp(-n\eta), k \geq 0, n \geq 0\}, \quad (2.15)$$

takes the following form

$$f(\eta) = a_{0,0}^0 + \sum_{n=0}^{\infty} \sum_{k=0}^{\infty} a_{m,n}^k \eta^k \exp(-n\eta), \quad (2.16)$$

$$\theta(\eta) = \sum_{n=0}^{\infty} \sum_{k=0}^{\infty} b_{m,n}^k \eta^k \exp(-n\eta), \quad (2.17)$$

in which $a_{m,n}^k$ and $b_{m,n}^k$ are the coefficients. Moreover, the initial guesses and linear operators are chosen as follows

$$f_0(\eta) = \epsilon\eta + (1 - \epsilon)(1 - e^{-\eta}), \quad (2.18)$$

$$\theta_0(\eta) = e^{-\eta} + \frac{\eta}{2}(e^{-\eta}). \quad (2.19)$$

The auxiliary linear operators

$$L_f = f''' - f', \quad L_\theta = \theta'' - \theta, \quad (2.20)$$

have the properties as follows:

$$L_f(C_1 + C_2e^\eta + C_3e^{-\eta}) = 0, \quad L_\theta(C_4e^\eta + C_5e^{-\eta}) = 0, \quad (2.21)$$

in which C_i ($i = 1 - 5$) are the arbitrary constants.

Nonlinear operators N_f and N_θ are defined by

$$\begin{aligned} N_f[f(\eta, p), \theta(\eta, p)] &= \frac{\partial^3 f(\eta, p)}{\partial \eta^3} - \left(f(\eta, p) + \frac{1}{2}\eta\alpha^* \right) \frac{\partial^2 f(\eta, p)}{\partial \eta^2} - \alpha^* \frac{\partial f(\eta, p)}{\partial \eta} \\ &\quad - \left(\frac{\partial f(\eta, p)}{\partial \eta} \right)^2 + \epsilon^2(1 - \varkappa_m) - \epsilon\alpha^*(1 - \varkappa_m) + \lambda_1\theta(\eta, p), \end{aligned} \quad (2.22)$$

$$\begin{aligned} N_\theta[\theta(\eta, p), f(\eta, p)] &= \left(1 + \frac{4}{3}R_d \right) \frac{\partial^2 \theta(\eta, p)}{\partial \eta^2} + \text{Pr} \left(f(\eta, p) + \frac{1}{2}\eta\alpha^* \right) \frac{\partial \theta(\eta, p)}{\partial \eta} \\ &\quad + 2\text{Pr}\alpha^*\theta(\eta, p). \end{aligned} \quad (2.23)$$

Zeroth order problems take the form

$$(1 - p)L_f[\hat{f}(\eta; p) - f_0(\eta)] = ph_f N_f[\hat{f}(\eta; p), \hat{\theta}(\eta; p)], \quad (2.24)$$

$$(1 - p)L_\theta[\hat{\theta}(\eta; p) - \theta_0(\eta)] = ph_\theta N_\theta[\hat{f}(\eta; p), \hat{\theta}(\eta; p)]. \quad (2.25)$$

$$\tilde{f}(0; p) = \epsilon, \quad \tilde{f}'(0; p) = -1, \quad \tilde{f}'(\infty; p) = 0, \quad \tilde{\theta}(0, p) = 1, \quad \tilde{\theta}(\infty, p) = 0, \quad (2.26)$$

in which p , h_f and h_θ are termed as the embedding parameter and non-zero auxiliary parameters.

By taking $p = 0$ and $p = 1$, one has

$$\tilde{f}(\eta; 0) = f_0(\eta), \quad \tilde{\theta}(\eta, 0) = \theta_0(\eta) \text{ and } \tilde{f}(\eta, 1) = f(\eta), \quad \tilde{\theta}(\eta, 1) = \theta(\eta). \quad (2.27)$$

When p lies between 0 to 1 then $f(\eta, p)$ and $\theta(\eta, p)$ vary from the initial guesses $f_0(\eta)$, $\theta_0(\eta)$ to the final solutions $f(\eta)$ and $\theta(\eta)$. By Taylor's series, we have

$$f(\eta, p) = f_0(\eta) + \sum_{m=1}^{\infty} f_m(\eta)p^m, \quad (2.28)$$

$$\theta(\eta, p) = \theta_0(\eta) + \sum_{m=1}^{\infty} \theta_m(\eta)p^m, \quad (2.29)$$

$$f_m(\eta) = \frac{1}{m!} \frac{\partial^m f(\eta; p)}{\partial \eta^m} \Big|_{p=0}, \quad \theta_m(\eta) = \frac{1}{m!} \frac{\partial^m \theta(\eta; p)}{\partial \eta^m} \Big|_{p=0}. \quad (2.30)$$

The non-zero auxiliary parameters h_f and h_θ are taken in an appropriate manner where both series converge at $p = 1$. Hence

$$f(\eta) = f_0(\eta) + \sum_{m=1}^{\infty} f_m(\eta), \quad (2.31)$$

$$\theta(\eta) = \theta_0(\eta) + \sum_{m=1}^{\infty} \theta_m(\eta). \quad (2.32)$$

The problems at the m^{th} order are given by

$$L_f [f_m(\eta) - \chi_m f_{m-1}(\eta)] = h_f R_f^m(\eta), \quad (2.33)$$

$$L_\theta [\theta_m(\eta) - \chi_m \theta_{m-1}(\eta)] = h_\theta R_\theta^m(\eta), \quad (2.34)$$

$$f_m(0) = f'_m(0) = f'_m(\infty) = 0, \quad \theta_m(0) = \theta_m(\infty) = 0, \quad (2.35)$$

$$\begin{aligned}
R_f^m(\eta) &= f_{m-1}'''(\eta) + \sum_{k=0}^{m-1} \left[f_{m-1-k} f_k'' + \frac{1}{2} \eta \alpha^* f_{m-1}'' \right] + \sum_{k=0}^{m-1} [\alpha^* f_{m-1}' - f_{m-1}''] \\
&\quad + \epsilon^2(1 - \chi_m) - \epsilon \alpha^*(1 - \chi_m) + \lambda_1 \sum_{k=0}^{m-1} \theta_{m-1-k},
\end{aligned} \tag{2.36}$$

$$R_\theta^m(\eta) = \left(1 + \frac{4}{3} R_d \right) \theta_{m-1}'' + \text{Pr} \sum_{k=0}^{m-1} \theta'_{m-1-k} f_k + \frac{1}{2} \text{Pr} \alpha^* \eta \theta_{m-1}' + 2 \text{Pr} \alpha^* \sum_{k=0}^{m-1} \theta_{m-1-k}, \tag{2.37}$$

$$\chi_m = \begin{cases} 0, & m \leq 1, \\ 1, & m > 1. \end{cases} \tag{2.38}$$

Denoting $f_m^*(\eta)$ and $\theta_m^*(\eta)$ as the special solutions we have the general solutions as follows:

$$f_m(\eta) = f_m^*(\eta) + C_1 + C_2 e^\eta + C_3 e^{-\eta}, \tag{2.39}$$

$$\theta_m(\eta) = \theta_m^*(\eta) + C_4 e^\eta + C_5 e^{-\eta}. \tag{2.40}$$

2.3 Convergence criteria

Series solutions (2.28) and (2.29) depend upon the nonzero auxiliary parameters \hbar_f and \hbar_θ to maintain the convergence of the HAM solutions. To check the for admissible values of \hbar_f and \hbar_θ , the \hbar -curves are plotted for 23rd-order of approximations. It is evident that Fig. 2.1 admits the appreciable range for \hbar_f and \hbar_θ i.e., $-0.75 \leq \hbar_f \leq -0.2$ and $-0.85 \leq \hbar_\theta \leq -0.1$. Furthermore, it is shown that the series converge in the whole region of η when $\hbar_f = \hbar_\theta = -0.5$.

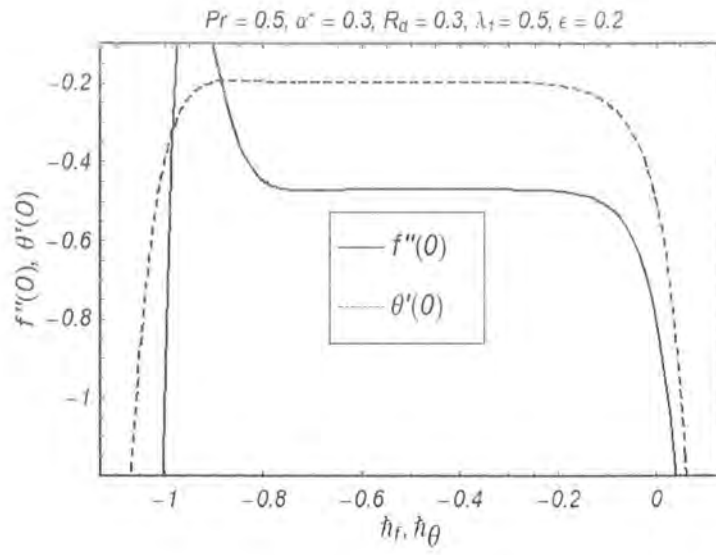


Fig. 2.1. h - curves for 23rd order of approximations.

Table: 2.1. Convergence of series solution when

$$\alpha^* = R_d = 0.3, \epsilon = 0.2, \lambda_1 = \text{Pr} = 0.5$$

$$\text{and } h_f = h_\theta = -0.5.$$

Order of approximations	$-f''(0)$	$-\theta'(0)$
1	0.65875	0.38056
5	0.48878	0.23125
10	0.47149	0.19983
15	0.47035	0.19687
20	0.47054	0.19709
25	0.47054	0.19715
30	0.47054	0.19715
35	0.47054	0.19715
40	0.47054	0.19715

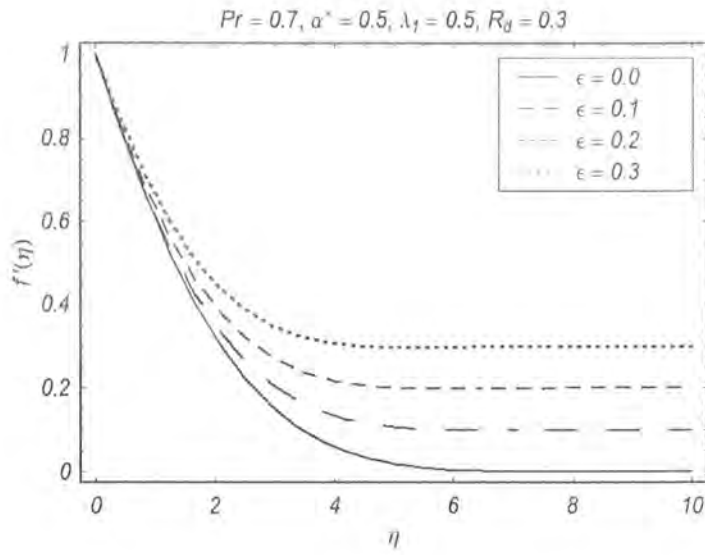


Fig. 2.2. Effect of ϵ on velocity profile f' .

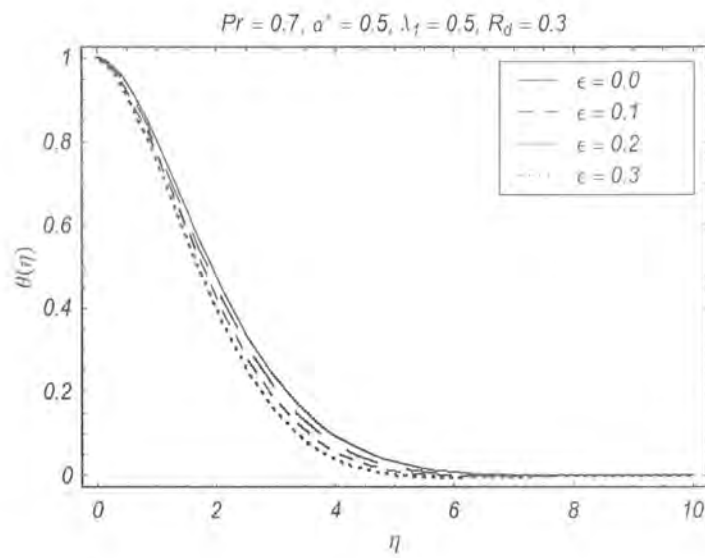


Fig. 2.3. Effect of ϵ on temperature profile θ .

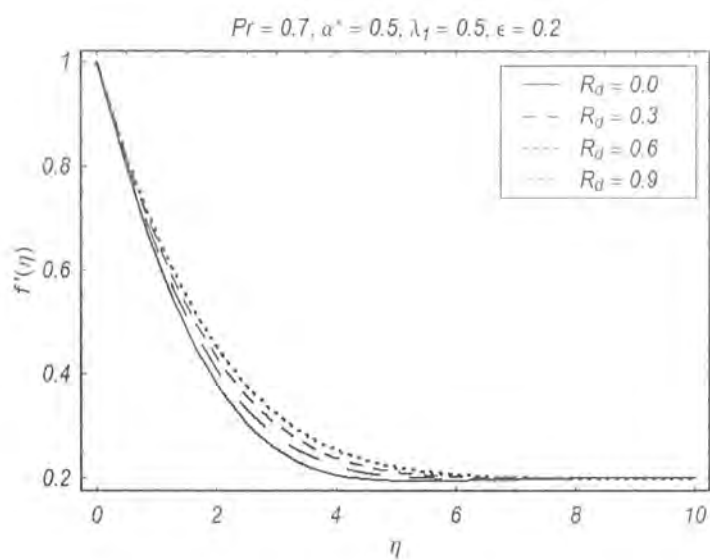


Fig. 2.4. Effect of R_d on velocity profile f' .

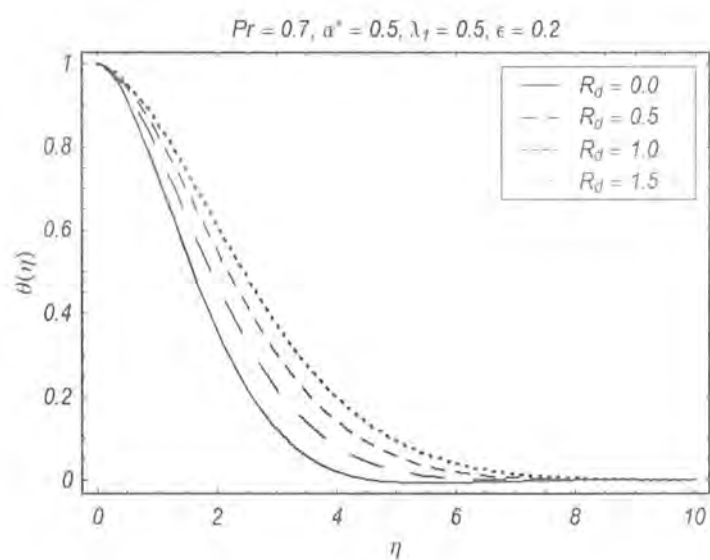


Fig. 2.5. Effect of R_d on temperature profile θ .

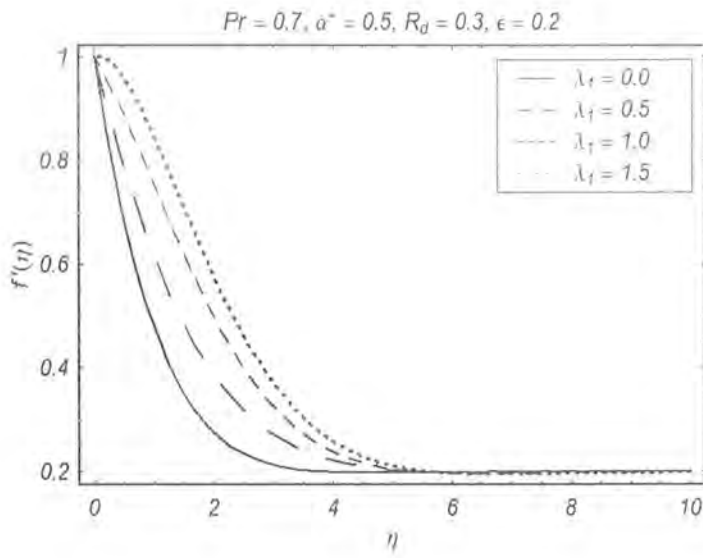


Fig. 2.6. Effect of λ_1 on velocity profile f' .

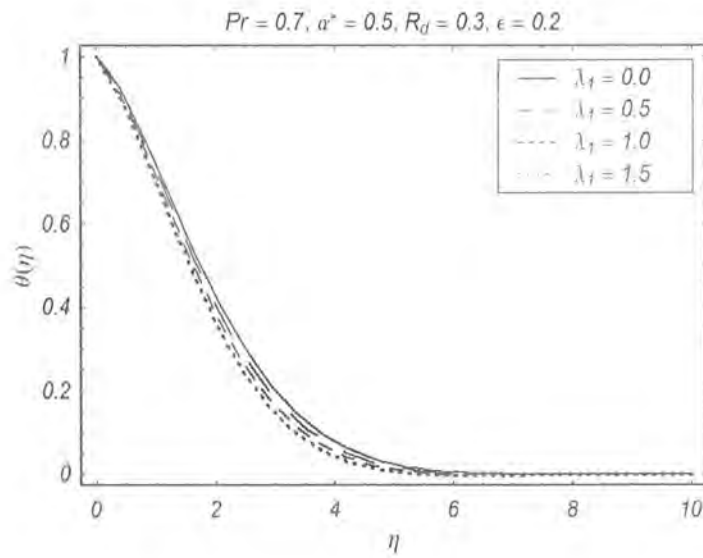


Fig. 2.7. Effect of λ_1 on temperature profile θ .

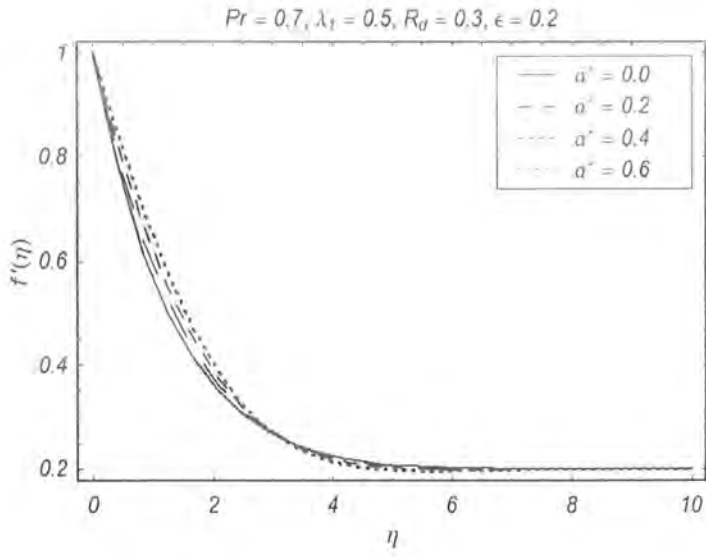


Fig. 2.8. Effect of a^* on velocity profile f' .

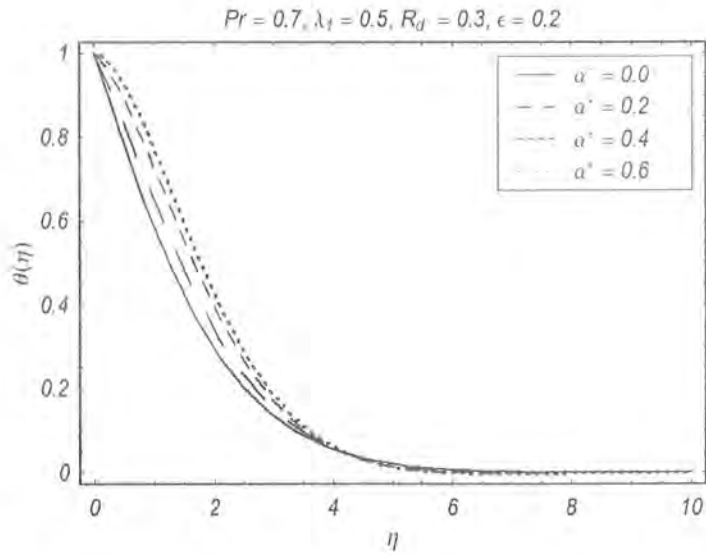


Fig. 2.9. Effect of a^* on temperature profile θ .

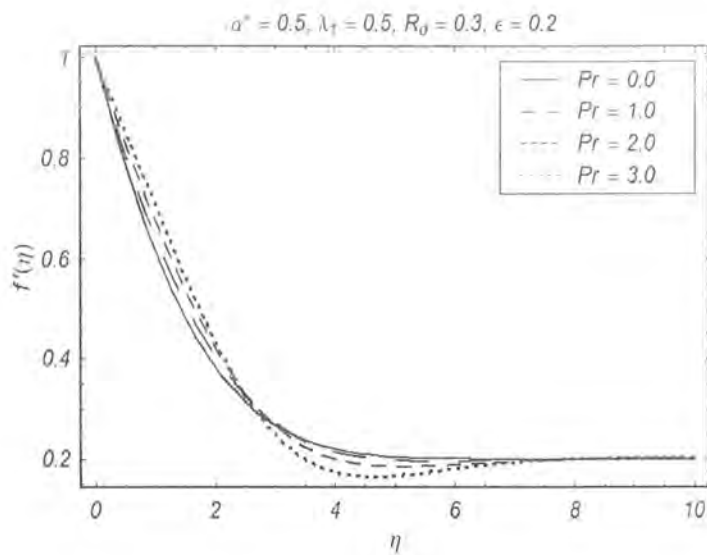


Fig. 2.10. Effect of Pr on velocity profile f' .

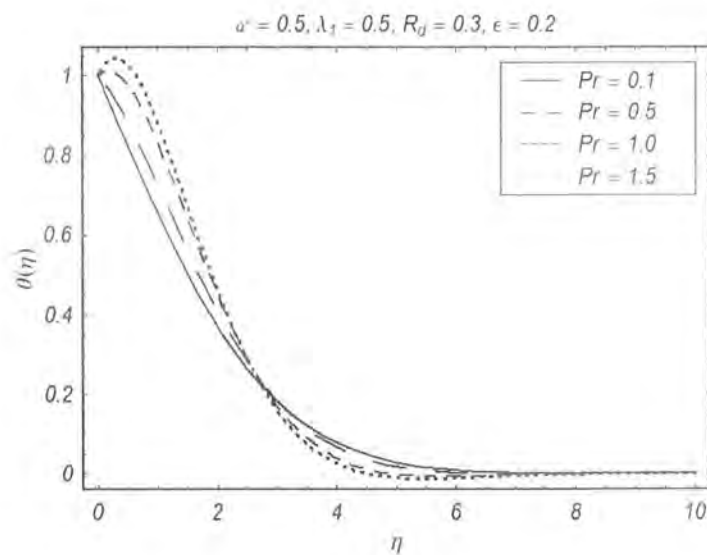


Fig. 2.11. Effect of Pr on temperature profile θ .

Table: 2.2. Comparison for different values of ϵ on $f''(0)$ relative to the results by Pop et al. [10] and Sharma and Singh [11].

ϵ	$f''(0)$		
	Pop et al. [10]	Sharma and Singh [11]	Present outcomes
0.1	-0.9694	-0.969386	-0.969386
0.2	-0.9181	-0.918107	-0.918107
0.5	-0.6673	-0.667263	-0.667264
1.0	2.0174	2.01749079	2.01895
2.0	4.7290	4.72922695	4.72654

Table: 2.3. Values of $f''(0)$ for different values of α^* , λ_1 and R_d when $\epsilon = 0.2$ and $Pr = 0.5$.

α^*	λ_1	R_d	$-f''(0)$
0.0	0.5	0.3	0.5885
0.3			0.4704
0.5			0.3914
1.0			0.1905
0.3	0.0		0.8452
	0.4		0.5384
	1.0		0.1589
	1.5		0.1242
		0.0	0.5022
		0.5	0.4543
		0.8	0.4350
		1.0	0.4244

Table: 2.4. Values of $\theta'(0)$ for different values of α^* , λ_1 and R_d when $\epsilon = 0.2$ and $\text{Pr} = 0.5$.

α^*	λ_1	R_d	$-\theta'(0)$
0.0	0.5	0.3	0.3720
0.3			0.1969
0.5			0.0738
1.0			-0.2519
0.3	0.0		0.1183
	0.4		0.1856
	1.0		0.2407
	1.5		0.2722
		0.0	0.2452
		0.5	0.1763
		0.8	0.1538
		1.0	0.1426

2.4 Graphical results and discussion

To monitor the effects of several non-dimensional parameters, namely ratio of constant parameter ϵ , mixed convection parameter λ_1 , radiation parameter R_d , parameter α^* and Prandtl number Pr on the velocity profile f' and temperature field θ' , we have prepared the Figs. 2.2 – 2.11. The values of skin friction coefficient and local Nusselt number for several values of emerging parameters are also given in the Tables 2.2 – 2.4.

Fig. 2.2 gives the variations of ϵ on the velocity f' . It is seen that velocity f' is enlarged for ϵ . Fig. 2.3 represents the effects of ϵ on the temperature field θ . For large values of ϵ , thermal boundary layer becomes weaker. Figs. 2.4 and 2.5 show the distributions of velocity f' and temperature field

θ for different values of R_d . Obviously, the fluid velocity and temperature increase by increasing R_d . Influence of λ_1 on velocity f' and temperature θ is shown in the Figs. 2.6 and 2.7. We observed that the velocity f' increases by increasing λ_1 and temperature field θ decreases by increasing λ_1 . Figs. 2.8 and 2.9 indicate the effects of α^* on both f' and θ . We observe that both the velocity and temperature increase by increasing α^* . Figs. 2.10 and 2.11 are plotted just to see the variations of Pr on both the velocity and temperature fields. We noticed that initially both fluid velocity and temperature increase but after $\eta = 0.25$, these decrease.

2.5 Conclusions

The main observations are listed below.

- Dimensionless velocity f' is an increasing function of ϵ .
- The velocity and temperature has quite opposite effects for ϵ .
- Both f' and θ increase by increasing R_d and α^* while λ_1 gives the reverse effects.
- Skin friction coefficient tends to decrease when α^* , λ_1 and R_d are increased.
- Magnitude of heat transfer increases when λ_1 increases.

Chapter 3

Slip effect in stagnation-point flow with thermal radiation

This chapter describes the magnetohydrodynamic (MHD) stagnation point flow over a stretching sheet. The problems formulation involve the consideration of both the velocity and thermal slip conditions. Appropriate transformations reduce the governing partial differential equations into the ordinary differential equations. Series solutions and related convergence analysis are presented. Results for velocity and temperature are plotted and studied. Further, the values of skin friction coefficient and local Nusselt number are computed and analyzed.

3.1 Development of the problems

Here we consider steady, stagnation point flow of magnetohydrodynamic (MHD) viscous fluid towards a stretched surface at $y = 0$. An incompressible fluid occupies $y > 0$. The fluid is conducting only in the presence of an applied magnetic field B_0 . Induced magnetic field is not taken into account. This situation is plausible when magnetic Reynolds number is small. Applied magnetic field acts in the y -direction. The heat transfer is considered in view of Rosseland approximation

for thermal radiative effect. The resulting boundary layer equations are

$$\frac{\partial u}{\partial x} + \frac{\partial v}{\partial y} = 0, \quad (3.1)$$

$$u \frac{\partial u}{\partial x} + v \frac{\partial u}{\partial y} = U_\infty(x) \frac{dU_\infty}{dx} + \nu \frac{\partial^2 u}{\partial y^2} + \frac{\sigma B_0^2}{\rho} (U_\infty - u), \quad (3.2)$$

$$\left[u \frac{\partial T}{\partial x} + v \frac{\partial T}{\partial y} \right] = \frac{\partial}{\partial y} \left[\left(\rho c_p \frac{16\sigma^* T_\infty^3}{3K^*} + \alpha \right) \frac{\partial T}{\partial y} \right], \quad (3.3)$$

in which u and v are the velocity components along the x and y -axes respectively, U_∞ the stagnation point velocity in the inviscid free stream assumed to vary proportional to distance x , ν the kinematic viscosity, ρ the fluid density, α the thermal diffusivity, c_p the specific heat, T the fluid temperature, T_∞ the ambient temperature, σ^* the Stefan-Boltzmann constant and K^* the mean absorption coefficient. Eq. (3.3) has been developed after using the Rosseland approximation for radiative heat flux.

The boundary conditions corresponding to velocity and thermal slips are

$$u = U_w(x) + N\mu \frac{\partial u}{\partial y}, \quad v = 0, \quad T = T_w(x) + K \frac{\partial T}{\partial y} \text{ at } y = 0, \quad (3.4)$$

$$u \rightarrow U_\infty(x) = bx, \quad T \rightarrow T_\infty \text{ as } y \rightarrow \infty, \quad (3.5)$$

where the linear stretching surface and ambient velocities are taken as $U_w = ax$ and $U_\infty(x) = bx$, μ being the dynamic viscosity, the stretching surface temperature $T_w = T_\infty + cx^n$ (n is constant and $c > 0$) and N and K are the dimensional slip parameters.

Defining the appropriate transformations for stream function ψ and T are

$$\eta = \left(\frac{a}{\nu} \right)^{1/2} y, \quad f(\eta) = \frac{\psi}{(a\nu)^{1/2} x}, \quad \theta(\eta) = \frac{T - T_\infty}{T_w - T_\infty}, \quad (3.6)$$

in which η being the similarity variable. The stream function relation with velocity components satisfy

$$u = \frac{\partial \psi}{\partial y}, \quad v = -\frac{\partial \psi}{\partial x}. \quad (3.7)$$

Now the continuity Eq. (3.1) is identically satisfied and Eqs. (3.2) and (3.3) take the following form

$$f''' + ff'' - f'^2 + \epsilon^2 + M(\epsilon - f') = 0, \quad (3.8)$$

$$\left(1 + \frac{4}{3}R_d\right)\theta'' + \text{Pr}(f\theta' - nf'\theta) = 0. \quad (3.9)$$

Here prime denotes the derivative with respect to η , the Hartman number $M = \sigma B_0^2/\rho a$, the ratio of rate constants $\epsilon = b/a$, the radiation parameter $R_d = \frac{4\sigma^* T_\infty^3}{\alpha K^*}$, the Prandtl number $\text{Pr} = \alpha/\mu c_p$ and n the temperature index parameter. In addition, the reduced boundary conditions after applying transformations are

$$f(0) = 0, \quad f'(0) - S_f f''(0) = 1, \quad f'(\eta) \rightarrow \epsilon \quad \text{as } \eta \rightarrow \infty, \quad (3.10)$$

$$\theta(0) = 1 + S_T \theta'(0), \quad \theta(\eta) \rightarrow 0, \quad \text{as } \eta \rightarrow \infty. \quad (3.11)$$

The coefficient of skin friction and local Nusselt number are defined below

$$C_f = \frac{\tau_w}{\rho U^2/2}, \quad Nu_x = \frac{xq_w}{k(T_w - T_\infty)} \quad (3.12)$$

$$\tau_w = \mu \left(\frac{\partial u}{\partial y}\right)_{y=0}, \quad q_w = -k \left(\frac{\partial T}{\partial y}\right)_{y=0}, \quad (3.13)$$

$$\frac{1}{2}C_f \text{Re}_x^{1/2} = f''(0), \quad Nu_x / \text{Re}_x^{1/2} = -\theta'(0). \quad (3.14)$$

Here the physical quantities involve the wall shear stress τ_w , the heat flux q_w , the thermal conductivity k and the local Reynolds number $\text{Re}_x = U_w x/\nu$.

3.2 Series solutions

To utilize the set of base functions are classified as

$$\{\eta^k \exp(-n\eta), k \geq 0, n \geq 0\}, \quad (3.15)$$

we have

$$f(\eta) = a_{0,0}^0 + \sum_{n=0}^{\infty} \sum_{k=0}^{\infty} a_{m,n}^k \eta^k \exp(-n\eta), \quad (3.16)$$

$$\theta(\eta) = \sum_{n=0}^{\infty} \sum_{k=0}^{\infty} b_{m,n}^k \eta^k \exp(-n\eta), \quad (3.17)$$

where $a_{m,n}^k$ and $b_{m,n}^k$ are the constant coefficients.

Initial guesses and auxiliary linear operators are selected in the forms:

$$f_0 = \epsilon\eta + \left(\frac{1-\epsilon}{1+S_f}\right) (1 - \exp(-\eta)), \quad \theta_0 = \left(\frac{1}{1+S_\theta}\right) \exp(-\eta), \quad (3.18)$$

$$L_f[f(\eta)] = \frac{d^3 f}{d\eta^3} - \frac{df}{d\eta}, \quad L_\theta[\theta(\eta)] = \frac{d^2 \theta}{d\eta^2} - \theta. \quad (3.19)$$

These operators satisfy

$$L_f [C_1 + C_2 \exp(-\eta) + C_3 \exp(\eta)] = 0, \quad (3.20)$$

$$L_\theta [C_4 \exp(\eta) + C_5 \exp(-\eta)] = 0. \quad (3.21)$$

The corresponding problems at zeroth and m^{th} orders are

$$(1-p)L_f [\hat{f}(\eta; p) - f_0(\eta)] = p\hbar_f N_f [\hat{f}(\eta; p), \hat{\theta}(\eta; p)], \quad (3.22)$$

$$(1-p)L_\theta [\hat{\theta}(\eta; p) - \theta_0(\eta)] = p\hbar_\theta N_\theta [\hat{\theta}(\eta; p), \hat{f}(\eta; p)], \quad (3.23)$$

$$\hat{f}(0; p) = 0, \quad \frac{\partial \hat{f}}{\partial \eta}(0; p) = 1 + S_f \frac{\partial^2 \hat{f}}{\partial \eta^2}(0; p), \quad \hat{\theta}(0; p) = 1 + S_\theta \frac{\partial \hat{\theta}}{\partial \eta}(0; p), \quad \eta = 0, \quad (3.24)$$

$$\frac{\partial \tilde{f}}{\partial \eta}(\eta) = \epsilon, \quad \tilde{\theta}(\eta) \longrightarrow 0, \quad \text{when } \eta \longrightarrow \infty, \quad (3.25)$$

$$L_f [f_m(\eta) - \chi_m f_{m-1}(\eta)] = \hbar_f R_{f,m}(\eta), \quad (3.26)$$

$$L_\theta [\theta_m(\eta) - \chi_m \theta_{m-1}(\eta)] = \hbar_\theta R_{\theta,m}(\eta), \quad (3.27)$$

$$f_m(0) = 0, \quad f'_m(0) = 0, \quad \theta_m(0) = 0, \quad (3.28)$$

$$f'_m(\eta) = 0, \quad \theta_m(\eta) = 0, \quad \text{when } \eta \longrightarrow \infty, \quad (3.29)$$

in which \hbar_f and \hbar_θ are the non-zero auxiliary parameters, $p \in [0, 1]$ the embedding parameter and the resulting nonlinear operators of the problems are

$$N_f[\tilde{f}(\eta; p)] = \frac{\partial^3 \tilde{f}}{\partial \eta^3} + \tilde{f} \frac{\partial^2 \tilde{f}}{\partial \eta^2} - \left(\frac{\partial \tilde{f}}{\partial \eta} \right)^2 + M \left(\epsilon - \frac{\partial \tilde{f}}{\partial \eta} \right) + \epsilon^2, \quad (3.30)$$

$$N_\theta[\tilde{\theta}(\eta; p)] = \left(1 + \frac{4}{3} R_d \right) \frac{\partial^2 \tilde{\theta}}{\partial \eta^2} + \text{Pr} \left(\tilde{f} \frac{\partial \tilde{\theta}}{\partial \eta} - n \frac{\partial \tilde{f}}{\partial \eta} \tilde{\theta} \right), \quad (3.31)$$

$$R_{f,m}(\eta) = \frac{\partial^3 f_{m-1}}{\partial \eta^3} + \sum_{i=0}^{m-1} f_i \frac{\partial^2 f_{m-i-1}}{\partial \eta^2} - \sum_{i=0}^{m-1} \frac{\partial f_{m-i-1}}{\partial \eta} \frac{\partial f_i}{\partial \eta} - M \frac{\partial f_{m-1}}{\partial \eta} + [\epsilon^2 + M\epsilon] (1 - \chi_m), \quad (3.32)$$

$$R_{\theta,m}(\eta) = \left(1 + \frac{4}{3} R_d \right) \frac{\partial^2 \theta_{m-1}}{\partial \eta^2} + \text{Pr} \sum_{i=0}^{m-1} \left(f_{m-i-1} \frac{\partial \theta_i}{\partial \eta} - n \frac{\partial f_{m-1-i}}{\partial \eta} \theta_i \right). \quad (3.33)$$

Through Taylor's series

$$f(\eta; p) = f_0(\eta) + \sum_{m=0}^{\infty} f_m(\eta) p^m; \quad f_m(\eta) = \frac{1}{m!} \frac{\partial^m \tilde{f}(\eta, p)}{\partial p^m} \Big|_{p=0}, \quad (3.34)$$

$$\theta(\eta; p) = \theta_0(\eta) + \sum_{m=0}^{\infty} \theta_m(\eta) p^m; \quad \theta_m(\eta) = \frac{1}{m!} \frac{\partial^m \tilde{\theta}(\eta, p)}{\partial p^m} \Big|_{p=0}. \quad (3.35)$$

with

$$\hat{f}(\eta, 0) = f_0(\eta), \quad \hat{\theta}(\eta, 0) = \theta_0(\eta), \quad (3.36)$$

$$\hat{f}(\eta, 1) = f(\eta), \quad \hat{\theta}(\eta, 1) = \theta(\eta), \quad (3.37)$$

where the embedding parameter p increases from 0 to 1 then $\hat{f}(\eta, p)$ and $\hat{\theta}(\eta, p)$ are taken into account. We get the initial guesses $f_0(\eta)$ and $\theta_0(\eta)$ by letting $p = 0$ and final solution $f(\eta)$ and $\theta(\eta)$ by letting $p = 1$ respectively. The values of auxiliary parameters h_f and h_θ are taken in such a manner that the Taylor's series of $\hat{f}(\eta, p)$ and $\hat{\theta}(\eta, p)$ converge at $p = 1$ i.e.

$$f(\eta) = f_0(\eta) + \sum_{m=1}^{\infty} f_m(\eta), \quad \theta(\eta) = \theta_0(\eta) + \sum_{m=0}^{\infty} \theta_m(\eta). \quad (3.38)$$

The general solutions can be expressed as

$$f_m(\eta) = f_m^*(\eta) + C_1 + C_2 \exp(\eta) + C_3 \exp(-\eta), \quad (3.39)$$

$$\theta_m(\eta) = \theta_m^*(\eta) + C_4 \exp(\eta) + C_5 \exp(-\eta), \quad (3.40)$$

where the involvement of particular solutions f_m^* and θ_m^* can be easily solved by Mathematica software up to the order $m = 1, 2, 3, \dots$

3.3 Convergence of the homotopy solutions

Obviously, Eq. (3.35) includes the auxiliary parameter h_f and h_θ . These parameters are very helpful and provide a simple way in order to find the convergence and rate of obtained series solutions. The h -curves for velocity and temperature fields with and without velocity and thermal slip are plotted in Figs. 3.1 (a and b). These Figs. show that the 20th order of approximations are enough for good agreement regarding convergence. To guarantee convergence, we take the values of h_f and h_θ are

equal to -1 . The convergence of $f''(0)$ and $-\theta'(0)$ by varying the value of Hartman number M (while other parameters are fixed) is carried out in Table 3.1. From this table, it is observed that convergence of series solutions is sufficient at 20^{th} order of approximations.

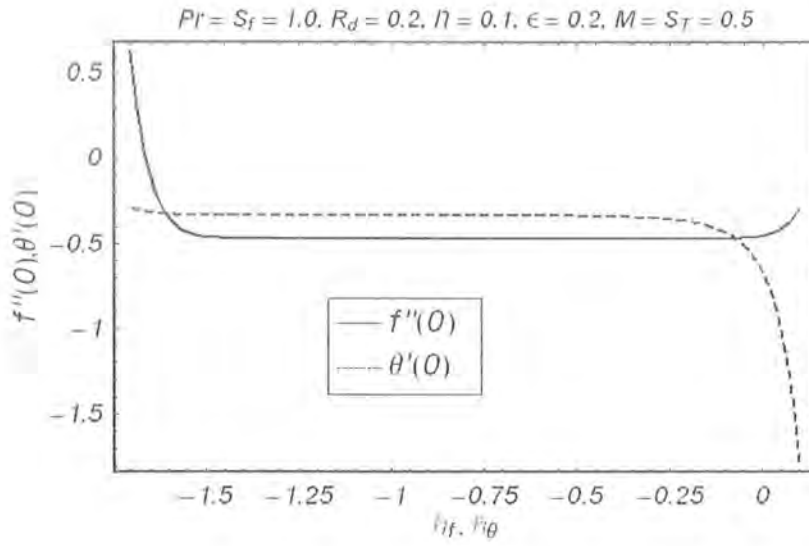


Fig. 3.1 (a) h - curves for 20th order of approximations.

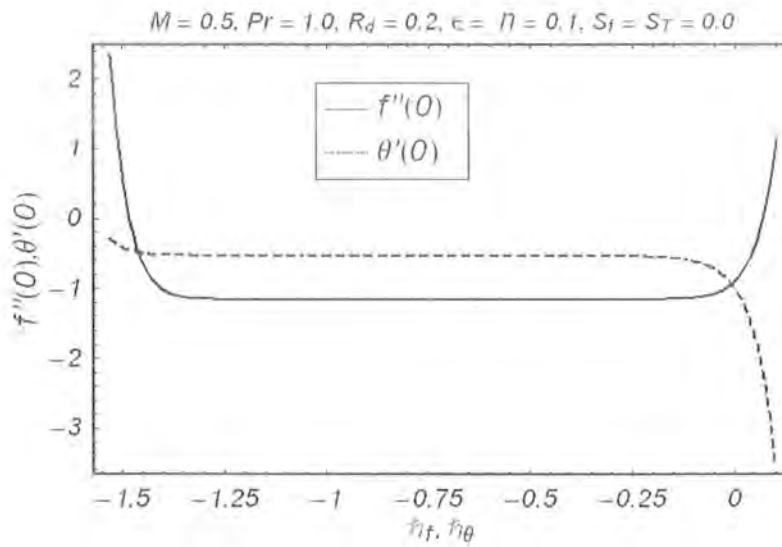


Fig. 3.1 (b) h - curves for 20th order of approximations.

Table: 3.1. Convergence of series solutions for different order of approximations.

Order of approximation	$M = 0.0$		$M = 0.3$		$M = 0.5$	
	$-f''(0)$	$-\theta'(0)$	$-f''(0)$	$-\theta'(0)$	$-f''(0)$	$-\theta'(0)$
1	0.41625	0.438519	0.450000	0.438519	0.4725	0.438519
5	0.416549	0.367609	0.450588	0.354157	0.469159	0.346999
10	0.416546	0.360951	0.450587	0.343306	0.469133	0.333959
15	0.416547	0.360509	0.450587	0.342068	0.469133	0.332191
20	0.416547	0.360479	0.450587	0.341918	0.469133	0.331931
25	0.416547	0.360477	0.450587	0.341899	0.469133	0.331893
30	0.416547	0.360477	0.450587	0.341897	0.469133	0.331887
35	0.416547	0.360477	0.450587	0.341897	0.469133	0.331887
40	0.416547	0.360477	0.450587	0.341897	0.469133	0.331887

Table: 3.2. Values of skin-friction coefficient $-f''(0)$
for the parameters M , S_f and ϵ .

M	S_f	ϵ	$-f''(0)$
0.0	5.0	0.1	0.139074
0.5			0.148789
1.0			0.153834
1.1			0.154577
0.5	0.0	0.1	1.158340
	2.0		0.302388
	10		0.081151
	20		0.042617
	30		0.028912
	50		0.017599
	100		0.008898
0.2	50	0.02	0.018893
		0.04	0.018557
		0.1	0.017494
		0.2	0.013720

Table: 3.3. Comparison of skin-friction coefficient $-f''(0)$
for various values of S_f when $M = \epsilon = 0$.

	[26]	HAM	[26]	HAM
S_f	$f'(0)$		$f''(0)$	
0.0	1.0000	1.000000	1.0000	1.000000
0.1	0.9128	0.912792	0.8721	0.872082
0.2	0.8447	0.844725	0.7764	0.776377
0.5	0.7044	0.704402	0.5912	0.591195
1.0	0.5698	0.569840	0.4302	0.430162
2.0	0.4320	0.432041	0.2840	0.283981
5.0	0.2758	0.275799	0.1448	0.144840
10	0.1876	0.187583	0.0812	0.081242
20	0.1242	0.124203	0.0438	0.043789
50	0.0702	0.070590	0.0186	0.018588
100	0.0450	0.045080	0.0095	0.009557

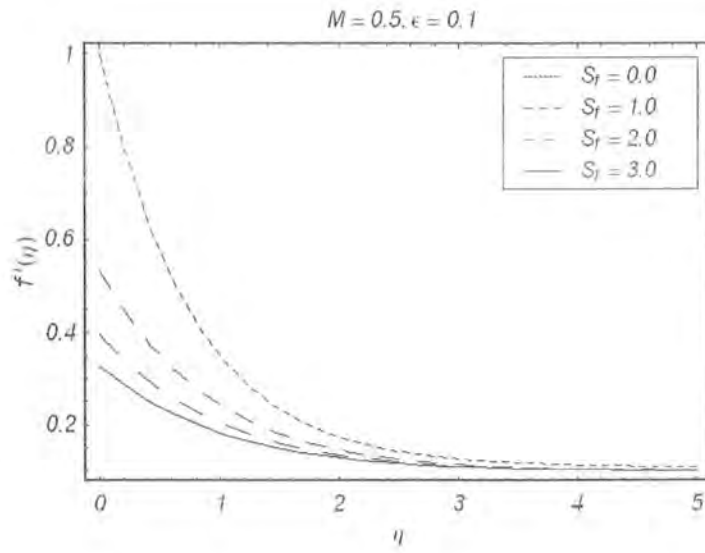


Fig. 3.2. Effect of S_f on velocity profile f' .

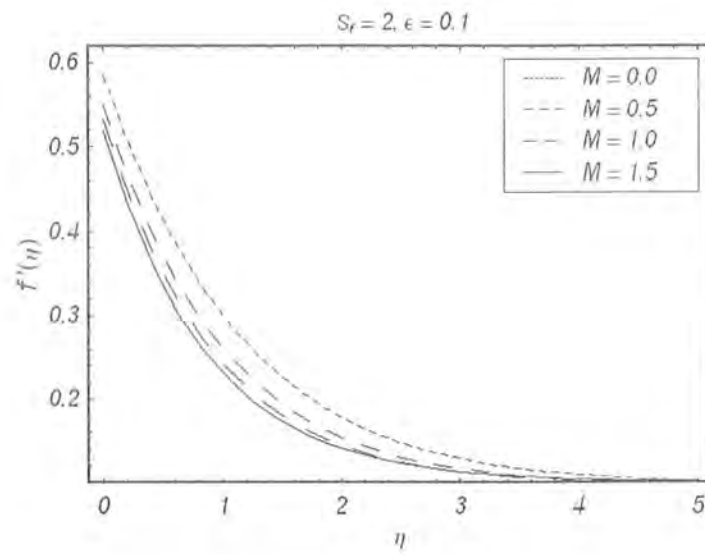


Fig. 3.3. Effect of M on velocity profile f' .

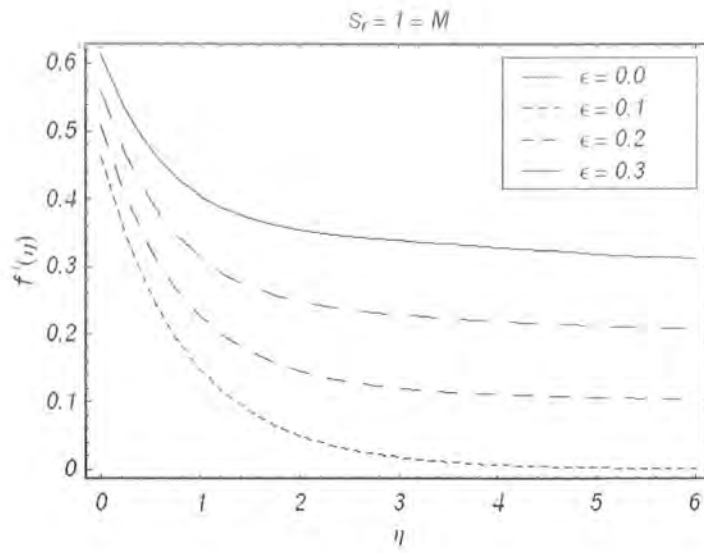


Fig. 3.4. Effect of ϵ on velocity profile f' .

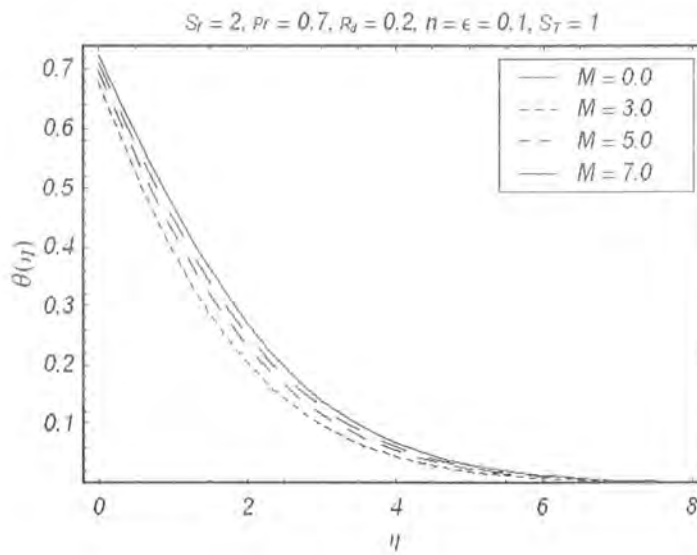


Fig. 3.5. Effect of M on temperature profile θ .

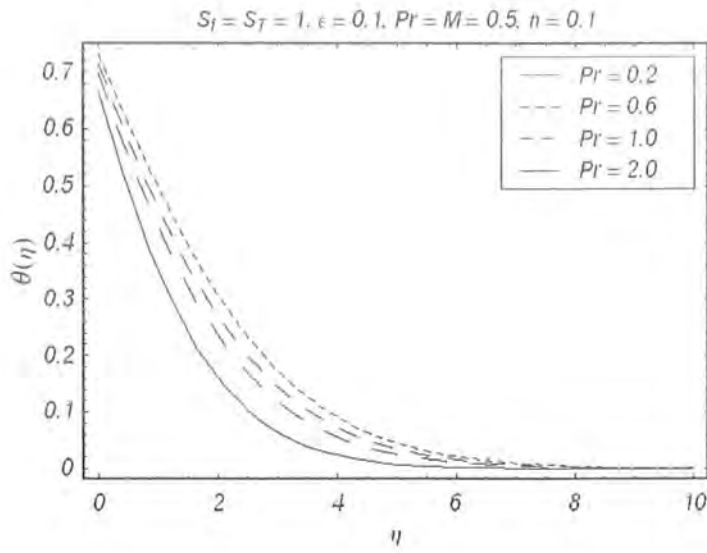


Fig. 3.6. Effect of Pr on temperature profile θ .

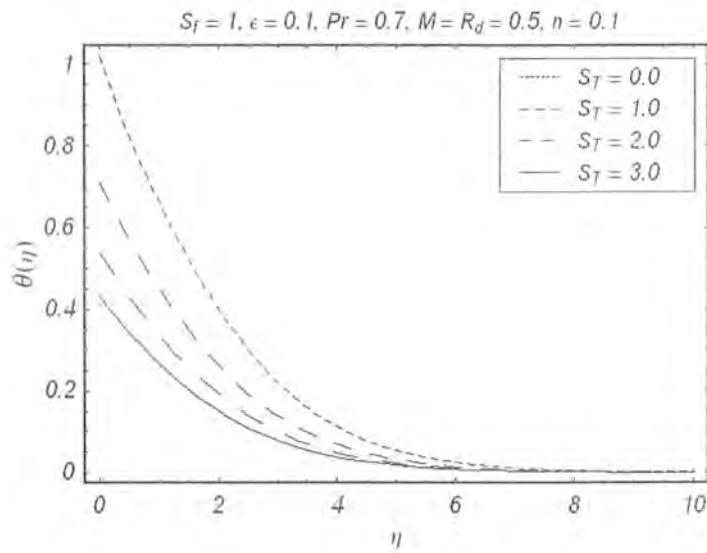


Fig. 3.7. Effect of S_T on temperature profile θ .

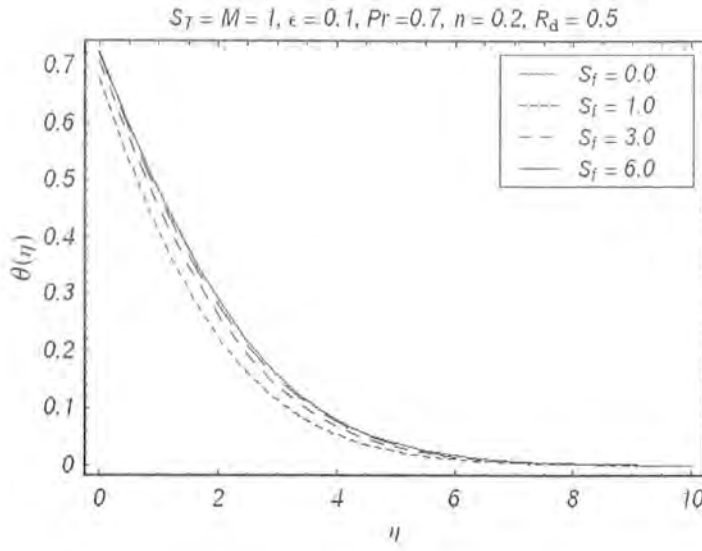


Fig. 3.8. Effect of S_f on temperature profile θ .

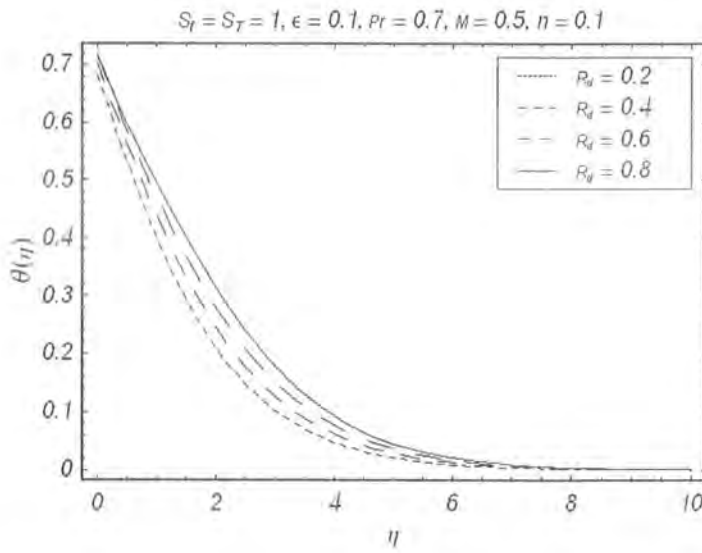


Fig. 3.9. Effect of R_d on temperature profile θ .

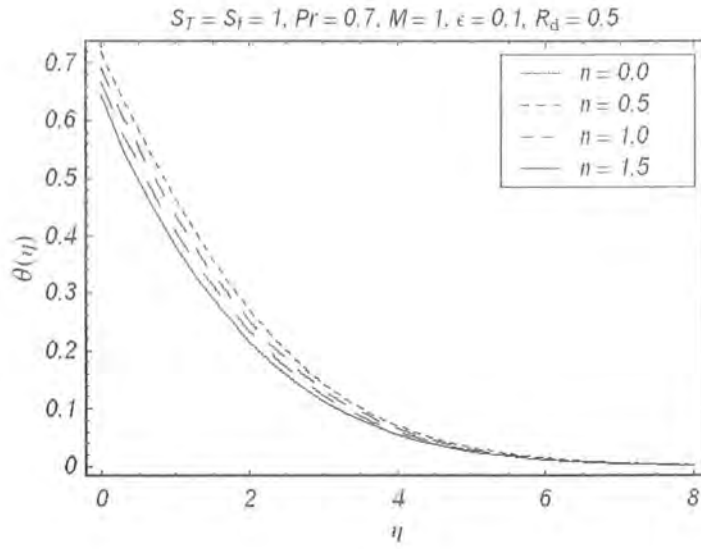


Fig. 3.10. Effect of n on temperature profile θ .

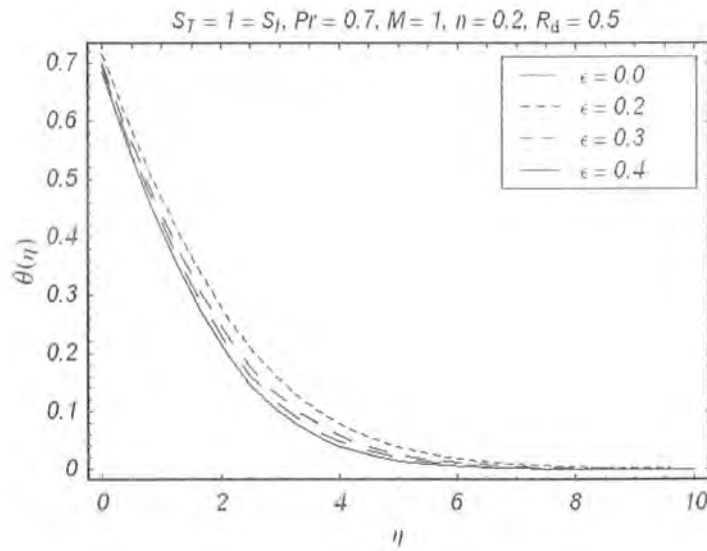


Fig. 3.11. Effect of ϵ on temperature profile θ .

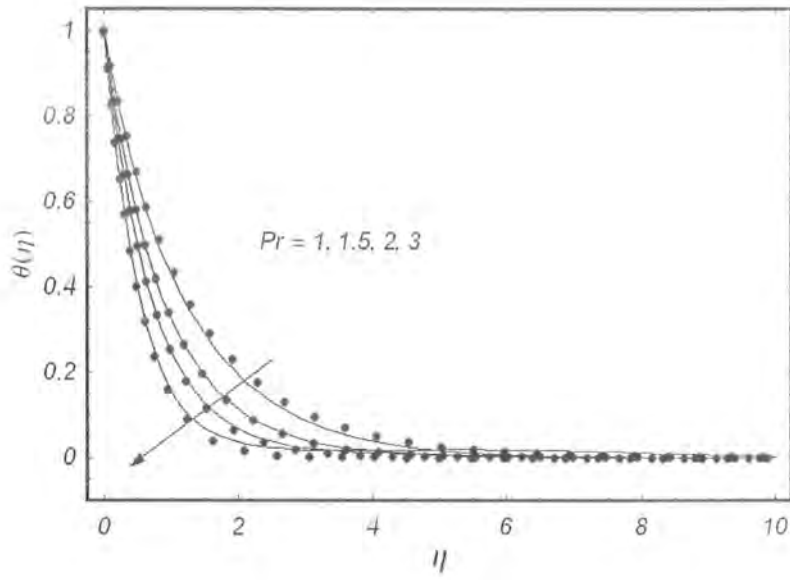


Fig. 3.12. Effect of Pr on temperature profile θ .

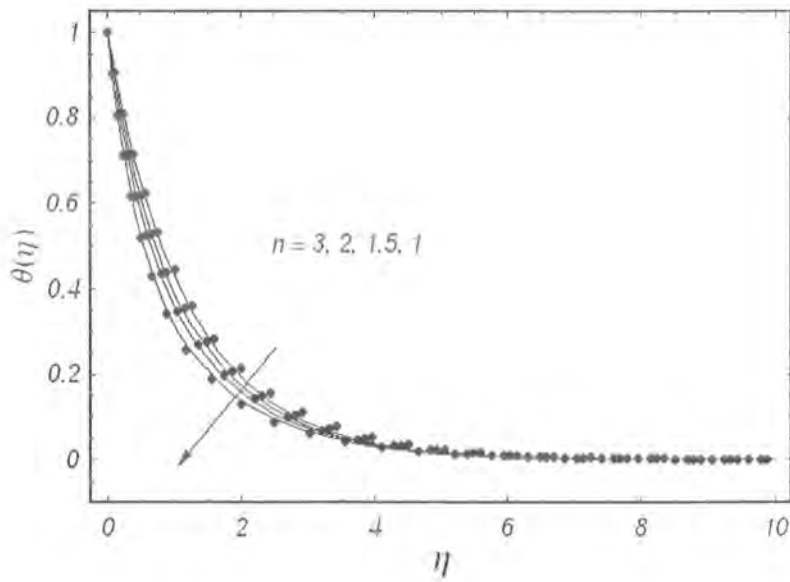


Fig. 3.13. Effect of n on temperature profile θ .

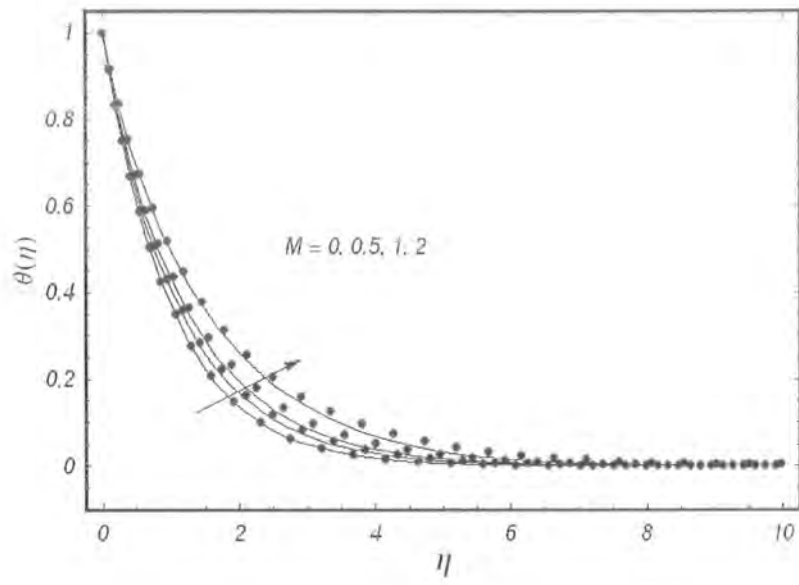


Fig. 3.14. Effect of M on temperature profile θ .

Table: 3.4. Values of $-\theta'(0)$ for parameters M , R_d and Pr when $S_f = S_T = 0$ and $\epsilon = n = 0.1$.

M	R_d	Pr	$-\theta'(0)$
0.2	0.2	1.0	0.530639
0.4			0.535615
0.6			0.525914
0.5	0.1		1.15834
	0.3		0.49661
	0.5		0.44208
0.2	0.2	0.6	0.3894
		0.72	0.43994
		1.1	0.581372
		1.2	0.615003
		1.3	0.64745

Table: 3.5. Values of skin-friction coefficient $-f''(0)$ and $-\theta'(0)$
when $\text{Pr} = 1$, $R_d = 0.2$, $S_T = 0.5$ and $n = 0.1$.

M	ϵ	S_f	$-f''(0)$	$-\theta'(0)$
0.0	0.1	2.0	0.274326	0.329742
0.3			0.292911	0.309954
0.5			0.302388	0.30001
0.7			0.310268	0.29191
0.1	0.01	1.0	0.445660	0.32610
	0.02		0.444257	0.32929
	0.1		0.428882	0.353734
	0.2		0.401170	0.038190
0.5	0.1	0.0	1.158340	0.419372
		5.0	0.148789	0.262772
		7.0	0.111513	0.2521
		10	0.081151	0.2427
		15	0.055872	0.23429

Table: 3.6. Comparison of local Nusselt number $-\theta'(0)$ for some values of M , Pr and n

when $R_d = \epsilon = 0 = S_f = S_T$.

M	Pr	n	HAM[25]	$-\theta'(0)$
0.0	2.0	0.1	0.981991	0.981707
0.3			0.950257	0.950258
0.5			0.931430	0.931430
0.8			0.905665	0.905665
1.0			0.889917	0.889855
0.5	1.0	0.2	0.625690	0.625689
	1.1		0.669087	0.669087
	1.3		0.750773	0.750773
	1.5		0.82675	0.82675
	2.0		0.997713	0.997713
0.5	1.0	0.1	0.58183	0.58183
		0.3	0.66843	0.66843
		0.5	0.750784	0.750782
		1.0	0.94090	0.94089
		3.0	1.55041	1.55041
		5.0	2.02104	2.02104

3.4 Discussion

In this section we look for the variations of the slip parameter S_f , the Hartman number M , the ratio parameter ϵ , thermal slip parameter S_T , Prandtl number Pr and radiation parameter R_d on the velocity and temperature fields. This can be achieved by plotting the Figs. 3.2 – 3.14. Fig. 3.2 presents the effect of S_f on the velocity f' . It is observed from this Fig. that boundary layer

thickness decreases by increasing S_f . Fig. 3.3 displays the velocity profile for various values of Hartman number M . The qualitative effects of M are found similar to that of S_f . Fig. 3.4 gives the variation of ϵ on the velocity component f' . The velocity component f' is an increasing function of ϵ . It is found that θ increases when M increases (Fig. 3.5). The variation of Prandtl number Pr is sketched in Fig. 3.6. As expected, it is found that θ decreases when Pr is increased. Fig. 3.7 gives the variation of S_f on the temperature field. It is observed from this Fig. that thermal boundary layer thickness decreases by increasing S_f . From Fig. 3.8 we have seen that θ increases by increasing S_f . Fig. 3.9 gives the effect of radiation parameter R_d on the temperature field. It has opposite result when compared with Fig. 3.6. Fig. 3.10 examines the effect of n parameter on the temperature profile. An increase in this parameter decreases the temperature. Fig. 3.11 clearly indicates that an increase in parameter ϵ decreases the temperature. To authenticate our HAM solution, a comparison is given in the Figs. 3.12 – 3.14 with already existing result in the literature. These solutions are in excellent agreement.

Table 3.1 shows that 15th order of approximations are sufficient for the convergent series solution. From Table 3.2 it is noticed that the magnitude of skin-friction coefficient increases for large values of M while it decreases by increasing S_f and ϵ . Table 3.3 indicates that HAM solution has a good agreement with the existing exact solution [26]. Tables (3.4 – 3.6) are prepared for the variations of skin-friction coefficient and local Nusselt numbers and the comparison with the work in ref. [25]. It is obvious from these tables that magnitude of $-\theta'(0)$ decreases by increasing M and n .

Chapter 4

MHD mixed convection flow near a stagnation-point towards a stretching sheet

This chapter addresses the magnetohydrodynamic (MHD) stagnation point flow near a stretching surface. The radiative effects which are high in temperature regime are also accounted. Both assisting and opposing flow cases are examined. The velocity and thermal slips are considered. Nonlinear mathematical analysis is performed using homotopy analysis method. Convergence of velocity and temperature are explicitly analyzed. The skin friction coefficient and local Nusselt number are examined in detail.

4.1 Mathematical description

We consider the MHD mixed convection stagnation-point flow of viscous fluid over stretching sheet. Electrically conducting fluid under uniform magnetic field B_0 has been taken. Here uniform magnetic field acts in the y -direction. Induced magnetic field is neglected for small magnetic Reynolds number. The electric field is taken zero. Further, the gravitational force is taken parallel to the

x -axis. Velocities of stretching surface and free stream are denoted by U_w and U_∞ . Mathematical expressions governing the present flow situation are given by

$$\frac{\partial u}{\partial x} + \frac{\partial v}{\partial y} = 0, \quad (4.1)$$

$$u \frac{\partial u}{\partial x} + v \frac{\partial u}{\partial y} = U_\infty(x) \frac{dU_\infty}{dx} + \nu \frac{\partial^2 u}{\partial y^2} + \frac{\sigma B_0^2}{\rho} (U_\infty - u) \pm g \beta_T (T - T_\infty), \quad (4.2)$$

$$\rho c_p \left[u \frac{\partial T}{\partial x} + v \frac{\partial T}{\partial y} \right] = \frac{\partial}{\partial y} \left[\left(\frac{16\sigma^* T_\infty^3}{3K^*} + \alpha \right) \frac{\partial T}{\partial y} \right], \quad (4.3)$$

$$u = U_w(x) + N\mu \frac{\partial u}{\partial y}, \quad v = v_w, \quad T = T_w(x) + K \frac{\partial T}{\partial y} \text{ at } y = 0, \quad (4.4)$$

$$u \longrightarrow U_\infty(x), \quad T \longrightarrow T_\infty \text{ as } y \longrightarrow \infty. \quad (4.5)$$

In above equations the velocity component u is along the x -axis and v along y -axis, g the gravitational acceleration, ν the kinematic viscosity, ρ the fluid density, β_T the thermal expansion coefficient, α the thermal diffusivity, c_p the specific heat, T the fluid temperature, T_∞ the ambient fluid temperature, σ^* the Stefan-Boltzmann constant and K^* the mean absorption coefficient, the surface temperature $T_w(x) = T_\infty(x) + cx^n$ with $T_w > T_\infty$, μ the dynamic viscosity and N and K the dimensional velocity and thermal slip parameters. Further the \pm signs in Eq. (4.2) correspond to the assisting and opposing flow. Defining

$$\eta = \left(\frac{a}{\nu} \right)^{1/2} y, \quad f(\eta) = \frac{\psi}{(a\nu)^{1/2} x}, \quad \theta(\eta) = \frac{T - T_\infty}{T_w - T_\infty}. \quad (4.6)$$

One finds that Eq. (4.1) is automatically satisfied while Eqs.(4.3) and (4.4) yield

$$u = \frac{\partial \psi}{\partial y}, \quad v = -\frac{\partial \psi}{\partial x}, \quad (4.7)$$

$$f''' + ff'' - f'^2 + \epsilon^2 + M(\epsilon - f') + \lambda_1 \theta = 0, \quad (4.8)$$

$$\left(1 + \frac{4}{3}R_d\right)\theta'' + \text{Pr}(f\theta' - n f'\theta) = 0. \quad (4.9)$$

The pertinent parameters which occur in Eqs. (4.8) and (4.9) are named as the Hartman number $M (= \sigma B_0^2/\rho a)$, the ratio of rate constants $\epsilon = b/a$, $\lambda_1 = Gr_x/\text{Re}_x^2$ the buoyancy or mixed convection parameter, $Gr_x = g\beta(T - T_\infty)x^3/\nu^2$ the local Grashof number, $\text{Re}_x = U_w x/\nu$, the local Reynold number, the radiation parameter $R_d = \frac{4\sigma^* T_\infty^3}{\alpha K^*}$, the Prandtl number $\text{Pr} = \alpha/\mu c_p$ and n the temperature index parameter. Now the dimensionless boundary conditions with velocity and thermal slips are

$$f(0) = S_0, \quad f'(0) - S_f f''(0) = 1, \quad f'(\eta) \rightarrow \epsilon \quad \text{as } \eta \rightarrow \infty, \quad (4.10)$$

$$\theta(0) = 1 + S_T \theta'(0), \quad \theta(\eta) \rightarrow 0, \quad \text{as } \eta \rightarrow \infty, \quad (4.11)$$

in which $S_0 = -v_w/(c\nu)^{1/2}$ and $S_0 > 0$ corresponds to suction case whereas $S_0 < 0$ yields blowing.

The skin friction coefficient and local Nusselt number are

$$C_f = \frac{\tau_w}{\rho U^2/2}, \quad Nu_x = \frac{xq_w}{k(T_w - T_\infty)}, \quad (4.12)$$

$$\tau_w = \mu \left(\frac{\partial u}{\partial y}\right)_{y=0}, \quad q_w = -k \left(\frac{\partial T}{\partial y}\right)_{y=0}. \quad (4.13)$$

Substitution of Eq. (4.12) into Eq. (4.13) yields

$$\frac{1}{2}C_f \text{Re}_x^{1/2} = f''(0), \quad Nu_x/\text{Re}_x^{1/2} = -\theta'(0), \quad (4.14)$$

4.2 Homotopy analysis solutions

The solutions defined by set of base functions

$$\{\eta^k \exp(-n\eta), k \geq 0, n \geq 0\}, \quad (4.15)$$

are given by

$$f(\eta) = a_{0,0}^0 + \sum_{n=0}^{\infty} \sum_{k=0}^{\infty} a_{m,n}^k \eta^k \exp(-n\eta), \quad (4.16)$$

$$\theta(\eta) = \sum_{n=0}^{\infty} \sum_{k=0}^{\infty} b_{m,n}^k \eta^k \exp(-n\eta), \quad (4.17)$$

where $a_{m,n}^k$ and $b_{m,n}^k$ are the coefficients. The following initial guesses and auxiliary linear operators are chosen for the preferred solutions

$$f_0 = S_0 + \epsilon\eta + \left(\frac{1-\epsilon}{1+S_f}\right)(1 - \exp(-\eta)), \quad \theta_0 = \left(\frac{1}{1+S_T}\right)\exp(-\eta). \quad (4.18)$$

$$L_f[f(\eta)] = \frac{d^3 f}{d\eta^3} - \frac{df}{d\eta}, \quad L_\theta[\theta(\eta)] = \frac{d^2 \theta}{d\eta^2} - \theta. \quad (4.19)$$

The auxiliary linear operators defined in above equation possess the properties given below

$$L_f [C_1 + C_2 \exp(-\eta) + C_3 \exp(\eta)] = 0, \quad (4.20)$$

$$L_\theta [C_4 \exp(\eta) + C_5 \exp(-\eta)] = 0, \quad (4.21)$$

where $C_i (i = 1 - 5)$ are the integral constants. Moreover, the problems at zeroth and m^{th} orders are

$$(1-p)L_f \left(\hat{f}(\eta; p) - f_0(\eta) \right) = p\hbar_f N_f \left(\hat{f}(\eta; p), \hat{\theta}(\eta; p) \right), \quad (4.22)$$

$$(1-p)L_\theta \left(\hat{\theta}(\eta; p) - \theta_0(\eta) \right) = p\hbar_\theta N_\theta \left(\hat{\theta}(\eta; p), \hat{f}(\eta; p) \right), \quad (4.23)$$

$$\hat{f}(0; p) = S_0, \quad \frac{\partial \hat{f}}{\partial \eta}(0; p) = 1 + S_f \frac{\partial^2 \hat{f}}{\partial \eta^2}(0; p), \quad \hat{\theta}(0; p) = 1 + S_T \frac{\partial \hat{\theta}}{\partial \eta}(0; p), \quad \eta = 0, \quad (4.24)$$

$$\frac{\partial \tilde{f}}{\partial \eta}(\eta) = \epsilon, \quad \tilde{\theta}(\eta) \longrightarrow 0, \quad \text{when} \quad \eta \longrightarrow \infty, \quad (4.25)$$

$$L_f [f_m(\eta) - \chi_m f_{m-1}(\eta)] = h_f R_{f,m}(\eta), \quad (4.26)$$

$$L_\theta [\theta_m(\eta) - \chi_m \theta_{m-1}(\eta)] = h_\theta R_{\theta,m}(\eta), \quad (4.27)$$

$$f_m(0) = 0, \quad f'_m(0) = 0, \quad \theta_m(0) = 0, \quad (4.28)$$

$$f'_m(\eta) = 0, \quad \theta_m(\eta) = 0, \quad \text{when} \quad \eta \longrightarrow \infty, \quad (4.29)$$

where h_f , h_θ and $p \in [0, 1]$ are the non-zero auxiliary and embedding parameters. The expression of nonlinear operators are

$$N_f[\tilde{f}(\eta, p)] = \frac{\partial^3 f}{\partial \eta^3} + f \frac{\partial^2 f}{\partial \eta^2} - \left(\frac{\partial f}{\partial \eta} \right)^2 + M \left(\epsilon - \frac{\partial f}{\partial \eta} \right) = \epsilon^2 + \lambda_1 \theta, \quad (4.30)$$

$$N_\theta[\tilde{\theta}(\eta, p)] = \left(1 + \frac{4}{3} R_d \right) \frac{\partial^2 \theta}{\partial \eta^2} + \text{Pr} \left(f \frac{\partial \theta}{\partial \eta} - n \frac{\partial f}{\partial \eta} \theta \right), \quad (4.31)$$

$$\begin{aligned} R_{f,m}(\eta) &= \frac{\partial^3 f_{m-1}}{\partial \eta^3} + \sum_{i=0}^{m-1} f_i \frac{\partial^2 f_{m-i-1}}{\partial \eta^2} - \sum_{i=0}^{m-1} \frac{\partial f_{m-i-1}}{\partial \eta} \frac{\partial f_i}{\partial \eta} \\ &\quad - M \frac{\partial f_{m-1}}{\partial \eta} + \lambda_1 \theta + (\epsilon^2 + M\epsilon) (1 - \chi_m), \end{aligned} \quad (4.32)$$

$$R_{\theta,m}(\eta) = \left(1 + \frac{4}{3} R_d \right) \frac{\partial^2 \theta_{m-1}}{\partial \eta^2} + \text{Pr} \sum_{i=0}^{m-1} \left(f_{m-i-1} \frac{\partial \theta_i}{\partial \eta} - n \frac{\partial f_{m-1-i}}{\partial \eta} \theta_i \right). \quad (4.33)$$

The velocity and temperature fields in view of Taylor's series are

$$\tilde{f}(\eta; p) = f_0(\eta) + \sum_{m=0}^{\infty} f_m(\eta) p^m, \quad f_m(\eta) = \frac{1}{m!} \frac{\partial^m \tilde{f}(\eta, p)}{\partial p^m} \Big|_{p=0}, \quad (4.34)$$

$$\tilde{\theta}(\eta; p) = \theta_0(\eta) + \sum_{m=0}^{\infty} \theta_m(\eta) p^m, \quad \theta_m(\eta) = \frac{1}{m!} \frac{\partial^m \tilde{\theta}(\eta, p)}{\partial p^m} \Big|_{p=0}. \quad (4.35)$$

It is obvious that

$$\hat{f}(\eta, 0) = f_0(\eta), \quad \hat{\theta}(\eta, 0) = \theta_0(\eta), \quad (4.36)$$

$$\hat{f}(\eta, 1) = f(\eta), \quad \hat{\theta}(\eta, 1) = \theta(\eta). \quad (4.37)$$

At $p = 1$ both series converge by assuming the suitable values of auxiliary parameters h_f and h_θ .

Thus

$$f(\eta) = f_0(\eta) + \sum_{m=1}^{\infty} f_m(\eta), \quad \theta(\eta) = \theta_0(\eta) + \sum_{m=0}^{\infty} \theta_m(\eta), \quad (4.38)$$

and the general solutions $f_m(\eta)$ and $\theta_m(\eta)$ are

$$f_m(\eta) = f_m^*(\eta) + C_1 + C_2 \exp(\eta) + C_3 \exp(-\eta), \quad (4.39)$$

$$\theta_m(\eta) = \theta_m^*(\eta) + C_4 \exp(\eta) + C_5 \exp(-\eta). \quad (4.40)$$

Here the particular solutions are denoted by f_m^* and θ_m^* .

4.3 Homotopy solutions

It is clear that the series solutions enclose the auxiliary parameters h_f and h_θ which helps us to manage the convergence region and adjust the rate of approximate series solutions. The h_f and h_θ -curves are plotted in Fig. 4.1 at 18^{th} order of approximations. From this Fig. we see that $-1.26 \leq h_f \leq -0.18$ and $-1.4 \leq h_\theta \leq -0.20$ are the acceptable values of h_f and h_θ . The analysis of series solutions converge by putting the value of h_f and h_θ equal to -1 . The effects of Hartman number M on the magnitude of $f''(0)$ and $\theta(0)$ are computed in Table 4.1.

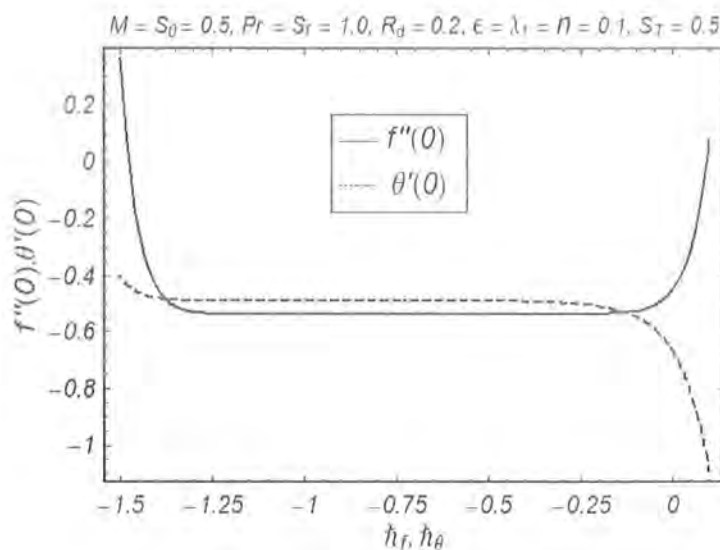


Fig. 4.1 h - curves for 18^{th} order of approximations.

Table: 4.1. Convergence of series solutions for different order of approximations.

Order of approximation	$M = 0.0$		$M = 0.4$		$M = 0.6$	
	$-f''(0)$	$-\theta'(0)$	$-f''(0)$	$-\theta'(0)$	$-f''(0)$	$-\theta'(0)$
1	0.5620830	0.660741	0.607083	0.660741	0.629583	0.660741
5	0.568342	0.653916	0.588574	0.6495	0.598247	0.647772
10	0.568572	0.653994	0.58817	0.649325	0.596059	0.647423
15	0.568581	0.653992	0.588173	0.649318	0.596324	0.64745
20	0.568582	0.653992	0.588171	0.649318	0.596281	0.647447
25	0.56858	0.653993	0.588171	0.649319	0.59629	0.647447
30	0.568584	0.653998	0.588173	0.64932	0.596284	0.647446
35	0.568584	0.653998	0.588188	0.649325	0.596284	0.647447

Table: 4.2. Values of skin-friction coefficient $-f''(0)$
for the parameters M , S_f and ϵ .

M	S_f	ϵ	$-f''(0)$
0.0	5	0.1	0.139074
0.5			0.148789
1.0			0.153834
1.1			0.154577
0.5	0.0	0.1	1.158340
	2.0		0.302388
	10		0.081151
	20		0.042617
	30		0.028912
	50		0.017599
	100		0.008898
0.2	50	0.02	0.0188931
		0.04	0.0185569
		0.1	0.0174941
		0.2	0.01372

Table: 4.3. Comparison of skin-friction coefficient $-f''(0)$
for diverse values of S_f when $M = S_0 = \lambda_1 = \epsilon = 0$.

S_f	[19]	HAM	[19]	HAM
	$f'(0)$		$f''(0)$	
0.0	1.0000	1.000000	1.0000	1.000000
0.1	0.9128	0.912792	0.8721	0.872082
0.2	0.8447	0.844725	0.7764	0.776377
0.5	0.7044	0.704402	0.5912	0.591195
1.0	0.5698	0.569840	0.4302	0.430162
2.0	0.4320	0.432041	0.2840	0.283981
5.0	0.2758	0.275799	0.1448	0.144840
10	0.1876	0.187583	0.0812	0.081242
20	0.1242	0.124203	0.0438	0.043789
50	0.0702	0.07059	0.0186	0.018588
100	0.0450	0.04508	0.0095	0.009557

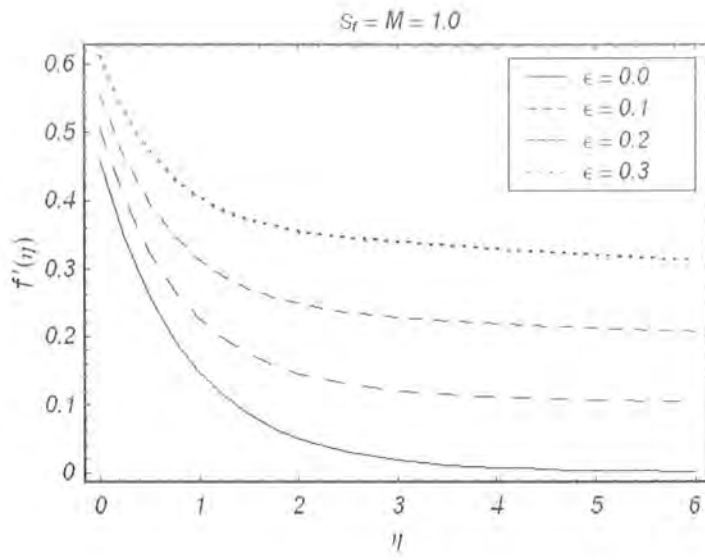


Fig. 4.2. Influence of ϵ on velocity profile f' .

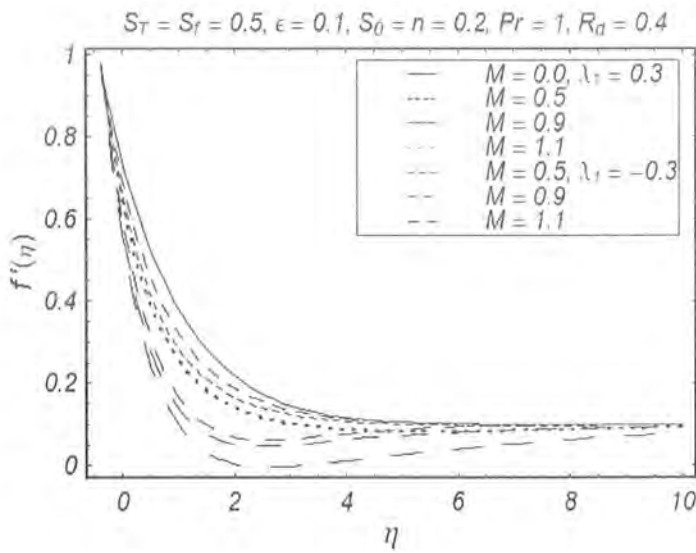


Fig. 4.3. Influence of M on velocity profile f' .

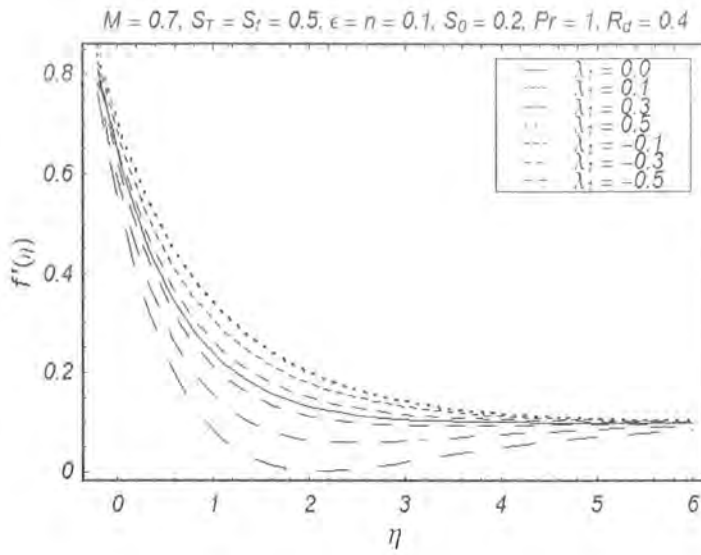


Fig. 4.4. Influence of λ_1 on velocity profile f' .

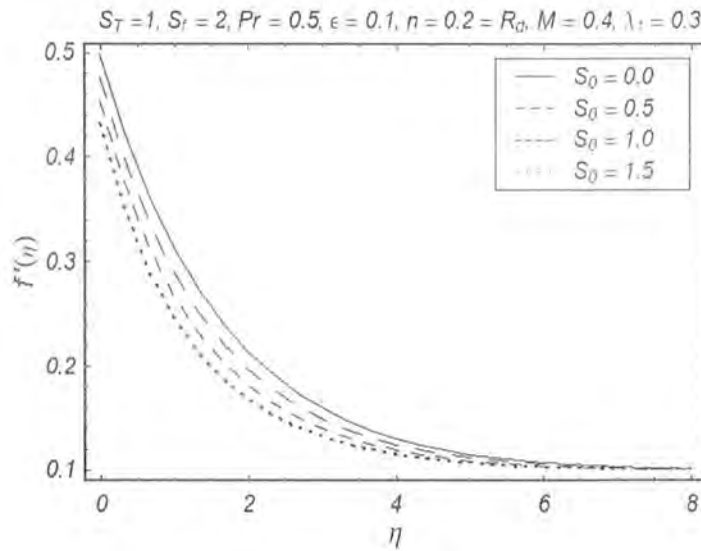


Fig. 4.5. Influence of S_0 on velocity profile f' .

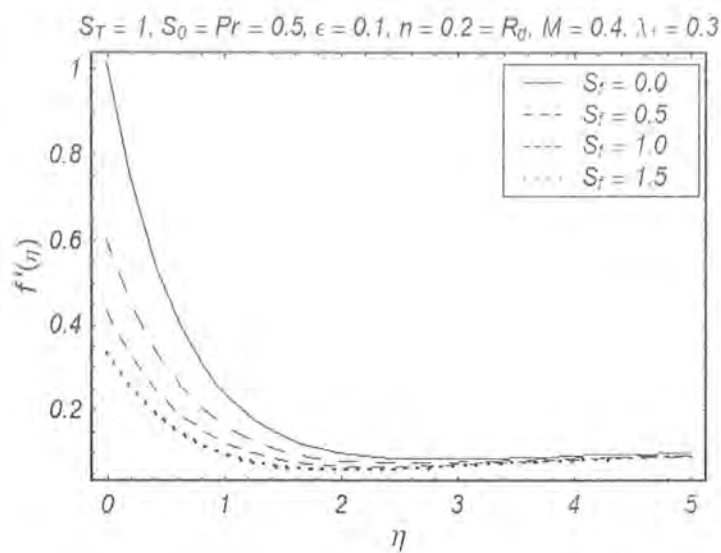


Fig. 4.6. Influence of S_f on velocity profile f' .

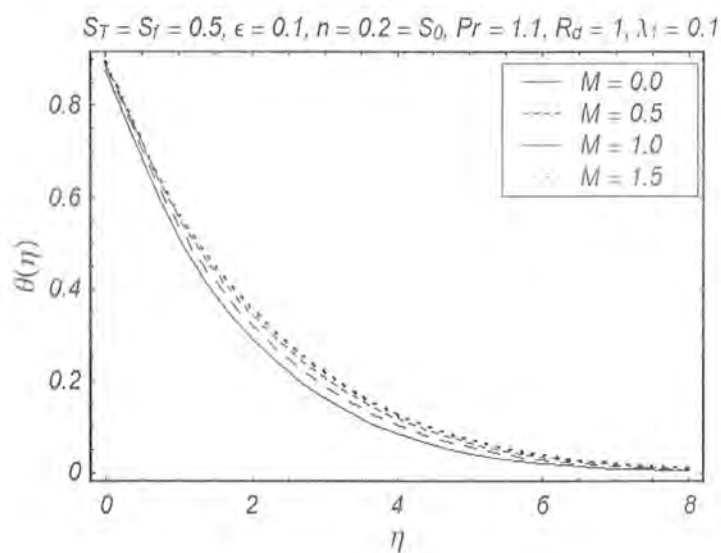


Fig. 4.7. Influence of M on temperature profile θ for assisting flow.

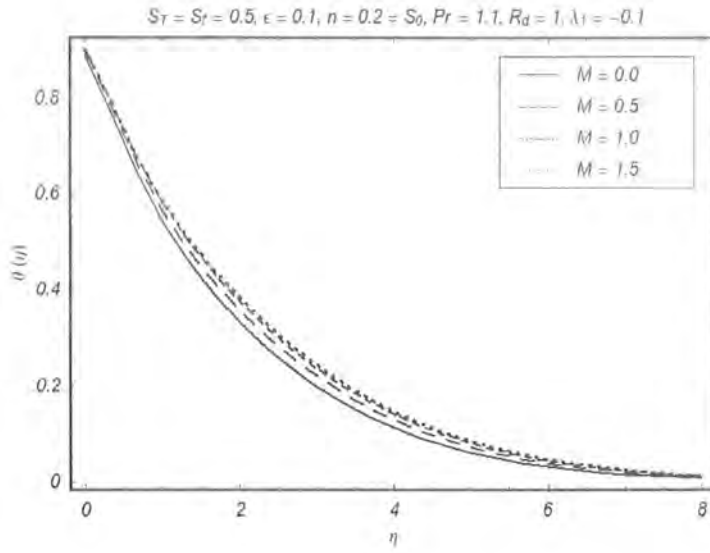


Fig. 4.8. Influence of M on temperature profile θ for opposing flow.

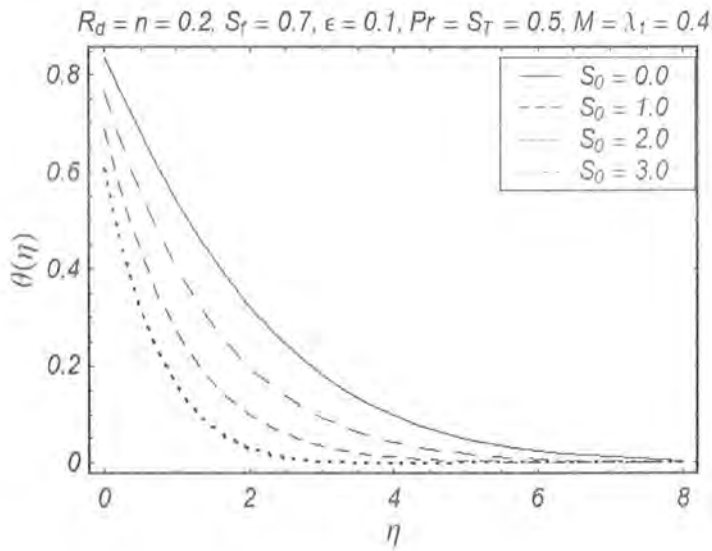


Fig. 4.9. Influence of S_0 on temperature profile θ .

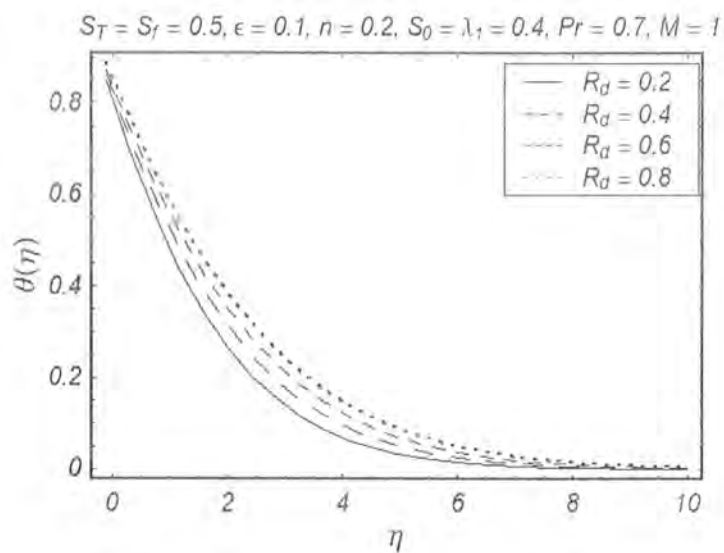


Fig. 4.10. Influence of R_d on temperature profile θ .

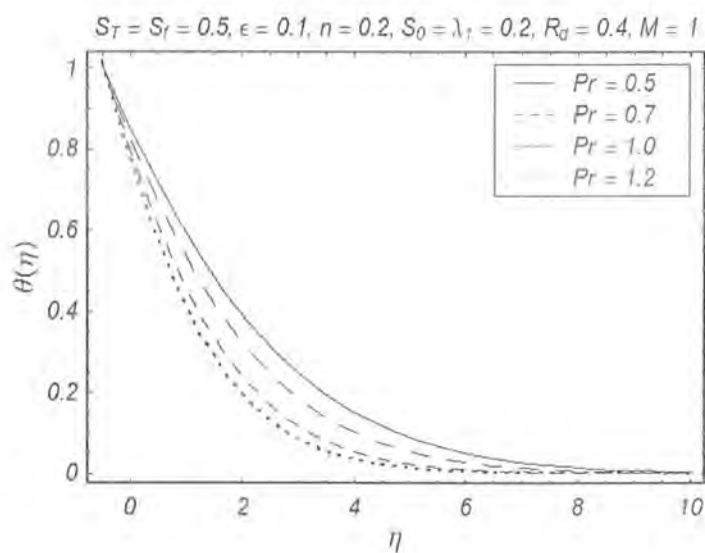


Fig. 4.11. Influence of Pr on temperature profile θ .

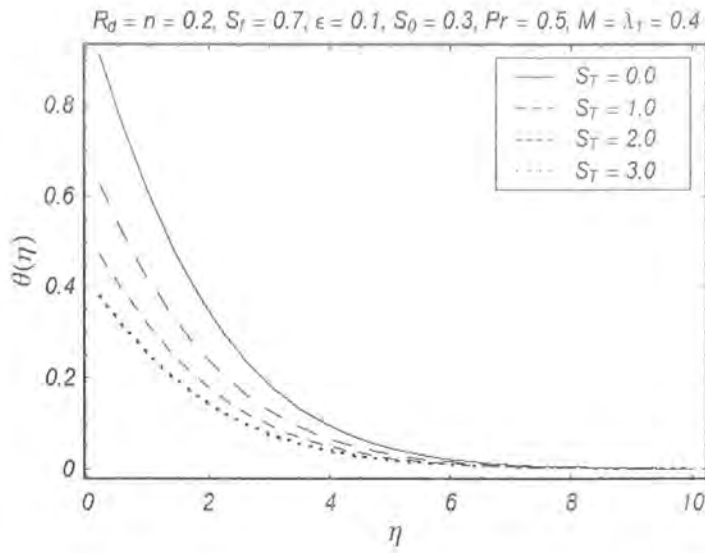


Fig. 4.12. Influence of S_T on temperature profile θ .

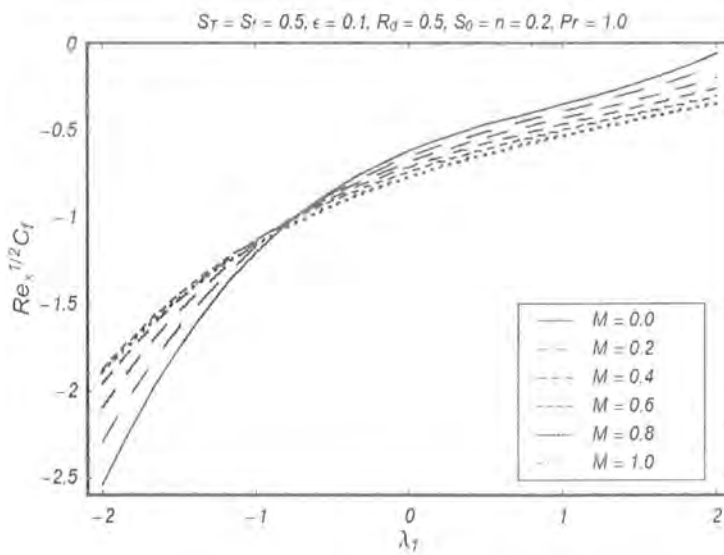


Fig. 4.13. Influence of M on $Re_x^{1/2} C_f$.

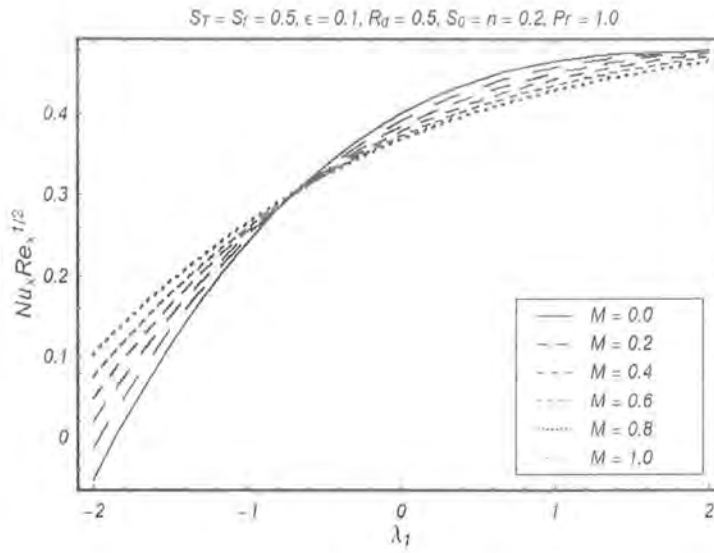


Fig. 4.14. Influence of M on $Nu_x Re_x^{1/2}$.

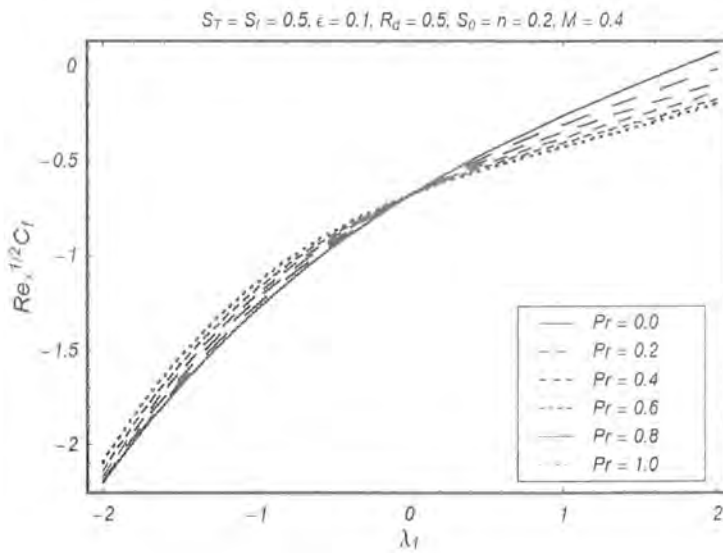


Fig. 4.15. Influence of Pr on $Re_x^{1/2} C_f$.

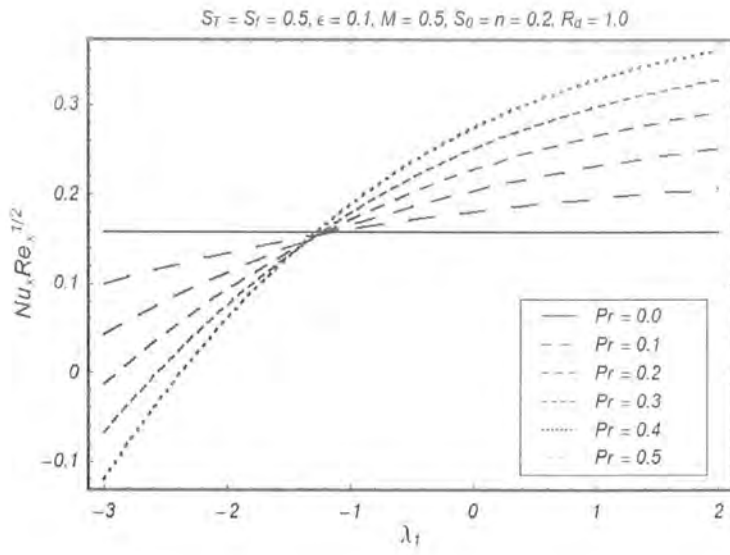


Fig. 4.16. Influence of Pr on $Nu_x Re_x^{1/2}$.

Table: 4.4. Values of $-\theta'(0)$ for parameters M , R_d , S_0 and n when $S_f = S_T = 0$, $\epsilon = 0.1$, $\lambda_1 = 0.2$ and $\text{Pr} = 1$.

M	R_d	S_0	n	$-\theta'(0)$
0.1	0.2	0.4	0.1	0.77779
0.3				0.768694
0.5				0.760436
0.7				0.752891
0.9				0.74596
0.2	0.0	0.4	0.5	1.074460
	0.2			0.907940
	0.4			0.793023
	0.6			0.747740
0.2	0.2	0.2	0.1	0.666714
		0.3		0.719025
		0.5		0.828924
		0.6		0.886293
0.2	0.2	0.4	0.4	0.875372
			0.6	0.939829
			1.0	1.061210
			1.5	1.201130
			2.0	1.330410

Table: 4.5. Values of skin-friction coefficient $-f''(0)$ and $-\theta'(0)$
when $\text{Pr} = 1$, $S_T = 0.5$ and $n = \epsilon = 0.1$.

M	S_0	λ_1	R_d	S_f	$-f''(0)$	$-\theta'(0)$
0.0	1.0	0.2	0.2	1.0	0.50022	0.67302
0.2					0.51555	0.66923
0.4					0.52893	0.66595
0.6					0.54073	0.66307
0.5	0.1	0.1	0.2	0.5	0.646438	0.403532
	0.3				0.683541	0.465849
	0.5				0.721271	0.528051
	0.7				0.759171	0.589035
	0.9				0.79681	0.64801
0.5	0.2	0.1		1.0	0.466658	0.410795
		0.2			0.446499	0.421359
		0.5			0.392488	0.446116
0.2	0.6	0.1	0.0	0.3	0.86056	0.659842
			0.1		0.858098	0.616144
			0.3		0.853654	0.546673
			0.5		0.849743	0.493664
			0.4	0.5	0.696141	0.506919
				1.0	0.482523	0.488838
				1.2	0.430602	0.483975
				3.0	0.220863	0.461827

Table: 4.6. Comparison of local Nusselt number $-\theta'(0)$ for some values M .

Pr and n when $R_d = \epsilon = \lambda_1 = 0 = S_f = S_0 = S_T$.

M	Pr	n	HAM[5]	$-\theta'(0)$
0.0	2.0	0.1	0.981991	0.981707
0.3			0.950257	0.950258
0.5			0.931430	0.931430
0.8			0.905665	0.905665
1.0			0.889917	0.889855
0.5	1.1	0.2	0.62569	0.625689
	1.1		0.669087	0.669087
	1.3		0.750773	0.750773
	1.5		0.82675	0.82675
	2.0		0.997713	0.997713
0.5	1.0	0.1	0.58183	0.58183
		0.3	0.66843	0.66843
		0.5	0.750784	0.750782
		1.0	0.94090	0.94089
		3.0	1.55041	1.55041
		5.0	2.02104	2.02104

4.4 Results and discussion

This section aims to explore the effects of different relevant parameters on velocity and temperature fields. For this purpose the Figs. 4.2–4.16 are prepared. Fig. 4.2 plots the effects of ϵ on the velocity field f' . The velocity field f' increases with an increase in ϵ significantly. Influence of magnetic parameter M for assisting and opposing flow cases are portrayed in Fig. 4.3. For assisting flow

($\lambda_1 > 0$), the velocity field f' decreases for positive values of M whereas for opposing flow ($\lambda_1 < 0$), the velocity field f' increases with an increase in M . Since in assisting flow case ($\lambda_1 > 0$), the positive values of gravitational forces g and magnetic field M simultaneously act as the retarding forces which result a decrease in the velocity field. From physical point of view when magnetic field is applied on any fluid then the apparent viscosity of the fluid increases. Thus the motion of fluid can be controlled by varying magnetic field which gives rise to many engineering applications including MHD power generation and electromagnetic casting etc.

Fig. 4.4 plots the influence of assisting flow case ($\lambda_1 > 0$) and opposing flow case ($\lambda_1 < 0$) on f' . $\lambda_1 > 0$ causes reduction in f' while $\lambda_1 < 0$ magnifies it. Fig. 4.5 predicts the effect of S_0 on f' . It is obvious that the reason of reduction in f' is suction S_0 near the boundary but for $\eta > 2$ it reveals opposite behaviour. Fig. 4.6 elucidates the variation of velocity slip parameter S_f on the velocity field f' . This Fig. illustrates the slip parameter S_f retards the fluid flow.

Figs. 4.7 – 4.12 illustrate the influences of M , S_0 , R_d , Pr and S_T on the temperature profile θ . It is observed from Figs. 4.7 and 4.8 that the temperature field θ and associated thermal boundary layer decrease with an increase in magnetic parameter M for both assisting ($\lambda_1 > 0$) and opposing ($\lambda_1 < 0$) flow cases. The change in temperature field θ for suction parameter S_0 is demonstrated in Fig. 4.9. This Fig. shows that suction S_0 causes a rapid decrease in the temperature field and associated boundary layer thickness. Fig. 4.10 plots the variation of radiation parameter R_d on θ . This Fig. clearly points out that θ increases by increasing R_d . Fig. 4.11 presents the effects of Prandtl number Pr on temperature field θ . It is noted that an increase in Pr results a decrease in θ . This is reasonable in the sense that larger Prandtl number corresponds to weaker thermal diffusivity and thinner boundary layer. The influence of thermal slip parameter S_T on temperature field θ is shown in Fig. 4.12. Since slip effects cause a decrease in fluid motion which means lesser molecular interaction. Thus due to lesser molecular interaction, the temperature field θ rapidly decreases by increasing slip parameter. Figs. 4.13 and 4.14 indicate the influence of magnetic parameter M with mixed convection parameter λ_1 . So the skin friction coefficient and local Nusselt number have the

similar effects and increase in assisting flow and decrease for opposing flow. Fig. 4.15 is prepared to show the effects of Prandtl number on skin friction coefficient $\text{Re}_x^{1/2} C_f$. The difference between assisting and opposing flows can easily visualized in this Fig. Further, the skin friction coefficient is decreasing in assisting case and increases in opposing case. Since the physical quantity local Nusselt which is used for heat transfer from the wall and from Fig. 4.16, it is noticed that for particular values of Prandtl number for assisting flow, the local Nusselt number is increased and quite opposite for opposing flow.

From Table 4.2 it is originated that the magnitude of $-f''(0)$ decreases for huge values of S_f . Table 4.3 presents a comparison of $-f''(0)$ with the numerical result reported in [19] for various values of S_f when $M = S_0 = \lambda_1 = \epsilon = 0$. The magnitude of local Nusselt number and skin-friction coefficient are given in the Tables 4.4 and 4.5. It is visible from these tables that the magnitude of $-\theta'(0)$ decreases for larger values of M and R_d . Table 4.6 is constructed to show the comparison of local Nusselt number $-\theta'(0)$ in limiting case [5]. This table indicates that magnitude of $-\theta'(0)$ increases when Pr and n are increased.

4.5 Concluding remarks

- The identical behavior of magnetic parameter M on f' in both cases assisting and opposing flows are observed but λ_1 has different effect, it shows an increasing effect for assisting and decreases in opposing flows.
- The results of suction, velocity slip, Prandtl and thermal slip parameters S_0 , S_f , Pr and S_T on f' and θ are similar. Here both velocity f' and temperature θ decrease with an increase in these parameters but the influence of R_d on θ is reverse.
- Magnitude of local Nusselt number decreases for large values of M and R_d .
- Local Nusselt number is an increasing function of S_0 and n .

Chapter 5

Series solution for stagnation-point flow of second grade fluid

This chapter reports the homotopy solution for stagnation point flow of a non-Newtonian fluid. An incompressible second grade fluid impinges on the wall either orthogonally or obliquely. The resulting nonlinear problems have been solved by homotopy analysis method (HAM). Convergence of the series solutions is checked. Such solutions are compared with the numerical solutions presented in a study [22]. Excellent agreement is noted between the numerical and series solutions.

5.1 Mathematical analysis

The continuity and momentum equations are

$$\operatorname{div} \mathbf{V}^* = 0, \quad (5.1)$$

$$\rho \mathbf{V}^* = \operatorname{div} \mathbf{T}, \quad (5.2)$$

where the constitutive equation for Cauchy stress tensor in a second grade fluid is

$$\mathbf{T} = -p^* \mathbf{I} + \mu \mathbf{A}_1 + \alpha_1 \mathbf{A}_2 + \alpha_2 \mathbf{A}_1^2, \quad (5.3)$$

$$\mathbf{A}_1 = (\text{grad } \mathbf{V}^*) + (\text{grad } \mathbf{V}^*)^T, \quad (5.4)$$

$$\mathbf{A}_2 = \frac{d\mathbf{A}_1}{dt} + (\text{grad } \mathbf{V}^*)^T \mathbf{A}_1 + \mathbf{A}_1 (\text{grad } \mathbf{V}^*), \quad (5.5)$$

where \mathbf{V}^* denotes the velocity vector, \mathbf{I} the identity tensor, p^* fluid pressure, μ , the dynamic viscosity, \mathbf{A}_1 , \mathbf{A}_2 the Rivlin Ericksen tensors, α_1 and α_2 the normal stresses and body forces are absent. The two-dimensional steady flow equations are

$$\frac{\partial u^*}{\partial x^*} + \frac{\partial v^*}{\partial y^*} = 0, \quad (5.6)$$

$$\begin{aligned} & u^* \frac{\partial u^*}{\partial x^*} + v^* \frac{\partial u^*}{\partial y^*} + \frac{1}{\rho} \frac{\partial p^*}{\partial x^*} \\ = & \nu \nabla^{*2} u^* + \frac{\alpha_1}{\rho} \left\{ \begin{array}{l} \frac{\partial}{\partial x^*} \left[\begin{array}{l} 2u^* \frac{\partial^2 u^*}{\partial x^{*2}} + 2v^* \frac{\partial^2 u^*}{\partial x^* \partial y^*} + 4 \left(\frac{\partial u^*}{\partial x^*} \right)^2 \\ + 2 \frac{\partial v^*}{\partial x^*} \left(\frac{\partial v^*}{\partial x^*} + \frac{\partial u^*}{\partial y^*} \right) \end{array} \right] \\ + \frac{\partial}{\partial y^*} \left[\begin{array}{l} \left(u^* \frac{\partial}{\partial x^*} + v^* \frac{\partial}{\partial y^*} \right) \\ \times \left(\frac{\partial v^*}{\partial x^*} + \frac{\partial u^*}{\partial y^*} \right) + 2 \frac{\partial u^*}{\partial x^*} \frac{\partial u^*}{\partial y^*} + 2 \frac{\partial v^*}{\partial x^*} \frac{\partial v^*}{\partial y^*} \end{array} \right] \end{array} \right\} \\ & + \frac{\alpha_2}{\rho} \frac{\partial}{\partial x^*} \left[4 \left(\frac{\partial u^*}{\partial x^*} \right)^2 + \left(\frac{\partial v^*}{\partial x^*} + \frac{\partial u^*}{\partial y^*} \right)^2 \right], \quad (5.7a) \end{aligned}$$

$$\begin{aligned}
u^* \frac{\partial v^*}{\partial x^*} + v^* \frac{\partial v^*}{\partial y^*} + \frac{1}{\rho} \frac{\partial p^*}{\partial y^*} &= \nu \nabla^{*2} u^* \\
&+ \frac{\alpha_1}{\rho} \left\{ \frac{\partial}{\partial x^*} \left[\begin{aligned} &2 \frac{\partial u^*}{\partial x^*} \frac{\partial v^*}{\partial y^*} + \left(u^* \frac{\partial}{\partial x^*} + v^* \frac{\partial}{\partial y^*} \right) \left(\frac{\partial v^*}{\partial x^*} + \frac{\partial u^*}{\partial y^*} \right) \\ &+ 2 \left(\frac{\partial v^*}{\partial x^*} \frac{\partial v^*}{\partial y^*} \right) \end{aligned} \right] \right. \\
&+ \frac{\partial}{\partial y^*} \left[\begin{aligned} &2 u^* \frac{\partial^2 v^*}{\partial x^* \partial y^*} + 4 \left(\frac{\partial v^*}{\partial y^*} \right)^2 + 2 v^* \frac{\partial^2 v^*}{\partial y^{*2}} \\ &+ 2 \frac{\partial u^*}{\partial y^*} \left(\frac{\partial v^*}{\partial x^*} + \frac{\partial u^*}{\partial y^*} \right) \end{aligned} \right] \left. \right\} \\
&+ \frac{\alpha_2}{\rho} \frac{\partial}{\partial y^*} \left[4 \left(\frac{\partial v^*}{\partial y^*} \right)^2 + \left(\frac{\partial v^*}{\partial x^*} + \frac{\partial u^*}{\partial y^*} \right)^2 \right], \tag{5.8}
\end{aligned}$$

where asterisk indicates the dimensional quantity, $\frac{d}{dt}$ the material time differentiation and ρ the fluid density. The following similarity transformations have been used to make the problem dimensionless.

$$x = x^* \sqrt{\frac{\beta}{\nu}}, \quad y = y^* \sqrt{\frac{\beta}{\nu}}, \tag{5.9}$$

$$u = \frac{1}{\sqrt{\nu\beta}} u^*, \quad v = \frac{1}{\sqrt{\nu\beta}} v^*, \quad p = \frac{1}{\rho\nu\beta} p^*, \tag{5.10}$$

in which ν is the kinematic viscosity. Dimensionless form of flow equations are

$$\frac{\partial u}{\partial x} + \frac{\partial v}{\partial y} = 0, \tag{5.11}$$

$$\begin{aligned}
&u \frac{\partial u}{\partial x} + v \frac{\partial u}{\partial y} + \frac{1}{\rho} \frac{\partial p}{\partial x} \\
&= \nabla^2 u + W_e \left\{ \begin{aligned} &\frac{\partial}{\partial x} \left[2u \frac{\partial^2 u}{\partial x^2} + 2v \frac{\partial^2 u}{\partial x \partial y} + 4 \left(\frac{\partial u}{\partial x} \right)^2 + 2 \frac{\partial v}{\partial x} \left(\frac{\partial v}{\partial x} + \frac{\partial u}{\partial y} \right) \right] \\ &+ \frac{\partial}{\partial y} \left[\left(u \frac{\partial}{\partial x} + v \frac{\partial}{\partial y} \right) \left(\frac{\partial v}{\partial x} + \frac{\partial u}{\partial y} \right) + 2 \frac{\partial u}{\partial x} \frac{\partial u}{\partial y} + 2 \frac{\partial v}{\partial x} \frac{\partial v}{\partial y} \right] \end{aligned} \right\} \\
&+ \lambda \frac{\partial}{\partial x} \left[4 \left(\frac{\partial u}{\partial x} \right)^2 + \left(\frac{\partial v}{\partial x} + \frac{\partial u}{\partial y} \right)^2 \right], \tag{5.12}
\end{aligned}$$

$$\begin{aligned}
& u \frac{\partial v}{\partial x} + v \frac{\partial v}{\partial y} + \frac{1}{\rho} \frac{\partial p}{\partial y} \\
= & \nabla^2 v + W_e \left\{ \begin{aligned} & \frac{\partial}{\partial x} \left[2 \frac{\partial v}{\partial x} \frac{\partial v}{\partial y} + \left(u \frac{\partial}{\partial x} + v \frac{\partial}{\partial y} \right) \left(\frac{\partial v}{\partial x} + \frac{\partial u}{\partial y} \right) + 2 \frac{\partial v}{\partial x} \frac{\partial v}{\partial y} \right] \\ & + \frac{\partial}{\partial y} \left[2u \frac{\partial^2 v}{\partial x \partial y} + 4 \left(\frac{\partial v}{\partial y} \right)^2 + 2v \frac{\partial^2 v}{\partial y^2} + 2 \frac{\partial u}{\partial y} \left(\frac{\partial v}{\partial x} + \frac{\partial u}{\partial y} \right) \right] \end{aligned} \right\} \\
& + \lambda \frac{\partial}{\partial y} \left[4 \left(\frac{\partial v}{\partial y} \right)^2 + \left(\frac{\partial v}{\partial x} + \frac{\partial u}{\partial y} \right)^2 \right]. \tag{5.13}
\end{aligned}$$

Using Eq. (5.11), we take the stream function $\psi(x, y)$ such that

$$u = \frac{\partial \psi}{\partial y}, v = -\frac{\partial \psi}{\partial x}. \tag{5.14}$$

By substituting Eq. (5.14) into Eqs. (5.12) and (5.13) and resulting equations become after elimination of pressure by using $p_{xy} = p_{yx}$, we have

$$\frac{\partial (\psi, \nabla^2 \psi)}{\partial (x, y)} - W_e \frac{\partial (\psi, \nabla^4 \psi)}{\partial (x, y)} + \nabla^4 \psi = 0, \tag{5.15}$$

where $W_e (= \alpha_1 \beta / \rho \nu)$ is the Weissenberg number, $\lambda (= \alpha_2 \beta / \rho \nu)$ and $\nabla^2 = \partial^2 / \partial x^2 + \partial^2 / \partial y^2$.

5.2 Orthogonal flow

The infinite plate is considered at $y = 0$ and fluid occupies the entire upper half plane $y > 0$. Furthermore we assume that the streamfunction far from the wall thus the boundary conditions are

$$\frac{\partial \psi}{\partial x} = 0, \text{ at } y = 0, \quad \psi(x, y) \sim y \text{ as } y \sim \infty, \tag{5.16}$$

with slip condition

$$\frac{\partial \psi}{\partial y} = \gamma \frac{\partial^2 \psi}{\partial y^2}, \tag{5.17}$$

where γ the slip parameter and

$$\psi = xf(y). \tag{5.18}$$

Using Eq. (5.18) in Eqs. (5.15) – (5.17), we get

$$f^{(iv)} + ff''' - f'f'' - We(ff^{(iv)} - f'f^{(iv)}) = 0, \quad (5.19)$$

$$f(0) = 0, f'(0) = \gamma f''(0), f'(\infty) = 1. \quad (5.20)$$

Now integrating the above equation with respect to y , we obtain

$$f''' + ff'' - f'^2 - We(ff^{(iv)} - 2f'f''' + f''^2) = -1, \quad (5.21)$$

$$f(0) = 0, f'(0) = \gamma f''(0), f'(\infty) = 1. \quad (5.22)$$

5.3 Oblique flow

The stream function far from the wall is defined as

$$\psi(x, y) \sim ky^2 + xy, \quad (5.23)$$

where k is the constant. Thus stream function has the form

$$\psi(x, y) = xf(y) + g(y), \quad (5.24)$$

with

$$\begin{aligned} f(0) &= 0, f'(0) = \gamma f''(0), g(0) = 0, g'(0) = \gamma g''(0), \\ f(y) &\sim y, g(y) \sim ky^2 \text{ as } y \rightarrow \infty. \end{aligned} \quad (5.25)$$

Employing Eq. (5.23) in Eq. (5.15) and we obtain an equation with terms of $O(x)$ and $O(1)$. The terms of $O(x)$ stand for ODE for $f(y)$ and the terms of $O(1)$ stand for an equation $g(y)$. Thus the second grade incompressible fluid invaded on the wall either orthogonal and oblique. Mathematical

problems for orthogonal flow is

$$f''' + ff'' - f'^2 - W_e(ff^{(iv)} - 2f'f''' + f''^2) = -1 \quad (5.26)$$

$$f(0) = 0, \quad f'(0) = \gamma f''(0), \quad f'(\infty) = 1, \quad (5.27)$$

where the slip parameter $\gamma = A_p\sqrt{\beta\nu}$ and β has units of inverse time. For oblique flow we have

$$f''' + ff'' - f'^2 - W_e(ff^{(iv)} - 2f'f''' + f''^2) = -1, \quad (5.28)$$

$$f(0) = 0, \quad f'(0) = \gamma f''(0), \quad f'(\infty) = 1, \quad (5.29)$$

$$g'' + fg' - f'g - W_e(fg'' - f'g' + f''g' - f'''g) = 0, \quad (5.30)$$

$$g(0) = \gamma g'(0), \quad g'(\infty) = 1. \quad (5.31)$$

Note that the constant of integration in Eq. (5.30) is taken zero. Here tangential component of flow is g .

5.4 Series solutions

Choosing the set of base functions

$$\{\eta^k \exp(-n\eta), \quad k \geq 0, n \geq 0\}, \quad (5.32)$$

one writes the solutions

$$f(\eta) = a_{0,0}^0 + \sum_{n=0}^{\infty} \sum_{k=0}^{\infty} a_{m,n}^k \eta^k \exp(-n\eta), \quad (5.33)$$

$$\theta(\eta) = \sum_{n=0}^{\infty} \sum_{k=0}^{\infty} b_{m,n}^k \eta^k \exp(-n\eta), \quad (5.34)$$

in which $a_{m,n}^k$ and $b_{m,n}^k$ are the coefficients.

The selection of initial guesses and linear operators are

$$f_0 = -\left(\frac{1}{1+\gamma}\right) + y + \frac{1}{1+\gamma} \exp(-y), \quad (5.35)$$

$$g_0 = (-\gamma - 1) + y + \exp(-2y), \quad (5.36)$$

$$L_f [f(y)] = \frac{\partial^3 f}{\partial y^3} - \frac{\partial f}{\partial y}, \quad (5.37)$$

$$L_g [g(y)] = \frac{\partial^2 g}{\partial y^2} - g, \quad (5.38)$$

through the properties

$$L_f [C_1 + C_2 \exp(y) + C_3 \exp(-y)] = 0, \quad (5.39)$$

$$L_g [C_4 \exp(y) + C_5 \exp(-y)] = 0, \quad (5.40)$$

where $C_i (i = 1 - 5)$ are the constants. The zeroth and m^{th} order problems are given below

$$(1-p)L_f [\hat{f}(y;p) - f_0(y)] = p h_f N_f[\hat{f}(y;p)], \quad (5.41)$$

$$(1-p)L_g [\hat{g}(y;p) - g_0(y)] = p h_g N_g[\hat{g}(y;p), \hat{f}(y;p)], \quad (5.42)$$

$$\hat{f}(0;p) = 0, \quad \frac{\partial \hat{f}}{\partial y}(0;p) = \gamma \frac{\partial^2 \hat{f}}{\partial y^2}(0;p), \quad (5.43)$$

$$g(0;p) = \gamma \frac{\partial \hat{g}}{\partial y}(0;p), \quad y = 0, \quad (5.44)$$

$$\frac{\partial \hat{f}}{\partial y}(y) = 1, \quad \frac{\partial \hat{g}}{\partial y}(y) \rightarrow 1 \text{ when } y \rightarrow \infty, \quad (5.45)$$

$$L_f [f_m(y) - \chi_m f_{m-1}(y)] = h_f R_{f,m}(y), \quad (5.46)$$

$$L_g [g_m(y) - \chi_m g_{m-1}(y)] = h_g R_{g,m}(y), \quad (5.47)$$

$$f_m(0) = 0, \quad f'_m(0) = \gamma f''_m(0), \quad g_m(0) = \gamma g'_m(0), \quad (5.48)$$

$$f'_m(y) = 0, \quad g'_m(y) = 0, \text{ when } y \rightarrow \infty, \quad (5.49)$$

where h_f and h_g are the non-zero parameters, $p \in [0, 1]$ is the embedding parameter and

$$N_f[\bar{f}(y; p)] = \frac{\partial^3 f}{\partial y^3} + f \frac{\partial^2 f}{\partial y^2} - \left(\frac{\partial f}{\partial y} \right)^2 - W_e \left(f \frac{\partial^4 f}{\partial y^4} - 2 \frac{\partial f}{\partial y} \frac{\partial^3 f}{\partial y^3} + \left(\frac{\partial^2 f}{\partial y^2} \right)^2 \right) + 1, \quad (5.50)$$

$$N_g[\bar{g}(y; p)] = \frac{\partial^2 g}{\partial y^2} + f \frac{\partial g}{\partial y} - \frac{\partial f}{\partial y} g - W_e \left(f \frac{\partial^3 g}{\partial y^3} - \frac{\partial f}{\partial y} \frac{\partial^2 g}{\partial y^2} + \frac{\partial^2 f}{\partial y^2} \frac{\partial g}{\partial y} - \frac{\partial^3 f}{\partial y^3} g \right), \quad (5.51)$$

$$\begin{aligned} R_{f,m}(y) &= \frac{\partial^3 f_{m-1}}{\partial y^3} + \sum_{i=0}^{m-1} f_i \frac{\partial^2 f_{m-i-1}}{\partial y^2} - \sum_{i=0}^{m-1} \frac{\partial f_{m-i-1}}{\partial y} \frac{\partial f_i}{\partial y} \\ &\quad - W_e \left(\sum_{i=0}^{m-1} f_i \frac{\partial^4 f_{m-i-1}}{\partial y^4} - 2 \sum_{i=0}^{m-1} \frac{\partial f_i}{\partial y} \frac{\partial^3 f_{m-i-1}}{\partial y^3} + \sum_{i=0}^{m-1} \frac{\partial^2 f_{m-i-1}}{\partial y^2} \frac{\partial^2 f_i}{\partial y^2} \right) \\ &\quad + (1 - \chi_m), \end{aligned} \quad (5.52)$$

$$\begin{aligned} R_{g,m}(y) &= \frac{\partial^2 g_{m-1}}{\partial y^2} + \sum_{i=0}^{m-1} f_i \frac{\partial g_{m-i-1}}{\partial y} - \sum_{i=0}^{m-1} \frac{\partial f_{m-i-1}}{\partial y} g_i \\ &\quad - W_e \left(\begin{aligned} &\sum_{i=0}^{m-1} f_i \frac{\partial^3 g_{m-i-1}}{\partial y^3} - \sum_{i=0}^{m-1} \frac{\partial f_i}{\partial y} \frac{\partial^2 g_{m-i-1}}{\partial y^2} \\ &+ \sum_{i=0}^{m-1} \frac{\partial^2 f_{m-i-1}}{\partial y^2} \frac{\partial g_i}{\partial y} - \sum_{i=0}^{m-1} \frac{\partial^3 f_{m-i-1}}{\partial y^3} g_i \end{aligned} \right). \end{aligned} \quad (5.53)$$

Note that

$$\bar{f}(y; 0) = f_0(y), \quad \bar{g}(y; 0) = g_0(y), \quad (5.54)$$

$$\bar{f}(y; 1) = f(y), \quad \bar{g}(y; 1) = g(y). \quad (5.55)$$

The general solutions after following the methodology in the previous chapter are

$$f_m(y) = f_m^*(y) + C_1 + C_2 \exp(y) + C_3 \exp(-y), \quad (5.56)$$

$$g_m(y) = g_m^*(y) + C_4 \exp(y) + C_5 \exp(-y), \quad (5.57)$$

where f_m^* and g_m^* indicate the special solutions.

5.5 Analysis of solutions

It is known that an auxiliary parameter plays a vital role in the convergence region and rate of approximation of the series solution. In view of adequate values of auxiliary parameters h_f and h_g the h -curves in Figs. 5.1 and 5.2 are depicted. The admissible regions are formed to be $-2.0 \leq h_f \leq -0.5$ and $-1.6 \leq h_g \leq -0.2$. Further, homotopy Pade-approximation is employed for the values presented in the Tables 5.1 and 5.2. These tables clearly indicate that convergence of the series solutions is accelerated through homotopy Pade approximation.

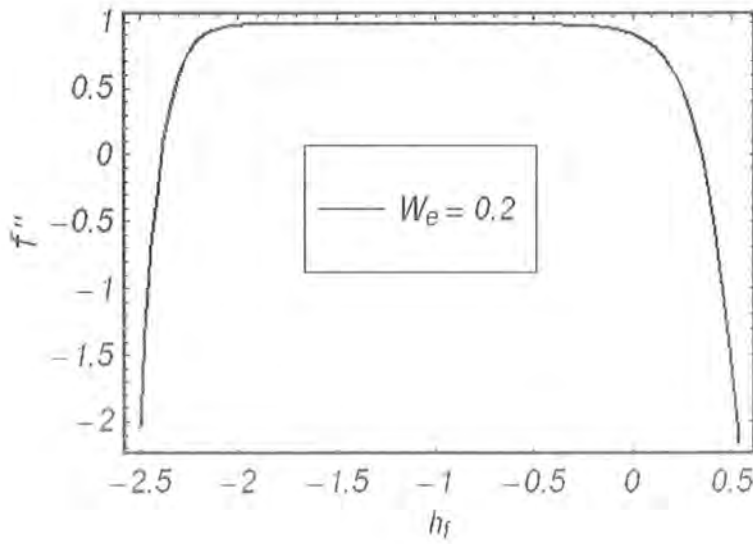


Fig. 5.1. h -curve for $f''(0)$ at the 22nd-order of approximation with $W_e = 0.2$ and $\gamma = 0.1$.

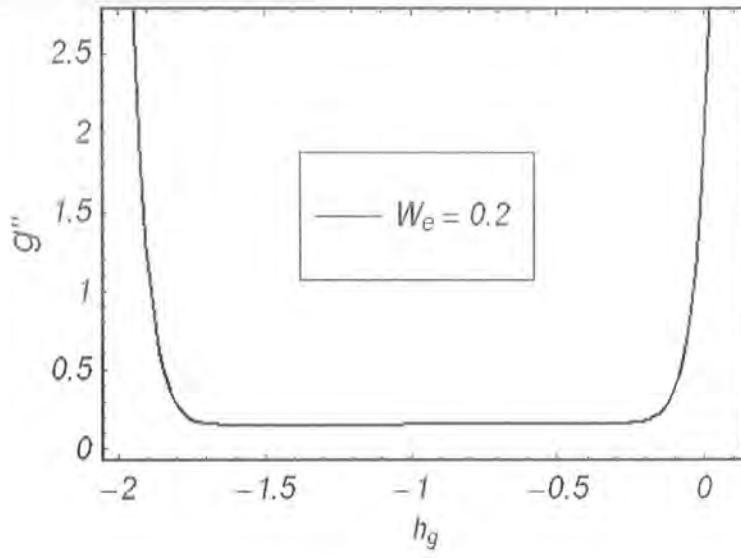


Fig. 5.2. h -curve for $g''(0)$ at the 22nd-order of approximation
with $h_f = -1.7$, $W_e = 0.2$ and $\gamma = 0.3$.

Table: 5.1. Convergence of series solutions of $f'''(0)$ with the various values of W_ε and γ by using homotopy-Pade approximation.

γ	$W_\varepsilon = 0$		$W_\varepsilon = 0.1$		$W_\varepsilon = 0.2$		$W_\varepsilon = 0.3$	
	[22]	[HAM]	[22]	[HAM]	[22]	[HAM]	[22]	[HAM]
0.0	1.23259	1.2326	1.13425	1.1341	1.05818	1.05818	0.99689	0.99684
0.2	1.04258	1.0426	0.96871	0.96872	0.91085	0.91085	0.86361	0.86361
0.4	0.88634	0.88634	0.83155	0.83155	0.78785	0.78786	0.75169	0.75170
0.6	0.76428	0.7643	0.72290	0.72291	0.68939	0.68939	0.66131	0.66131
0.8	0.66896	0.66897	0.63696	0.63696	0.61068	0.61068	0.58844	0.58844
1.0	0.59346	0.59346	0.56810	0.56810	0.54706	0.54706	0.52909	0.52909
2.0	0.37588	0.37589	0.36556	0.36556	0.35671	0.3567	0.34895	0.34895
5.0	0.17726	0.17726	0.17494	0.17494	0.17289	0.17289	0.17105	0.1711
10	0.09402	0.09403	0.09338	0.09338	0.09279	0.09279	0.09226	0.09226
20	0.04847	0.04847	0.04829	0.04829	0.04814	0.04814	0.04799	0.04799

γ	$W_e = 0.4$		$W_e = 0.5$		$W_e = 1$		$W_e = 2$	
	[22]	[HAM]	[22]	[HAM]	[22]	[HAM]	[22]	[HAM]
0.0	0.94588	0.94588	0.90248	0.90248	0.75276	0.75276	0.59677	0.59677
0.2	0.82393	0.82393	0.78989	0.78988	0.67021	0.67021	0.54170	0.54170
0.4	0.72098	0.72098	0.69437	0.69437	0.59900	0.59900	0.49323	0.49323
0.6	0.63721	0.63721	0.61616	0.61616	0.53933	0.53933	0.45154	0.45154
0.8	0.56919	0.56919	0.55225	0.55225	0.48943	0.48943	0.41575	0.41575
1.0	0.51343	0.51343	0.49956	0.49956	0.44743	0.44743	0.38488	0.38488
2.0	0.34203	0.34203	0.33578	0.33578	0.31125	0.31125	0.27945	0.27945
5.0	0.16936	0.16937	0.16782	0.16782	0.16144	0.16144	0.15241	0.15241
10	0.09177	0.09177	0.09131	0.09131	0.08939	0.08939	0.08655	0.08655
20	0.04786	0.04786	0.04773	0.04773	0.04720	0.04720	0.04640	0.04640

Table: 5.2. Convergence of series solutions of $g'(0)$ with the various values of W_e and γ by using homotopy-Pade approximation.

γ	$W_e = 0.0$		$W_e = 0.1$		$W_e = 0.2$	
	[22]	[HAM]	[22]	[HAM]	[22]	[HAM]
0	1.40643	0.570	1.36622	0.517	1.33539	0.477
0.2	1.09253	0.511	1.07934	0.475	1.06938	0.445
0.4	0.87852	0.445	0.87974	0.420	0.88121	0.394
0.6	0.72933	0.379	0.73788	0.359	0.74541	0.356
0.8	0.62130	0.332	0.63352	0.322	0.64422	0.315
1	0.54015	0.288	0.55413	0.282	0.56643	0.275
2	0.32442	0.124	0.33851	0.140	0.35120	0.139
5	0.14650	0.003	0.15514	0.007	0.16313	0.008

γ	$W_e = 0.3$		$W_e = 0.4$		$W_e = 0.5$	
	[22]	[HAM]	[22]	[HAM]	[22]	[HAM]
0.0	1.31046	0.445	1.28971	0.418	1.27217	0.396
0.2	1.0613	0.422	1.05456	0.396	1.04887	0.386
0.4	0.88263	0.384	0.88392	0.366	0.885206	0.355
0.6	0.75201	0.345	0.75781	0.355	0.76307	0.311
0.8	0.65362	0.283	0.66191	0.285	0.66943	0.277
1.0	0.57730	0.272	0.58694	0.268	0.59571	0.255
2.0	0.36270	0.999	0.37312	0.144	0.38276	0.141
5.0	0.17056	0.008	0.17747	0.009	0.18398	0.001

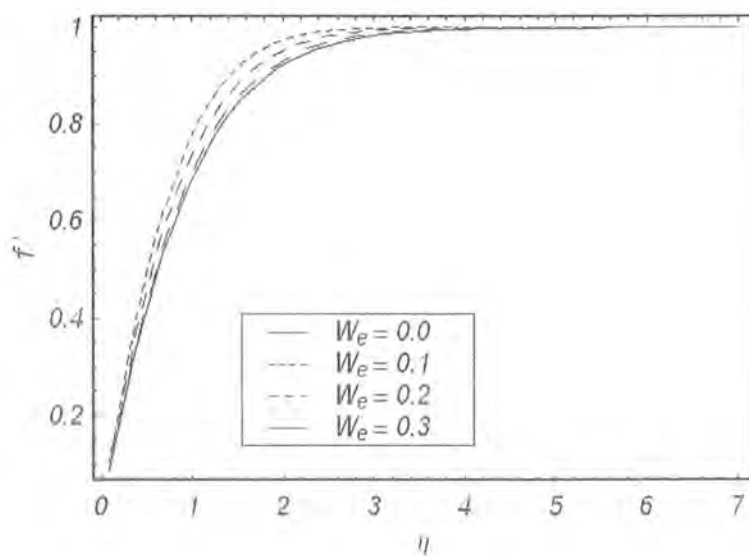


Fig. 5.3. Influence of f' with different values of W_e when $\gamma = 0$.

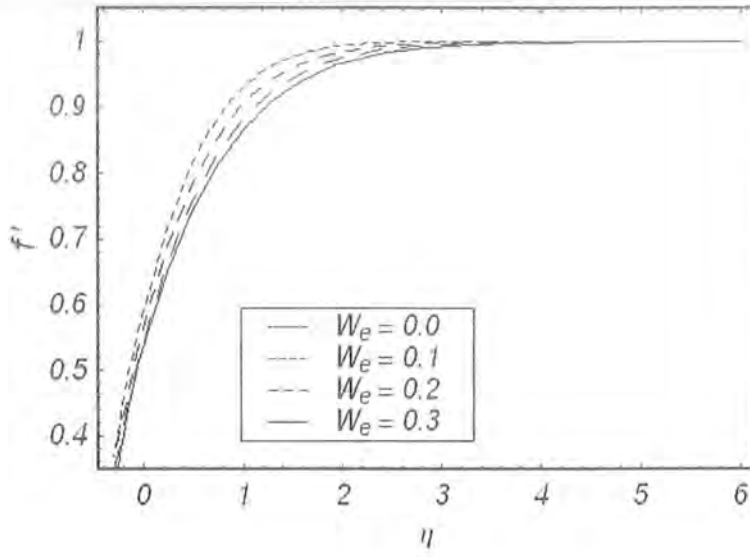


Fig. 5.4. Influence of f' with different values of W_e when $\gamma = 1$.

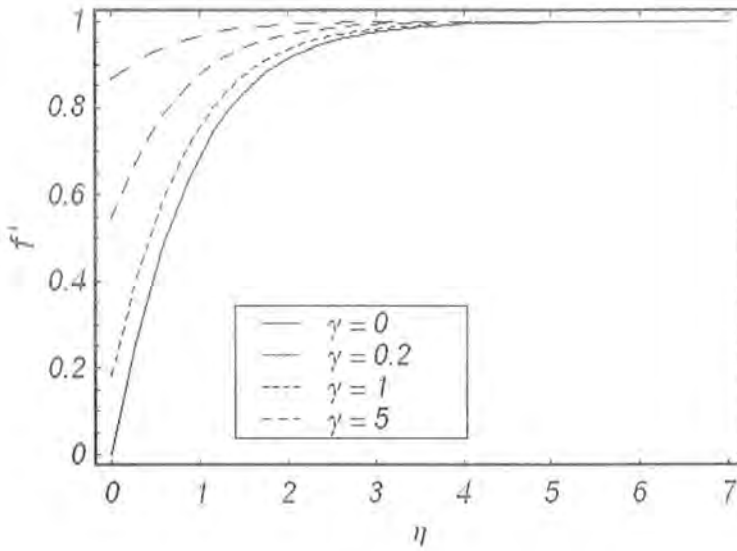


Fig. 5.5. Influence of f' with different values of γ when $W_e = 0.2$.

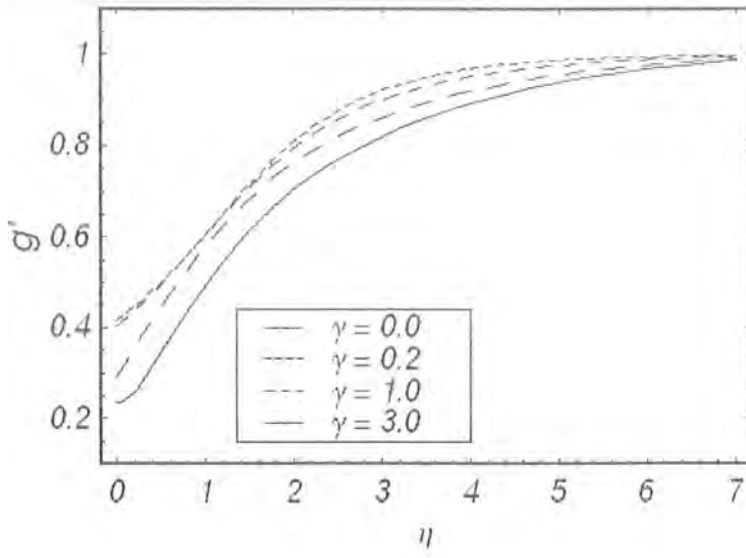


Fig. 5.6. Influence of g' with different values of γ when $W_e = 0.2$.

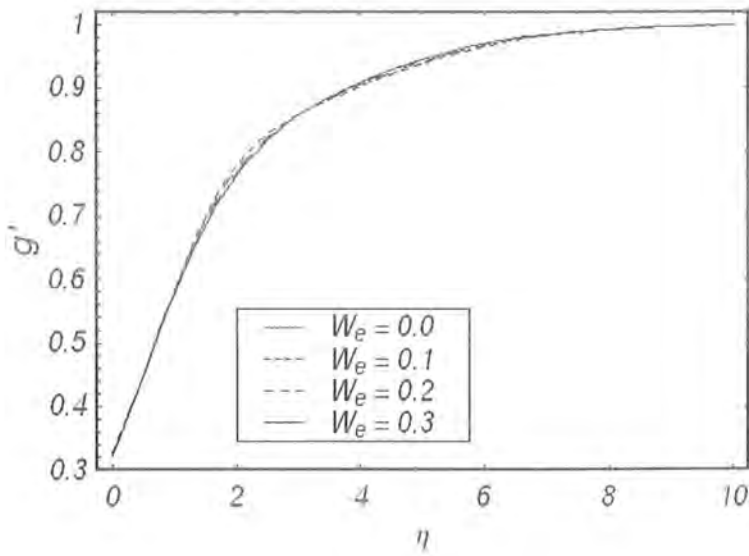


Fig. 5.7. Influence of g' with different values of W_e when $\gamma = 1$.

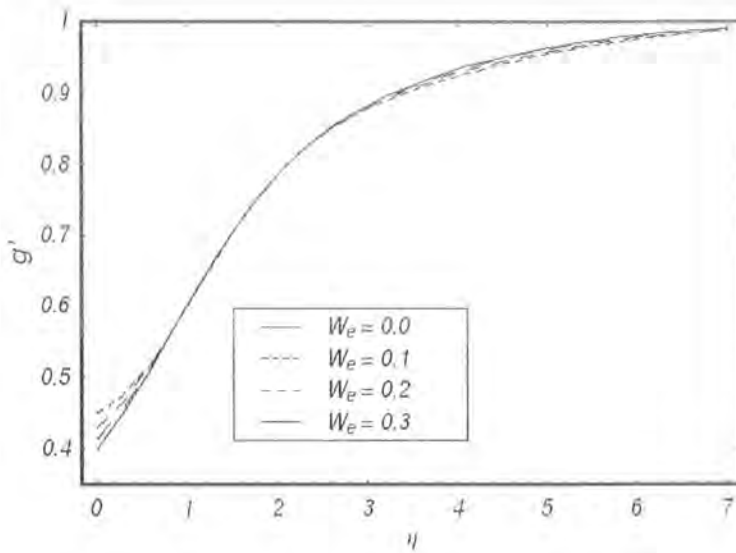


Fig. 5.8. Influence of g' with different values of W_e when $\gamma = 0.4$.

5.6 Discussion

Here Figs. 5.3 and 5.4 display the effects of Weissenberg number W_e on f' when $\gamma = 0$ and $\gamma = 1$, respectively. It is seen that f' is an increasing function of W_e . Further, f' in no-slip case is less than the slip case. From Table 5.1 it is further found that $f''(0)$ in no-slip situation is greater than the slip case. This observation is true for both viscous and second grade fluids. However $f''(0)$ in viscous fluid is larger than the second grade fluid for both slip and no-slip cases. Further the variations of γ and W_e on $f''(0)$ are similar in a qualitative sense. It is interesting to note that $f''(0)$ decreases when W_e increases. Decrease in $f''(0)$ by increasing W_e is less when compared with that of γ . This table also depicts that a comparison between the present series solution by homotopy analysis method and numerical solution in ref. [22] is in complete agreement. The variations of γ and W_e on $g'(0)$ are computed in Table 5.2. It is found that $g'(0)$ in slip situation is less than for no-slip case. Further $g'(0)$ in viscous fluid is greater than second grade fluid. More, the parameters

γ and W_e on $g'(0)$ have similar role qualitatively. The variation of γ on f' is shown in Fig. 5.5. This Fig. depicts that f' increases when γ increases. In view of Figs. 5.5 and 5.6 it is noticed that the variations of γ on f' and g' are quite opposite. From Fig. 5.7 it is found that there is slight increase/decrease in g' near the wall when γ varies.

Chapter 6

Stagnation-point flow of Maxwell fluid with thermal radiation and source/sink

The objective of this chapter is to examine the magnetohydrodynamic (MHD) mixed convection flow near a stagnation point over non-conducting stretching surface. Analysis has been modeled with thermal radiation and heat source/sinks. Thermal conductivity is taken variable and radiation heat flux is approximated under the Rosseland approximation. The partial differential equations are transformed into the ordinary differential equations. The solutions have been computed with the help of homotopy analysis method. Comparison with previous published results is presented in the special cases. Influence of various parameters of interest is discussed. Local Nusselt number is computed and analyzed.

6.1 Mathematical model

We consider the mixed convection flow of MHD Maxwell fluid with variable thermal conductivity. The stagnation point flow near a stretching sheet is considered. The x - and y -axes in the Cartesian

coordinate system are chosen along and perpendicular to the sheet, respectively. Further, the analysis is carried out in the presence of heat source/sink and thermal radiation. A uniform magnetic field B_0 is applied in the y -direction and induced magnetic field is not considered in terms of assumption of small magnetic Reynold number. The gravitational force acts parallel to x -axis. The equations governing the boundary layer flow are

$$\frac{\partial u}{\partial x} + \frac{\partial v}{\partial y} = 0, \quad (6.1)$$

$$\begin{aligned} u \frac{\partial u}{\partial x} + v \frac{\partial u}{\partial y} + \lambda \left(u^2 \frac{\partial^2 u}{\partial x^2} + v^2 \frac{\partial^2 u}{\partial y^2} + 2uv \frac{\partial^2 u}{\partial x \partial y} \right) &= U_\infty \frac{dU_\infty}{dx} + \lambda U_\infty^2 \frac{d^2 U_\infty}{dx^2} + \nu \frac{\partial^2 u}{\partial y^2} \\ &+ \frac{\sigma B_0^2}{\rho} \left(U_\infty - u - \lambda v \frac{\partial u}{\partial y} \right) \\ &\pm g \beta_T (T - T_\infty), \end{aligned} \quad (6.2)$$

$$\rho c_p \left(u \frac{\partial T}{\partial x} + v \frac{\partial T}{\partial y} \right) = \frac{\partial}{\partial y} \left(K^* \frac{\partial T}{\partial y} \right) + Q (T - T_\infty) + \frac{16\sigma^* T_\infty^3}{3K_1} \frac{\partial^2 T}{\partial y^2}, \quad (6.3)$$

where u and v the velocity components parallel to the x and y axes respectively, λ the relaxation time, ρ the fluid density, ν kinematic viscosity, g gravitational force per unit mass, β_T thermal expansion coefficient, c_p specific heat at constant pressure and term $(T - T_\infty)$ shows that temperature of sheet is higher than ambient temperature. Eq. (6.3) is derived by using Rosseland approximation. Expression of variable thermal conductivity is defined as $K^* = K(1 + \epsilon\theta)$ where K denotes the uniform thermal conductivity, σ^* Stefan-Boltzmann constant, K_1 mean absorption coefficient and θ dimensionless fluid temperature.

The above equations are solved subject to the following boundary conditions

$$u = U_w(x) = ax, \quad v = 0, \quad T = T_w(x) \text{ at } y = 0, \quad (6.4)$$

$$u \longrightarrow U_\infty(x) = bx, \quad T \longrightarrow T_\infty \text{ as } y \longrightarrow \infty. \quad (6.5)$$

Considering

$$\eta = \left(\frac{a}{\nu}\right)^{1/2} y, \quad (a\nu)^{1/2} x f(\eta) = \psi, \quad \theta(\eta) = \frac{T - T_\infty}{T_w - T_\infty}, \quad (6.6)$$

$$u = \frac{\partial \psi}{\partial y}, \quad v = -\frac{\partial \psi}{\partial x}. \quad (6.7)$$

The continuity equation (6.1) is automatically satisfied and Eqs. (6.2) and (6.3) yields

$$f''' - f'^2 + f f'' (1 + M\beta) - M f' + \beta (2f f' f'' - f^2 f''') + (\epsilon^2 + M\epsilon) \pm \lambda_1 \theta = 0, \quad (6.8)$$

$$\epsilon^* \theta'^2 + \left(1 + \frac{4}{3} R_d\right) ((1 + \epsilon^* \theta) \theta'' + \text{Pr} f \theta' - \text{Pr} S \theta) = 0, \quad (6.9)$$

The boundary conditions are given by

$$f(0) = 0, \quad f'(0) = 1, \quad f'(\eta) \rightarrow \epsilon \quad \text{as } \eta \rightarrow \infty, \quad (6.10)$$

$$\theta(0) = 1, \quad \theta(\eta) \rightarrow 0, \quad \text{as } \eta \rightarrow \infty, \quad (6.11)$$

where prime stands for the derivative with respect to η , the Hartman number $M = \sigma B_0^2 / \rho a$, the Deborah number $\beta = \lambda a$, the ratio of rate constants $\epsilon = b/a$, $R_d = \frac{4\sigma^* T_\infty^3}{\alpha K^*}$ the radiation parameter, the buoyancy or mixed convection parameter $\lambda_1 = Gr_x / \text{Re}_x^2$, $Gr_x = g\beta(T - T_\infty)x^3/\nu^2$ the local Grashof number, $\text{Re}_x = U_w x / \nu$ the local Reynolds number and the Prandtl number $\text{Pr} = \epsilon / \mu c_p$. Here a and b signify the rates of dimension time^{-1} . Local Nusselt number is defined as

$$Nu_x = \frac{x q_w}{K(T_w - T_\infty)}, \quad q_w = -K \left(\frac{\partial T}{\partial y} \right)_{y=0}. \quad (6.12)$$

6.2 Homotopy analysis solutions

In order to obtain the series solution, the leading expressions of f and θ are easily defined by the set of base functions $\{\eta^k \exp(-n\eta) | k \geq 0, n \geq 0\}$ in the following types

$$f(\eta) = a_{0,0}^0 + \sum_{n=0}^{\infty} \sum_{k=0}^{\infty} a_{m,n}^k \eta^k \exp(-\eta k), \quad \theta(\eta) = \sum_{n=0}^{\infty} \sum_{k=0}^{\infty} b_{m,n}^k \eta^k \exp(-\eta k), \quad (6.13)$$

where $a_{m,n}^k$ and $b_{m,n}^k$ are the coefficients. For the sake of HAM solutions, the following initial guesses and auxiliary linear operators are selected as follows

$$f_0 = \epsilon \eta + (1 - \epsilon)(1 - \exp(-\eta)), \quad \theta_0 = \exp(-\eta), \quad (6.14)$$

$$L_f[f(\eta)] = \frac{d^3 f}{d\eta^3} - \frac{df}{d\eta}, \quad L_\theta[\theta(\eta)] = \frac{d^2 \theta}{d\eta^2} - \theta. \quad (6.15)$$

The operators have the following properties

$$L_f[C_1 + C_2 \exp(-\eta) + C_3 \exp(\eta)] = 0, \quad L_\theta[C_4 \exp(\eta) + C_5 \exp(-\eta)] = 0, \quad (6.16)$$

in which $C_i (i = 1 \text{ to } 5)$ are the integral constants. Such integral constants can be determined using the boundary conditions. We construct the problems at zeroth and m^{th} orders. These are

$$(1-p)L_f[\hat{f}(\eta; p) - f_0(\eta)] = ph_f N_f[\hat{f}(\eta; p), \hat{\theta}(\eta; p)], \quad (6.17)$$

$$(1-p)L_\theta[\hat{\theta}(\eta; p) - \theta_0(\eta)] = ph_\theta N_\theta[\hat{\theta}(\eta; p), \hat{f}(\eta; p)], \quad (6.18)$$

$$\hat{f}(0; p) = 0, \quad \frac{\partial \hat{f}}{\partial \eta}(0; p) = 1, \quad \hat{\theta}(0; p) = 1, \quad \eta = 0, \quad (6.19)$$

$$\frac{\partial \hat{f}}{\partial \eta}(\eta) = \epsilon, \quad \hat{\theta}(\eta) \rightarrow 0, \quad \text{when } \eta \rightarrow \infty, \quad (6.20)$$

$$L_f[f_m(\eta) - \chi_m f_{m-1}(\eta)] = h_f R_{f,m}(\eta), \quad (6.21)$$

$$L_\theta[\theta_m(\eta) - \chi_m \theta_{m-1}(\eta)] = h_\theta R_{\theta,m}(\eta), \quad (6.22)$$

$$f_m(0) = 0, \quad f'_m(0) = 0, \quad \theta_m(0) = 0, \quad (6.23)$$

$$f'_m(\eta) = 0, \quad \theta_m(\eta) = 0, \quad \text{when } \eta \longrightarrow \infty, \quad (6.24)$$

where $p \in [0, 1]$ is the embedding parameter and h_f and h_θ the nonzero auxiliary parameters. The nonlinear operators are

$$\begin{aligned} N_f [\tilde{f}(\eta; p)] &= \frac{\partial^3 f}{\partial \eta^3} - \left(\frac{\partial f}{\partial \eta} \right)^2 + f \frac{\partial^2 f}{\partial \eta^2} (1 + M^2 \beta) - M^2 \frac{\partial f}{\partial \eta} \\ &\quad + \beta \left(2f \frac{\partial f}{\partial \eta} \frac{\partial^2 f}{\partial \eta^2} - f^2 \frac{\partial^3 f}{\partial \eta^3} \right) + (\epsilon^2 + M\epsilon) \pm \lambda_1 \theta, \end{aligned} \quad (6.25)$$

$$N_\theta [\hat{\theta}(\eta; p)] = \frac{\partial^2 \theta}{\partial \eta^2} \left(1 + \frac{4}{3} R_d \right) (1 + \epsilon^* \theta) + \epsilon^* \left(\frac{\partial \theta}{\partial \eta} \right)^2 + \text{Pr} f \frac{\partial \theta}{\partial \eta} + \text{Pr} S \theta, \quad (6.26)$$

$$\begin{aligned} R_{f,m}(\eta) &= \frac{\partial^3 f_{m-1}}{\partial \eta^3} - \sum_{i=0}^{m-1} \frac{\partial f_{m-i-1}}{\partial \eta} \frac{\partial f_i}{\partial \eta} + (1 + M^2 \beta) \sum_{i=0}^{m-1} f_i \frac{\partial^2 f_{m-i-1}}{\partial \eta^2} - M^2 \frac{\partial f_{m-1}}{\partial \eta} \\ &\quad + \beta \sum_{i=0}^{m-1} f_{m-i-1} \sum_{l=0}^i \left(2 \frac{\partial f_{i-l}}{\partial \eta} \frac{\partial^2 f_l}{\partial \eta^2} - f_{i-l} \frac{\partial^3 f_l}{\partial \eta^3} \right) + [\epsilon^2 + M\epsilon] (1 - \chi_m) \pm \lambda_1 \theta, \end{aligned} \quad (6.27)$$

$$R_{\theta,m}(\eta) = \epsilon^* \left(\frac{\partial \theta_{m-1}}{\partial \eta} \right)^2 + \sum_{i=0}^{m-1} (1 + \epsilon^* \theta_i) \left(1 + \frac{4}{3} R_d \right) \frac{\partial^2 \theta_{m-i-1}}{\partial \eta^2} + \text{Pr} \sum_{i=0}^{m-1} \left(f_{m-i-1} \frac{\partial \theta_i}{\partial \eta} + S \theta_i \right). \quad (6.28)$$

The definition of χ_m is defined as

$$\chi_m = \begin{cases} 0, & m = 1, \\ 1, & m > 1. \end{cases}$$

For $p = 0$ and $p = 1$, one obtains

$$\hat{f}(\eta, 0) = f_0(\eta), \quad \hat{\theta}(\eta, 0) = \theta_0(\eta), \quad (6.29)$$

$$\hat{f}(\eta, 1) = f(\eta), \quad \hat{\theta}(\eta, 1) = \theta(\eta). \quad (6.30)$$

According to the Taylor's series we have

$$f(\eta; p) = f_0(\eta) + \sum_{m=0}^{\infty} f_m(\eta) p^m, \quad f_m(\eta) = \frac{1}{m!} \frac{\partial^m \hat{f}(\eta, p)}{\partial p^m} \Big|_{p=0}, \quad (6.31)$$

$$\theta(\eta; p) = \theta_0(\eta) + \sum_{m=0}^{\infty} \theta_m(\eta) p^m, \quad \theta_m(\eta) = \frac{1}{m!} \frac{\partial^m \hat{\theta}(\eta, p)}{\partial p^m} \Big|_{p=0}. \quad (6.32)$$

The values of auxiliary parameters \hbar_f and \hbar_θ are chosen in such a way that the Taylor series of $\hat{f}(\eta, p)$ and $\hat{\theta}(\eta, p)$ for $p = 1$. Hence

$$f(\eta) = f_0(\eta) + \sum_{m=1}^{\infty} f_m(\eta), \quad \theta(\eta) = \theta_0(\eta) + \sum_{m=0}^{\infty} \theta_m(\eta). \quad (6.33)$$

General solutions $f_m(\eta)$ and $\theta_m(\eta)$ are given by

$$f_m(\eta) = f_m^*(\eta) + C_1 + C_2 \exp(\eta) + C_3 \exp(-\eta), \quad (6.34)$$

$$\theta_m(\eta) = \theta_m^*(\eta) + C_4 \exp(\eta) + C_5 \exp(-\eta), \quad (6.35)$$

where the constants are determined using the Eqs. (6.23) and (6.24).

6.3 Analysis of solutions

It is well established argument that the convergence and rate of approximation for HAM solutions depend upon the values of involved auxiliary parameters \hbar_f and \hbar_θ . In order to get the admissible values of non-zero auxiliary parameters \hbar_f and \hbar_θ , we plotted the \hbar_f and \hbar_θ -curves at the 20th

order of approximations in Fig. 6.1. The admissible range for h_f and h_θ are $-0.96 \leq h_f \leq -0.1$ and $-1 \leq h_\theta \leq -0.1$. Suitable values of h_f and h_θ are -0.7 respectively.

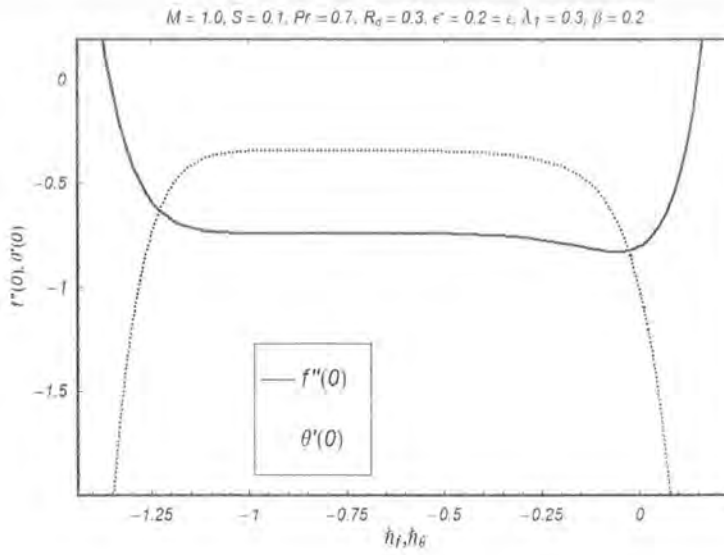


Fig. 6.1. h -curves for 20^{th} order of approximations.

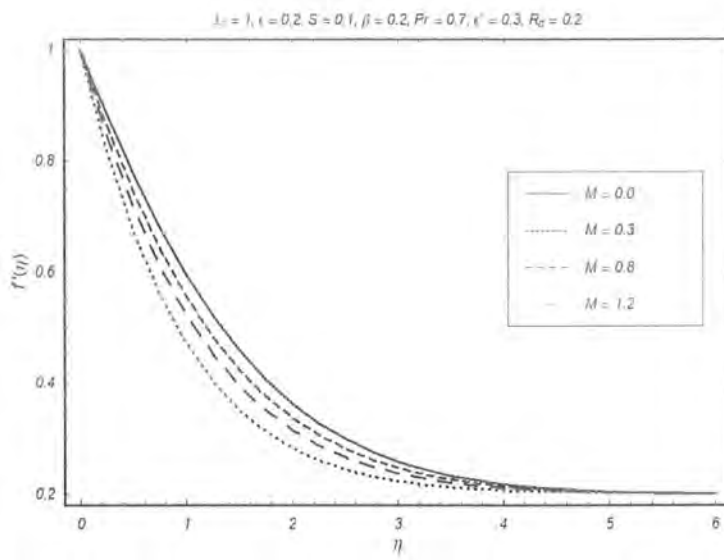


Fig. 6.2. Variation of M on the velocity $f'(\eta)$.

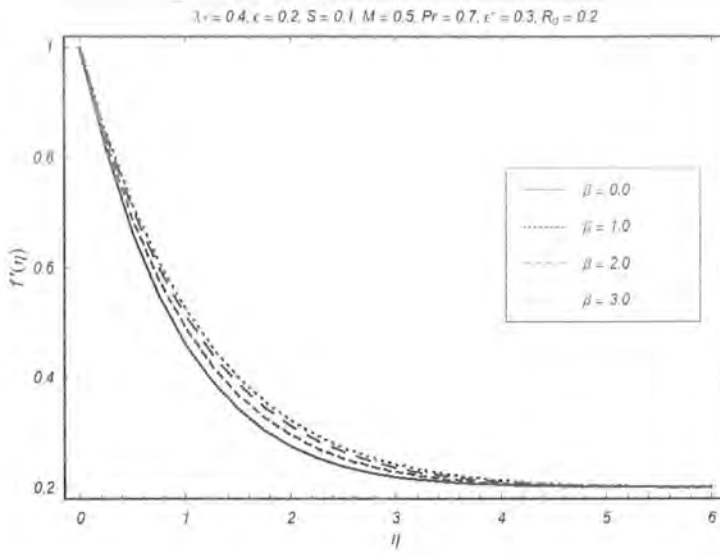


Fig. 6.3. Variation of β on the velocity $f'(\eta)$.

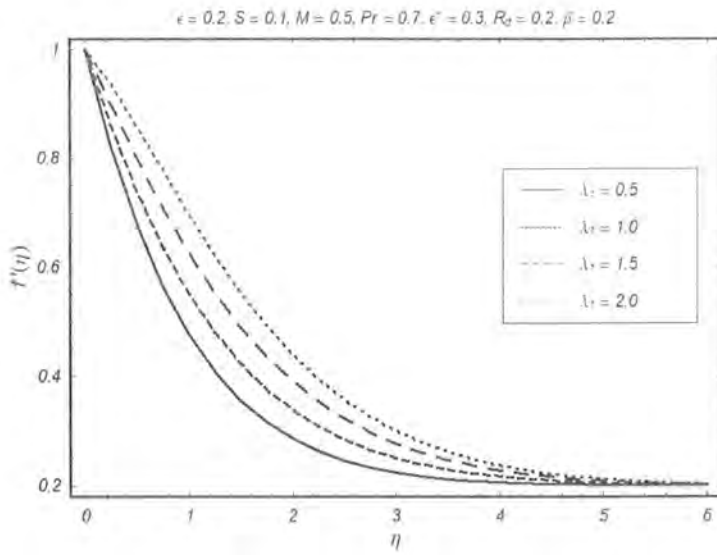


Fig. 6.4. Variation of λ_1 on the velocity $f'(\eta)$.

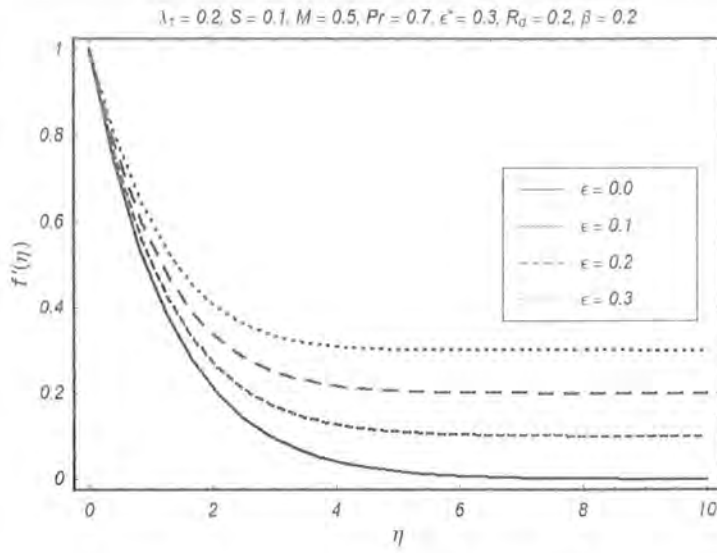


Fig. 6.5. Variation of ϵ on the velocity $f'(\eta)$.

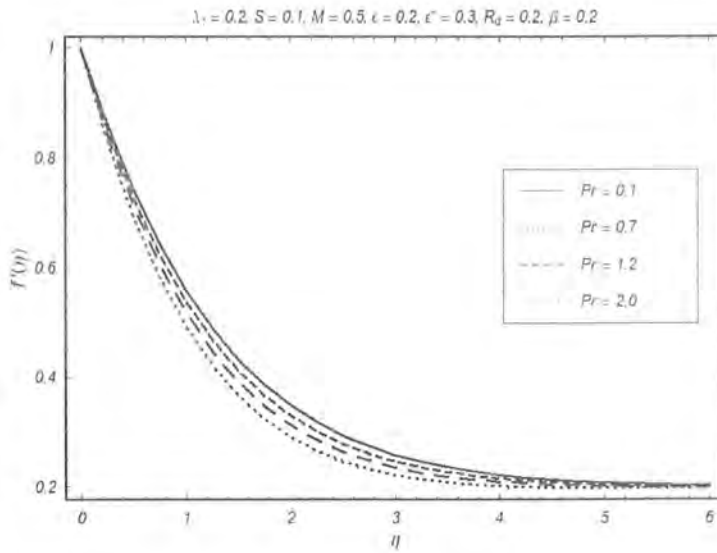


Fig. 6.6. Variation of Pr on the velocity $f'(\eta)$.

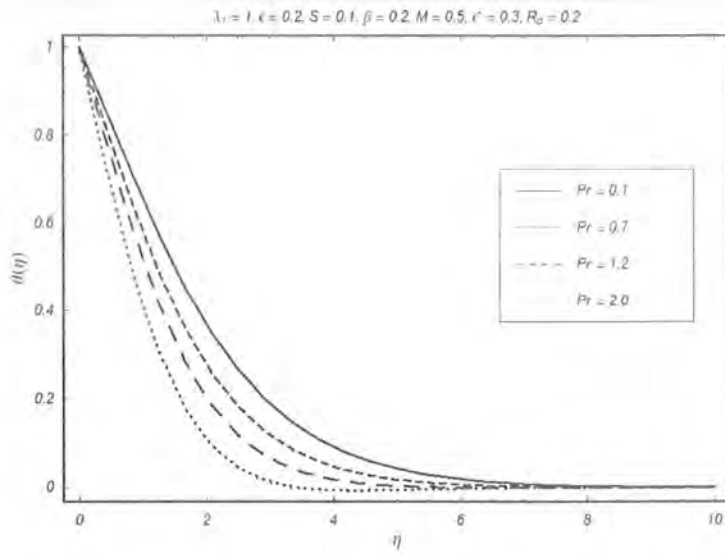


Fig. 6.7. Variation of Pr on the temperature $\theta(\eta)$.

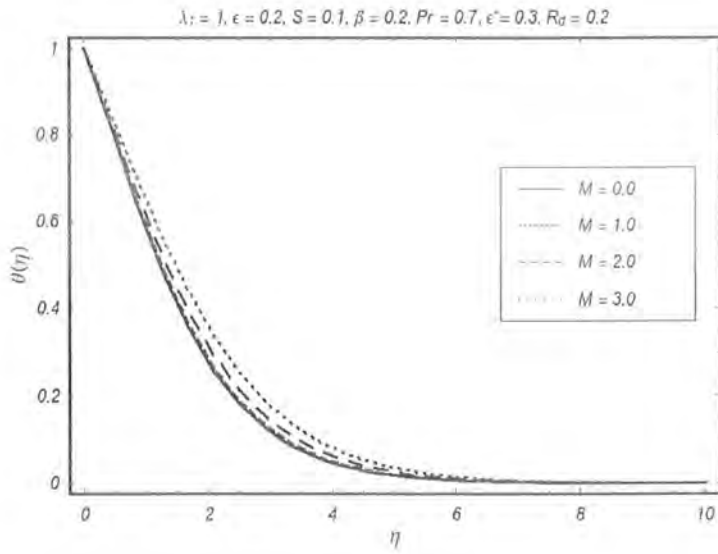


Fig. 6.8. Variation of M on the temperature $\theta(\eta)$.

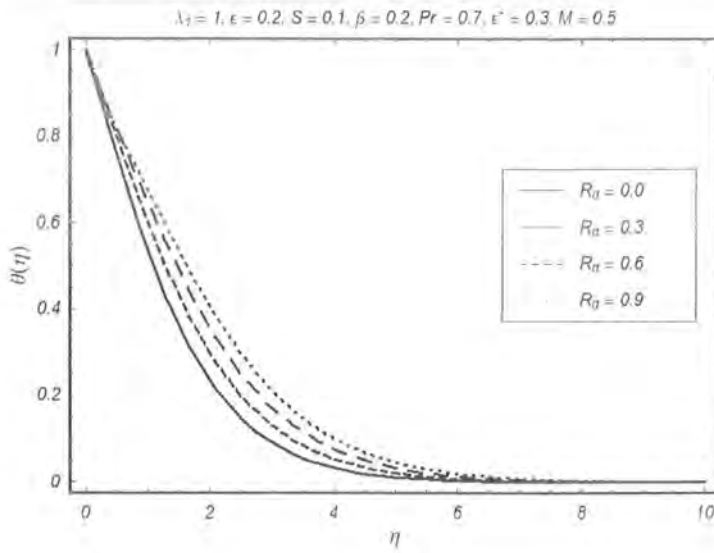


Fig. 6.9. Variation of R_d on the temperature $\theta(\eta)$.

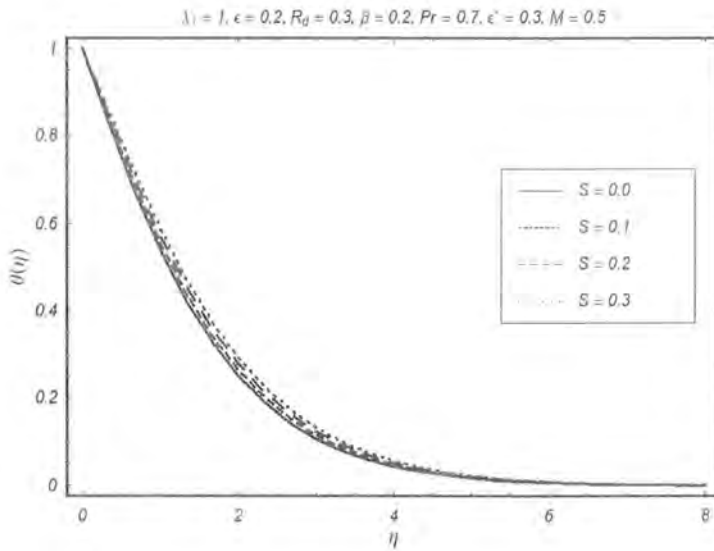


Fig. 6.10. Variation of S on the temperature $\theta(\eta)$.

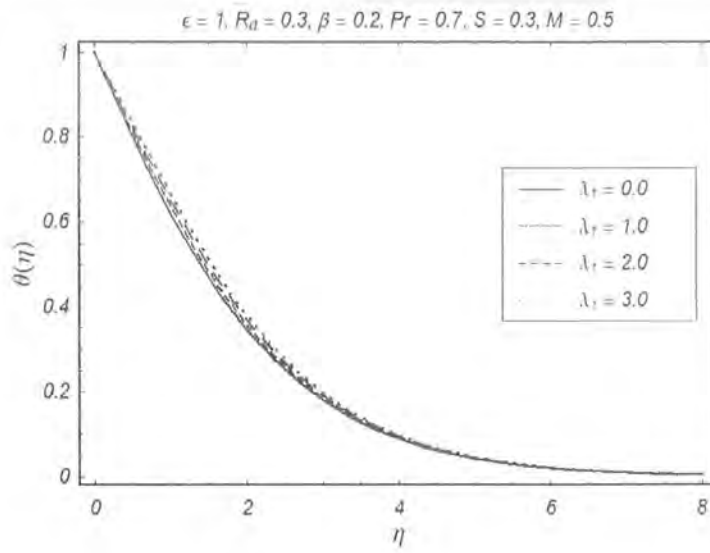


Fig. 6.11. Variation of λ_1 on the temperature $\theta(\eta)$.

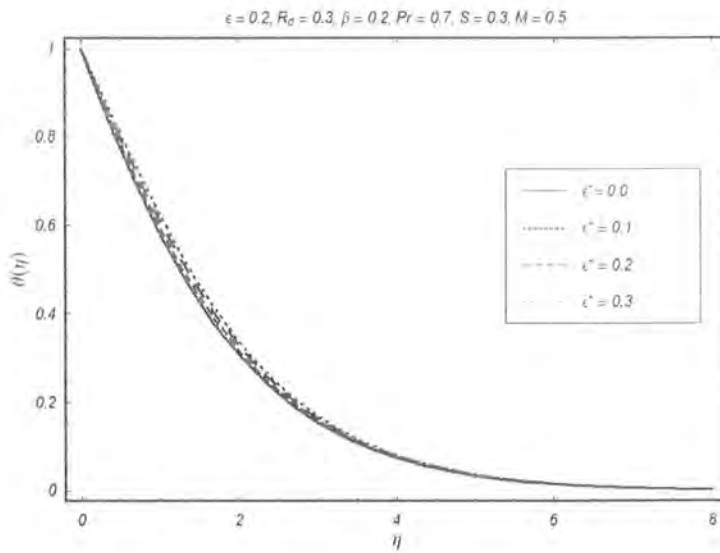


Fig. 6.12. Variation of ϵ^* on the temperature $\theta(\eta)$.

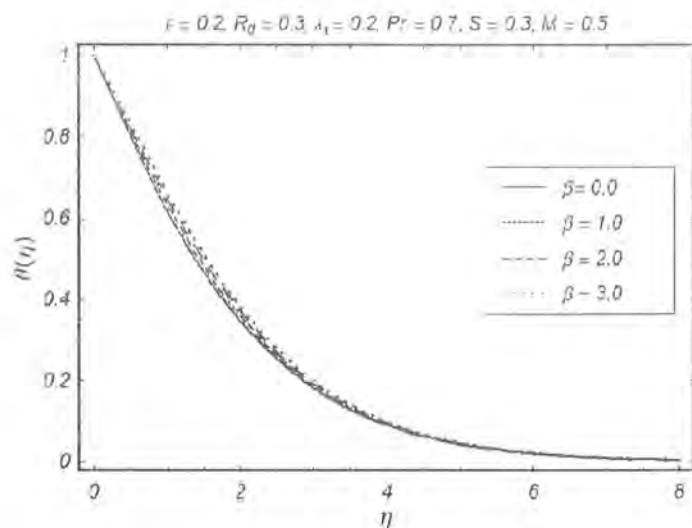


Fig. 6.13. Variation of β on the temperature $\theta(\eta)$.

Table: 6.1. Convergence of HAM solutions for different order of approximations

when $\beta = \epsilon = 0.2 = R_d$, $S = 0.1$, $Pr = 0.7$, $\epsilon^* = 0.3$ and $\lambda_1 = 1.0$.

Order of convergence	$-f''(0)$	$-\theta'(0)$
1	0.87074	0.46333
5	0.74315	0.35061
10	0.73646	0.33929
15	0.73707	0.34012
20	0.73718	0.34033
25	0.73718	0.34033
30	0.73718	0.34033

Table: 6.2. Comparison of $f''(0)$ for different values of α and M when $\beta = 0 = \lambda_1$.

M	$-f''(0)$					
	$\epsilon = 0.1$		$\epsilon = 0.2$		$\epsilon = 0.5$	
	[11]	HAM	[11]	HAM	[11]	HAM
0.0	0.969386	0.969386	0.9181069	0.9181069	0.667263	0.667263
0.1	0.97350851	0.973509	0.921466	0.921466	0.666102	0.666102
0.5	1.067898	1.067898	1.00469	1.004692	0.71189085	0.711887
1.0	1.321111	1.321111	0.2156222	0.215587	0.83215208	0.832652
1.5	1.66020742	1.662587	1.50849937	1.508986	1.00168146	1.001253

6.4 Discussion

Our interest here is to analyze the effects of Hartman number M , Deborah number β , local buoyancy parameter λ_1 , parameter ϵ , Prandtl number Pr , thermal radiation R_d , heat source/sink parameter S and ϵ^* the perturbation parameter on velocity f' and temperature θ . Therefore Figs. (6.2 – 6.13) have been plotted. Fig. 6.2 gives the variation of Hartman number M on the flow. It is found that the velocity profile decreases due to increase in Hartman number when $\epsilon < 1$. This is in view of the fact that an increase of M signifies the increase of Lorentz force thereby decreasing the magnitude of velocity. Magnetic field is a powerful mechanism for controlling the momentum of the boundary layer regime flow in actual applications. Hence magnetic field can control flow characteristics. The velocity profile for different values of Deborah number β is plotted in Fig. 6.3. It is observed that boundary layer thickness increases because of an increase in β . The variations of parameters ϵ and λ_1 on the velocity are shown in the Figs. 6.4 and 6.5. It is found that f' is an increasing function of both parameters ϵ and λ_1 . When $\epsilon = 0$ there is no stagnation point flow. Infact increasing values of λ_1 corresponds to the stronger buoyancy force which causes an increase in flow velocity. Fig.

6.6 describes the effects of Pr on f' . Prandtl number Pr decreases the velocity profile. Infact an increase in the Prandtl number leads to an increase in fluid viscosity which causes a decrease in the flow velocity.

The effects of Prandtl number Pr on the temperature is shown in Fig. 6.7. It is revealed from this Fig. that the thermal boundary layer thickness is reduced when Pr increases. A higher Prandtl number fluid has a thinner thermal boundary layer and this increases the gradient of the temperature. Figs. 6.8 and 6.9 are presented for the variations of M and radiation parameter R_d . These Figs. depict that the temperature profile increases by increasing M and R_d . Thus radiation should be minimized to have the cooling process at a faster rate. The increasing frictional drag due to the Lorentz force is responsible for increasing the thermal boundary layer thickness. Fig. 6.10 elucidates that with the increase in the value of S , the temperature profile increases. Further, we conclude that the effect of volumetric rate of heat generation/absorption reduces the temperature θ for low Prandtl number. Effects of λ_1 and ϵ^* on the temperature are displayed in the Figs. 6.11 and 6.12. These Figs. indicate that the temperature profile decreases when there is an increase in λ_1 and has opposite behavior for ϵ^* . Fig. 6.13 elucidates the influence of β on temperature field θ . It is obvious that temperature field increases by increasing β . Table 6.1 is displayed to examine the convergence of series solution which indicates that convergence is achieved at 20^{th} order of approximations. Tables 6.2 shows the comparison of the values of HAM solution with the numerical solution in the limiting cases.

Chapter 7

MHD stagnation point flow of Maxwell fluid with radiation effects

Two-dimensional stagnation point flow of Maxwell fluid over a stretched surface with heat transfer is examined in this chapter. The fluid is electrically conducting in the presence of uniform applied magnetic field. Radiation effect in the energy equation is taken into account. The arising nonlinear problem is solved by a homotopy analysis method (HAM). Convergence of the series solutions is checked. The values of skin friction coefficient and local Nusselt number are computed and discussed.

7.1 Problem Statement

We consider the stagnation point flow of magnetohydrodynamic (MHD) fluid bounded by a stretching surface. A magnetic field of strength B_0 is exerted in the y -direction. The magnetic Reynold number of the flow is taken to be small enough so that the induced magnetic field is negligible. The electric field is negligible. Here we consider $T_w(x) = T_\infty + cx^n$ as the prescribed temperature of sheet (where T_∞ is taken as ambient fluid temperature), c and n are constants with $c > 0$.

(heated surface). The equations which can govern the present flow are

$$\frac{\partial u}{\partial x} + \frac{\partial v}{\partial y} = 0, \quad (7.1)$$

$$u \frac{\partial u}{\partial x} + v \frac{\partial u}{\partial y} + \lambda_1 \left[u^2 \frac{\partial^2 u}{\partial x^2} + v^2 \frac{\partial^2 u}{\partial y^2} + 2uv \frac{\partial^2 u}{\partial x \partial y} \right] = U_\infty(x) \frac{dU_\infty}{dx} + \nu \frac{\partial^2 u}{\partial y^2} + \frac{\sigma B_0^2}{\rho} \left(U_\infty - u - \lambda_1 v \frac{\partial u}{\partial y} \right), \quad (7.2)$$

$$\rho c_p \left[u \frac{\partial T}{\partial x} + v \frac{\partial T}{\partial y} \right] = \frac{\partial}{\partial y} \left[\left(\frac{16\sigma^* T_\infty^3}{3k^*} + \alpha \right) \frac{\partial T}{\partial y} \right], \quad (7.3)$$

in which the velocity components u and v are taken along x -and y -directions. ν , ρ , λ_1 , σ , c_p , α and T are the kinematic viscosity, the density of fluid, relaxation time, the electrical conductivity, specific heat having constant pressure, the thermal diffusivity and the temperature of fluid. Note that Eq. (7.2) holds only if the velocity of outer flow $U_\infty(x)$ is linear dependent on x coordinate. The simplified form of Eq. (7.3) for radiative heat flux has been achieved after applying Rosseland approximation. The relevant boundary conditions for the present flow are

$$u = U_w(x) = ax, \quad v = 0, \quad T = T_w(x) \text{ at } y = 0, \quad (7.4)$$

$$u \longrightarrow U_\infty(x) = bx, \quad T \longrightarrow T_\infty, \quad \text{as } y \longrightarrow \infty, \quad (7.5)$$

$$\eta = \left(\frac{a}{\nu} \right)^{1/2} y, \quad f(\eta) = \frac{\psi}{(a\nu)^{1/2} x}, \quad \theta(\eta) = \frac{T - T_\infty}{T_w - T_\infty} \quad (7.6)$$

Letting equation (7.1) is satisfied while Eqs. (7.2) – (7.5) are reduced as

$$f''' - f'^2 + ff''(1 + M\beta) - Mf' + \beta(2ff'f'' - f^2f''') + (\epsilon^2 + M\epsilon) = 0, \quad (7.7)$$

$$\left(1 + \frac{4}{3}R_d \right) \theta'' + \text{Pr}(f\theta' - n f'\theta) = 0, \quad (7.8)$$

$$f(0) = 0, \quad f'(0) = 1, \quad \theta(0) = 1, \quad (7.9)$$

$$f'(\eta) \rightarrow \epsilon, \quad \theta(\eta) \rightarrow 0, \quad \text{as } \eta \rightarrow \infty, \quad (7.10)$$

in which prime points out the derivative with respect to the variable η , M the magnetic parameter, ϵ the velocity ratio parameter, R_d the radiation parameter and Pr the Prandtl number. The definitions of these variables are

$$M = \sigma B_0^2 / \rho a, \quad \epsilon = b/a, \quad R_d = \frac{4\sigma^*}{\alpha K^*} T_\infty^3, \quad \text{Pr} = \alpha / \mu c_p. \quad (7.11)$$

The mathematical expressions of physical quantities such as skin friction coefficient and local Nusselt number are

$$C_f = \frac{\tau_w}{\rho U^2 / 2}, \quad Nu_x = \frac{x q_w}{k(T_w - T_\infty)}. \quad (7.12)$$

Here τ_w and q_w are the wall skin friction and wall heat flux i.e.

$$\tau_w = \mu \left(\frac{\partial u}{\partial y} \right)_{y=0}, \quad q_w = -k \left(\frac{\partial T}{\partial y} \right)_{y=0}. \quad (7.13)$$

In dimensionless form we have

$$\frac{1}{2} C_f \text{Re}_x^{1/2} = f''(0), \quad Nu_x / \text{Re}_x^{1/2} = -\theta'(0), \quad (7.14)$$

where the local Reynolds number is $\text{Re}_x = U_w x / \nu$.

7.2 Solution by Homotopy Analysis Method

The set of base functions are

$$\{\eta^k \exp(-n\eta), k \geq 0, n \geq 0\}, \quad (7.15)$$

lead to the following expressions

$$f(\eta) = a_{0,0}^0 + \sum_{n=0}^{\infty} \sum_{k=0}^{\infty} a_{m,n}^k \eta^k \exp(-n\eta), \quad (7.16)$$

$$\theta(\eta) = \sum_{n=0}^{\infty} \sum_{k=0}^{\infty} b_{m,n}^k \eta^k \exp(-n\eta), \quad (7.17)$$

in which $a_{m,n}^k$ and $b_{m,n}^k$ are the coefficients.

The initial guesses and linear operators are as follows

$$f_0(\eta) = (1 - \epsilon)(1 - \exp(-\eta)) + \epsilon\eta, \quad (7.18)$$

$$\theta_0(\eta) = \exp(-\eta) + \frac{\eta}{2}\exp(-\eta), \quad (7.19)$$

$$L_f[f(\eta)] = \frac{d^3 f}{d\eta^3} - \frac{df}{d\eta}, \quad (7.20)$$

$$L_\theta[\theta(\eta)] = \frac{d^2 \theta}{d\eta^2} - \theta. \quad (7.21)$$

The relations which satisfies the following linear operators are

$$L_f [C_1 + C_2 \exp(-\eta) + C_3 \exp(\eta)] = 0, \quad (7.22)$$

$$L_\theta [C_4 \exp(\eta) + C_5 \exp(-\eta)] = 0. \quad (7.23)$$

In above Eqs. $C_1 - C_5$ are the arbitrary constants. Now the expressions of zeroth and m^{th} order problems are

$$(1 - p)L_f[\tilde{f}(\eta; p) - f_0(\eta)] = p\hbar_f N_f[\tilde{f}(\eta; p), \tilde{\theta}(\eta; p)], \quad (7.24)$$

$$(1 - p)L_\theta[\tilde{\theta}(\eta; p) - \theta_0(\eta)] = p\hbar_\theta N_\theta[\tilde{\theta}(\eta; p), \tilde{f}(\eta; p)], \quad (7.25)$$

$$\tilde{f}(0; p) = 0, \quad \frac{\partial \tilde{f}}{\partial \eta}(0; p) = 1, \quad \tilde{\theta}(0; p) = 1, \quad (7.26)$$

$$\frac{\partial \tilde{f}}{\partial y}(\eta) \longrightarrow \epsilon, \quad \theta(\eta) \longrightarrow 0, \quad \text{when} \quad \eta \longrightarrow \infty, \quad (7.27)$$

$$L_f[f_m(\eta) - \chi_m f_{m-1}(\eta)] = h_f R_{f,m}(\eta), \quad (7.28)$$

$$L_\theta[\theta_m(\eta) - \chi_m \theta_{m-1}(\eta)] = h_\theta R_{\theta,m}(\eta), \quad (7.29)$$

$$f_m(0) = 0, \quad f'_m(0) = 0, \quad \theta_m(0) = 0, \quad (7.30)$$

$$f'_m(\eta) = 0, \quad \theta_m(\eta) = 0, \quad \text{when} \quad \eta \longrightarrow \infty, \quad (7.31)$$

$$\begin{aligned} N_f[\tilde{f}(\eta, p)] &= \frac{\partial^3 f}{\partial \eta^3} - \left(\frac{\partial f}{\partial \eta} \right)^2 + f \frac{\partial^2 f}{\partial \eta^2} (1 + M\beta) - M \frac{\partial f}{\partial \eta} \\ &\quad + \beta \left(2f \frac{\partial f}{\partial \eta} \frac{\partial^2 f}{\partial \eta^2} - f^2 \frac{\partial^3 f}{\partial \eta^3} \right) + (\epsilon^2 + M\epsilon), \end{aligned} \quad (7.32)$$

$$N_\theta[\tilde{\theta}(\eta; p)] = \left(1 + \frac{4}{3} R_d \right) \frac{\partial^2 \theta}{\partial \eta^2} + \text{Pr} \left(f \frac{\partial \theta}{\partial \eta} - n \frac{\partial f}{\partial \eta} \theta \right). \quad (7.33)$$

$$\begin{aligned} R_{f,m}(\eta) &= \frac{\partial^3 f_{m-1}}{\partial \eta^3} - \sum_{i=0}^{m-1} \frac{\partial f_{m-i-1}}{\partial \eta} \frac{\partial f_i}{\partial \eta} + (1 + M\beta) \sum_{i=0}^{m-1} f_i \frac{\partial^2 f_{m-i-1}}{\partial \eta^2} - M \frac{\partial f_{m-1}}{\partial \eta} \\ &\quad + \beta \sum_{i=0}^{m-1} f_{m-i-1} \sum_{l=0}^i \left(2 \frac{\partial f_{i-l}}{\partial \eta} \frac{\partial^2 f_l}{\partial \eta^2} - f_{i-l} \frac{\partial^3 f_l}{\partial \eta^3} \right) + (\epsilon^2 + M\epsilon) (1 - \chi_m), \end{aligned} \quad (7.34)$$

$$R_{\theta,m}(\eta) = \left(1 + \frac{4}{3} R_d \right) \frac{\partial^2 \theta_{m-1}}{\partial \eta^2} + \text{Pr} \sum_{i=0}^{m-1} \left(f_{m-i-1} \frac{\partial \theta_i}{\partial \eta} - n \frac{\partial f_{m-1-i}}{\partial \eta} \theta_i \right), \quad (7.35)$$

where p , h_f and h_θ indicate the embedding and auxiliary parameters. Further

$$\tilde{f}(\eta, 0) = f_0(\eta), \quad \tilde{\theta}(\eta, 0) = \theta_0(\eta), \quad (7.36)$$

$$\tilde{f}(\eta, 1) = f(\eta), \quad \tilde{\theta}(\eta, 1) = \theta(\eta). \quad (7.37)$$

It is noticed that when p increases from 0 to 1 then $\tilde{f}(\eta, p)$, $\tilde{\theta}(\eta, p)$ approach to $f_0(\eta)$, $\theta_0(\eta)$ and to

the final solutions $f(\eta)$ and $\theta(\eta)$ respectively. Taylor series of $\hat{f}(\eta; p)$ and $\hat{\theta}(\eta; p)$ converge at $p = 1$.

By Taylor series

$$f(\eta) = f_0(\eta) + \sum_{m=1}^{\infty} f_m(\eta), \quad (7.38)$$

$$\theta(\eta) = \theta_0(\eta) + \sum_{m=1}^{\infty} \theta_m(\eta), \quad (7.39)$$

$$f_m(\eta) = \frac{1}{m!} \frac{\partial^m \hat{f}(\eta; p)}{\partial p^m} \Big|_{p=0}, \quad (7.40)$$

$$\theta_m(\eta) = \frac{1}{m!} \frac{\partial^m \hat{\theta}(\eta; p)}{\partial p^m} \Big|_{p=0}. \quad (7.41)$$

The general solutions are computed as follows:

$$f_m(\eta) = f_m^*(\eta) + C_1 + C_2 \exp(\eta) + C_3 \exp(-\eta), \quad (7.42)$$

$$\theta_m(\eta) = \theta_m^*(\eta) + C_4 \exp(\eta) + C_5 \exp(-\eta), \quad (7.43)$$

where f_m^* and θ_m^* are the special solutions. With the use of boundary conditions one finds that

$$C_2 = C_4 = 0, \quad C_3 = \frac{\partial f_m^*}{\partial \eta}(0), \quad C_1 = -C_3 - f_m^*(0), \quad C_5 = \theta_m^*(0), \quad (7.44)$$

7.3 Analysis of solutions

For convergence we plot the h -curves at 18^{th} order of approximations. The admissible values of non-zero auxiliary parameters of $f''(0)$ and $\theta'(0)$ are shown in the Figs. 7.1 and 7.2. The acceptable values of h_f and h_θ are $-0.81 \leq h_f \leq -0.46$ and $1.5 \leq h_\theta \leq -0.2$. The series converge in the region when $h_f = -0.7$ and $h_\theta = -0.8$. Table 7.1 depicts that 10^{th} order approximations are sufficient for the convergent series solutions.

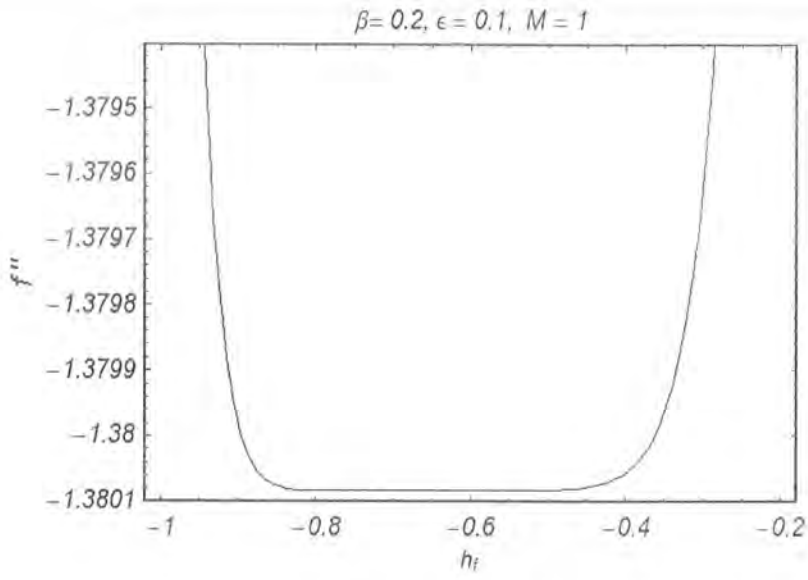


Fig. 7.1. h -curves for 18th order of approximations.

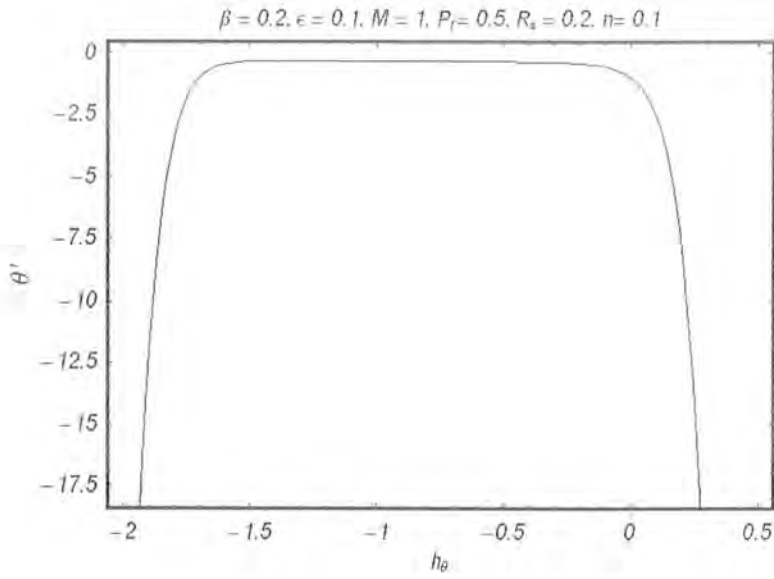


Fig. 7.2. h_θ -curves for 18th order of approximations.

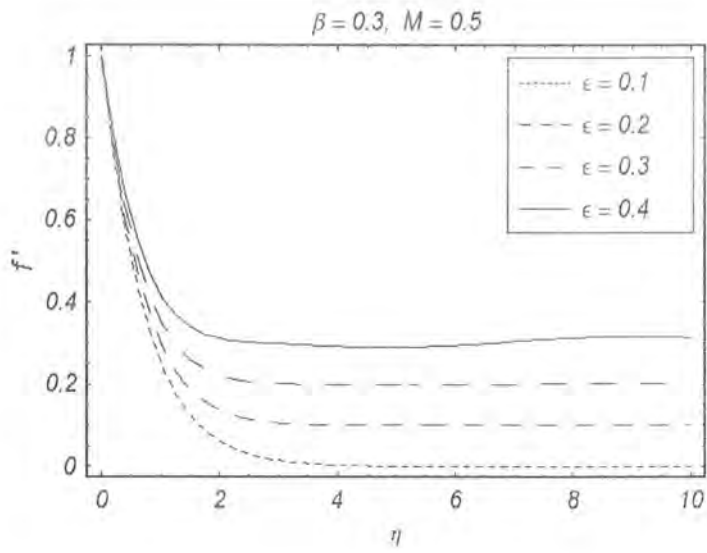


Fig. 7.3. Velocity profile $f'(\eta)$ vs η for different values of ϵ .

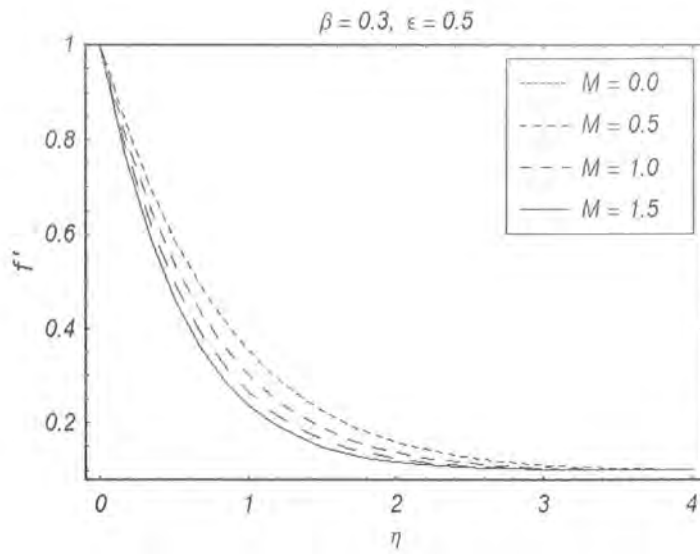


Fig. 7.4. Velocity profile $f'(\eta)$ vs η for different values of M .

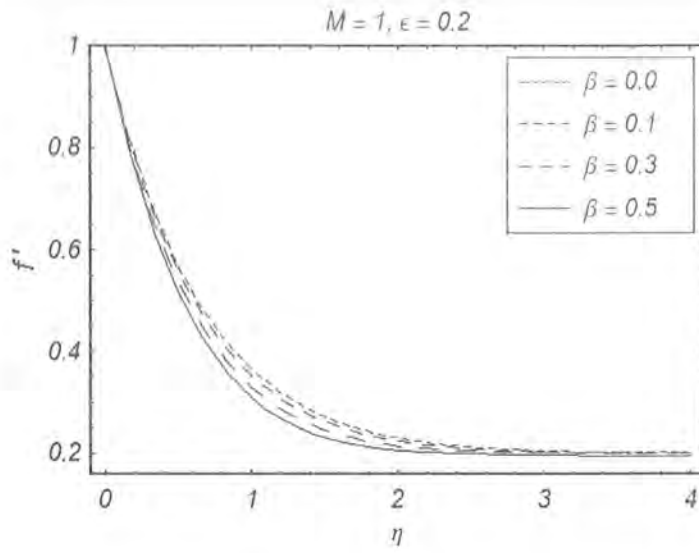


Fig. 7.5. Velocity profile $f'(\eta)$ vs η for different values of β .

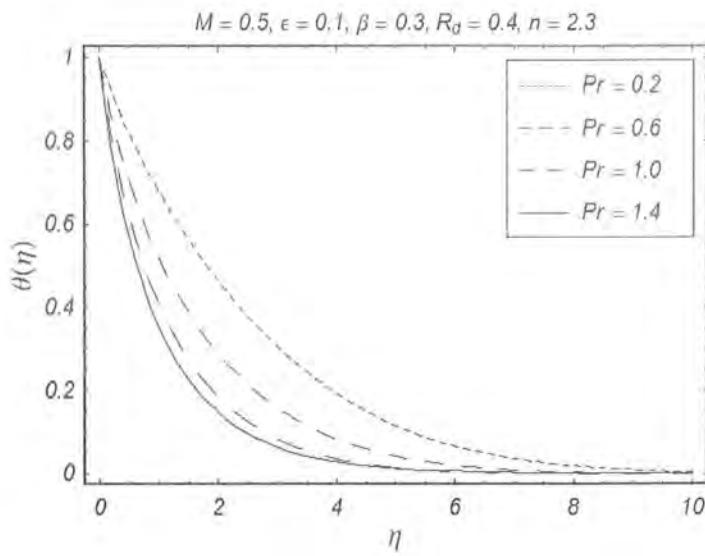


Fig. 7.6. Temperature $\theta(\eta)$ vs η for different values of Pr .

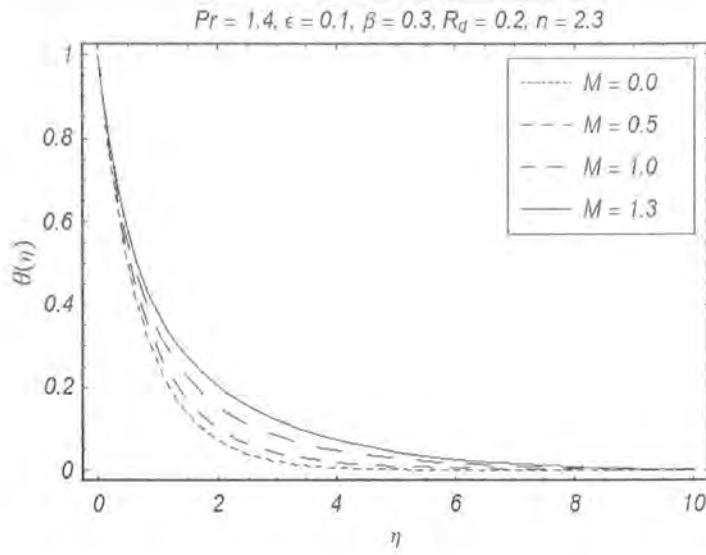


Fig. 7.7. Temperature $\theta(\eta)$ vs η for various values of M .

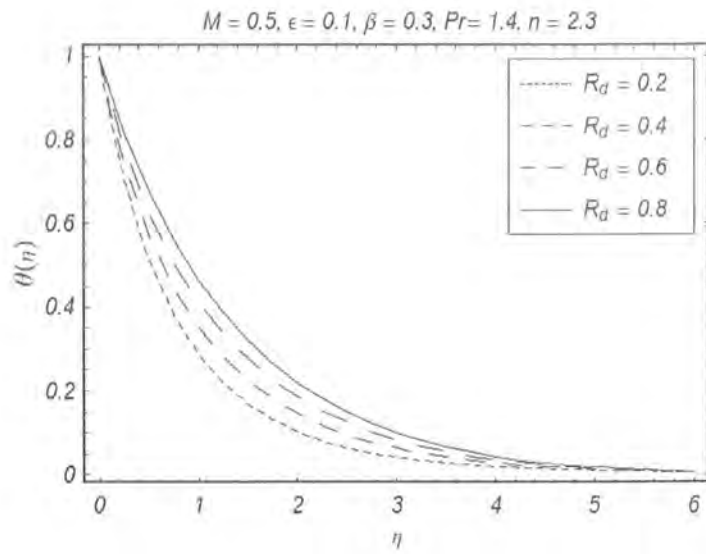


Fig. 7.8. Temperature $\theta(\eta)$ vs η for various values of R_d .

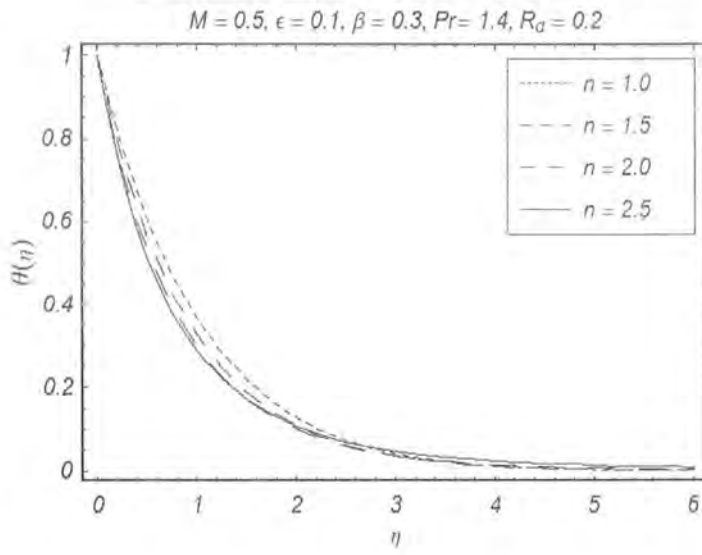


Fig. 7.9. Temperature $\theta(\eta)$ vs η for various values of n .

Table: 7.1. Convergence of HAM solution at different order of approximations

when $M = 1$, $\beta = 0.2$, $Pr = 1.1$, $R_d = 0.4$, $\epsilon = 0.1$ and $n = 2$.

Order of approximation	$-f''(0)$	$-\theta'(0)$
1	1.32021	1.21567
2	1.35615	0.96209
5	1.37975	1.01866
8	1.38008	1.01632
10	1.38008	1.01639
15	1.38008	1.01640
20	1.38008	1.01640
25	1.38008	1.01640
30	1.38008	1.01640
35	1.38008	1.01640
40	1.38008	1.01640

Table: 7.2. Values of $-\theta'(0)$ for some values of n, M, Pr, R_d

when $\beta = 0.2$ and $\epsilon = 0.1$.

n	M	Pr	R_d	$-\theta'(0)$
1.3	0.5	1.1	0.2	1.18269
1.5				1.03886
1.7				1.09783
2.0				1.18269
2.1				1.21010
2.3				1.26369
2.5				1.31577
1.3	0.5			0.97775
	0.7			0.96406
	1.0			0.94546
	1.3			0.92881
	1.5			0.91862
2.0	0.5		0.0	1.36690
			0.2	1.18269
			0.4	1.05005
			0.5	0.99639
			0.6	0.94903
			0.7	0.90685
		1.1	0.2	1.18269
		1.3		1.31045
		1.5		1.42927
		1.7		1.54077

Table: 7.3. Comparison of local Nusselt number $-\theta'(0)$ for some values of M , Pr and n when $R_d = \beta = \epsilon = 0 = S_f = S_T$.

M	Pr	n	HAM [5]	$-\theta'(0)$
0.0	2.0	0.1	0.981991	0.981707
0.3			0.950257	0.950258
0.5			0.931430	0.931430
0.8			0.905665	0.905665
1.0			0.889917	0.889855
0.5	1.0	0.2	0.62569	0.625689
	1.1		0.669087	0.669087
	1.3		0.750773	0.750773
	1.5		0.82675	0.82675
	2.0		0.997713	0.997713
0.5	1.0	0.1	0.58183	0.58183
		0.3	0.66843	0.66843
		0.5	0.750784	0.750782
		1.0	0.94090	0.94089
		3.0	1.55041	1.55041
		5.0	2.02104	2.02104

7.4 Graphical results and discussion

In this section Figs. 7.3 and 7.4 describe the effects of ϵ and the magnetic parameter M on f' . Fig. 7.3 shows that by increasing the value of ϵ the boundary layer thickness increases whereas Fig. 7.4 shows the opposite behavior for increasing M . Table 7.2 represents the values of $-\theta'(0)$ for different values of n , Hartman number M , Prandtl number Pr and radiation number R_d when $\beta = 0.2$ and

$\epsilon = 0.1$. Table 7.3 shows the comparison of Nusselt number given in the study [5].

Fig. 7.5 is plotted for different values of Deborah number β on f' . Here we can observe that boundary layer thickness for f' decreases when β increases. The variations of M , Pr , n and R_d on θ have been shown in the Figs. 7.6 – 7.9. The temperature profile θ decreases by increasing Pr and increases by increasing M (see Figs. 7.6 and 7.7). Fig. 7.8 shows the effects of R_d on θ . Here temperature profile θ increases when R_d increases but Fig. 7.9 shows the opposite behavior.

Chapter 8

Stagnation point flow of an Oldroyd-B fluid with variable thermal conductivity

This chapter is concerned with the boundary layer flow of an Oldroyd-B fluid near the stagnation-point towards the stretching sheet with thermal radiation. Variable thermal conductivity and surface temperature considered. Suitable transformations are invoked to convert the partial differential equations into the ordinary ones. The flow is governed by the Deborah numbers (β_1 and β_2), the velocity ratio (ϵ), the Prandtl number (Pr) and the radiation parameter (R_d). The dimensionless expressions of velocity and temperature are constructed in a series form by a homotopic approach. The results indicate a decrease in the temperature and the thermal boundary layer thickness with an increase in the fluid parameter (β_2). This reduction is associated with the larger heat transfer rate at the stretching sheet. Numerical values of local Nusselt number for different values of parameters are computed.

8.1 Governing problems

We consider the two-dimensional stagnation-point flow of an incompressible Oldroyd-B fluid over a stretching surface with thermal radiation and variable thermal conductivity. We choose a Cartesian coordinate system in such a way that x -axis is along the stretching surface and the y -axis perpendicular to it. In view of the boundary layer approximations, the governing equations for flow and temperature are

$$\frac{\partial u}{\partial x} + \frac{\partial v}{\partial y} = 0, \quad (8.1)$$

$$\begin{aligned} u \frac{\partial u}{\partial x} + v \frac{\partial u}{\partial y} = & \nu \frac{\partial^2 u}{\partial y^2} - \lambda_1 \left(u^2 \frac{\partial^2 u}{\partial x^2} + v^2 \frac{\partial^2 u}{\partial y^2} + 2uv \frac{\partial^2 u}{\partial x \partial y} \right) + a^2 x \\ & + \nu \lambda_2 \left(u \frac{\partial^3 u}{\partial x \partial y^2} + v \frac{\partial^3 u}{\partial y^3} - \frac{\partial u}{\partial x} \frac{\partial^2 u}{\partial y^2} - \frac{\partial u}{\partial y} \frac{\partial^2 v}{\partial y^2} \right), \end{aligned} \quad (8.2)$$

$$\rho c_p \left(u \frac{\partial T}{\partial x} + v \frac{\partial T}{\partial y} \right) = k \frac{\partial^2 T}{\partial y^2} - \frac{\partial q_r}{\partial y}, \quad (8.3)$$

with boundary conditions

$$u = cx, \quad v = 0, \quad T = T_w(x) = T_\infty + Dx^\alpha \quad \text{at } y = 0, \quad (8.4)$$

$$u = ax, \quad T = T_\infty \quad \text{as } y \rightarrow \infty. \quad (8.5)$$

The velocity components u and v are taken along the x - and y -directions, λ_1 and λ_2 are the relaxation and retardation times, respectively, $\nu = (\mu/\rho)$ is termed as the kinematic viscosity, T is named as the fluid temperature, ρ is the density of fluid, k the thermal conductivity, c_p the specific heat at constant pressure and q_r the radiative heat flux. After utilizing the appropriate Rosseland approximation the mathematical expression for radiative heat flux q_r is

$$q_r = -\frac{4\sigma^*}{3k_1} \frac{\partial T^4}{\partial y}. \quad (8.6)$$

Here, σ^* and k_1 are used for the Stefan-Boltzmann constant and the mean absorption coefficient.

The relation of T^4 in view of Taylor's series can be defined as

$$T^4 \cong 4T_\infty^3 T - 3T_\infty^4. \quad (8.7)$$

By employing Eqs. (8.6) and (8.7), Eq. (8.3) turns into

$$\rho c_p \left[u \frac{\partial T}{\partial x} + v \frac{\partial T}{\partial y} \right] = \frac{\partial}{\partial y} \left[k \frac{\partial T}{\partial y} \right] + \frac{16\sigma T_\infty^3}{3k^*} \frac{\partial^2 T}{\partial y^2}, \quad (8.8)$$

The associative similarity transformations are expressed as

$$u = cx f'(\eta), \quad v = -\sqrt{c\nu} f(\eta), \quad \eta = y \sqrt{\frac{c}{\nu}}, \quad \theta(\eta) = \frac{T - T_\infty}{T_w - T_\infty}, \quad (8.9)$$

where T_w is the variable wall temperature and $\theta(\eta)$ is the non-dimensional form of the temperature.

We consider $T = T_w(x) = T_\infty + D x^\alpha \theta(\eta)$ at $\eta = 0$. The variable thermal conductivity is $k = k_\infty (1 + \epsilon_0 \theta)$ (here D and α are positive constants, k_∞ is the fluid free stream conductivity) and ϵ_0 is given by

$$\epsilon_0 = \frac{k_w - k_\infty}{k_\infty}, \quad (8.10)$$

where c is a constant and prime denotes the differentiation with respect to η .

Equations (8.2) – (8.5) yield

$$f'''' + f f'' - f'^2 + \epsilon^2 + \beta_1 (2f f' f'' - f^2 f''') + \beta_2 (f''^2 - f f''''') = 0, \quad (8.11)$$

$$(1 + \epsilon_0 \theta) \theta'' + \epsilon_0 \theta'^2 + \frac{4}{3} R_d \theta'' = \text{Pr} (\alpha f' \theta - f' \theta), \quad (8.12)$$

$$f = 0, \quad f' = 1, \quad \theta' = 1 \quad \text{at } \eta = 0, \quad (8.13)$$

$$f' = \epsilon, \quad \theta = 0 \quad \text{as } \eta \rightarrow \infty, \quad (8.14)$$

where $\beta_1 = \lambda_1 c$ and $\beta_2 = \lambda_2 c$ are the dimensionless fluid material factors, $\epsilon = \frac{a}{c}$ ratio parameter,

$Pr = \frac{\rho C_p \nu}{k_\infty}$ the Prandtl number and $R_d = \frac{4\sigma T_\infty^3}{K k_\infty}$ the radiation parameter.

The local Nusselt number and heat flux expressions are

$$Nu_x = \frac{x q_w}{k(T_w - T_\infty)}, \quad q_w = -k \left(\frac{\partial T}{\partial y} \right)_{y=0}. \quad (8.15)$$

In dimensionless form we have

$$Nu/Re_x^{1/2} = -\theta'(0). \quad (8.16)$$

8.2 Homotopy analysis solutions

We can express f and θ by a set of base functions

$$\{\eta^k \exp(-n\eta), \quad k \geq 0, n \geq 0\}, \quad (8.17)$$

as follows

$$f(\eta) = a_{0,0}^0 + \sum_{n=0}^{\infty} \sum_{k=0}^{\infty} a_{m,n}^k \eta^k \exp(-n\eta), \quad (8.18)$$

$$\theta(\eta) = \sum_{n=0}^{\infty} \sum_{k=0}^{\infty} b_{m,n}^k \eta^k \exp(-n\eta), \quad (8.19)$$

in which $a_{m,n}^k$ and $b_{m,n}^k$ are the coefficients. Further the initial approximations and auxiliary linear operators are

$$f_0(\eta) = \epsilon \eta + (1 - \epsilon)(1 - \exp(-\eta)), \quad \theta_0(\eta) = \exp(-\eta), \quad (8.20)$$

$$L_f = f''' - f', \quad L_\theta = \theta'' - \theta, \quad (8.21)$$

with

$$L_f (C_1 + C_2 e^\eta + C_3 e^{-\eta}) = 0, \quad L_\theta (C_4 e^\eta + C_5 e^{-\eta}) = 0, \quad (8.22)$$

where C_i ($i = 1 - 5$) represent the arbitrary constants.

The problems at zeroth order deformation are

$$(1-p) L_f \left[\hat{f}(\eta; p) - f_0(\eta) \right] = q h_f N_f \left[\hat{f}(\eta; p) \right], \quad (8.23)$$

$$(1-p) L_\theta \left[\hat{\theta}(\eta; p) - \theta_0(\eta) \right] = q h_\theta N_\theta \left[\hat{f}(\eta; p), \hat{\theta}(\eta; p) \right], \quad (8.24)$$

$$\hat{f}(0; p) = 0, \quad \hat{f}'(0; p) = 1, \quad \hat{f}'(\infty; p) = \epsilon, \quad \hat{\theta}'(0, p) = 1, \quad \hat{\theta}(\infty, p) = 0. \quad (8.25)$$

The nonlinear operators N_f and N_θ with embedding parameter p are expressed as

$$\begin{aligned} N_f \left[\hat{f}(\eta, p) \right] &= \frac{\partial^3 \hat{f}(\eta, p)}{\partial \eta^3} - \hat{f}(\eta, p) \frac{\partial^2 \hat{f}(\eta, p)}{\partial \eta^2} - \left(\frac{\partial \hat{f}(\eta, p)}{\partial \eta} \right)^2 + \epsilon^2 \\ &+ \beta_1 \left[2\hat{f}(\eta, p) \frac{\partial \hat{f}(\eta, p)}{\partial \eta} \frac{\partial^2 \hat{f}(\eta, p)}{\partial \eta^2} - \left(\hat{f}(\eta, p) \right)^2 \frac{\partial^3 \hat{f}(\eta, p)}{\partial \eta^3} \right] \\ &+ \beta_2 \left[\frac{\partial^2 \hat{f}(\eta, p)}{\partial \eta^2} - \hat{f}(\eta, p) \frac{\partial^4 \hat{f}(\eta, p)}{\partial \eta^4} \right], \end{aligned} \quad (8.26)$$

$$\begin{aligned} N_\theta \left[\hat{\theta}(\eta, p), \hat{f}(\eta, p) \right] &= \left(1 + \frac{4}{3} R_d \right) \frac{\partial^2 \hat{\theta}(\eta, p)}{\partial \eta^2} + \epsilon_0 \hat{\theta}(\eta, p) \frac{\partial^2 \hat{\theta}(\eta, p)}{\partial \eta^2} + \epsilon_0 \left(\frac{\partial \hat{\theta}(\eta, p)}{\partial \eta} \right)^2 \\ &- \text{Pr} \alpha \hat{\theta}(\eta, p) \frac{\partial \hat{f}(\eta, p)}{\partial \eta} + \text{Pr} \hat{f}(\eta, p) \frac{\partial \hat{\theta}(\eta, p)}{\partial \eta}. \end{aligned} \quad (8.27)$$

By setting $q = 0$ and $q = 1$, we have

$$\hat{f}(\eta; 0) = f_0(\eta), \quad \hat{\theta}(\eta, 0) = \theta_0(\eta) \quad \text{and} \quad \hat{f}(\eta; 1) = f(\eta), \quad \hat{\theta}(\eta, 1) = \theta(\eta), \quad (8.28)$$

and when p increases from 0 to 1 then $f(\eta, q)$ and $\theta(\eta, q)$ vary from $f_0(\eta), \theta_0(\eta)$ to $f(\eta)$ and $\theta(\eta)$.

In view of Taylor's series we can expand

$$f(\eta, q) = f_0(\eta) + \sum_{m=1}^{\infty} f_m(\eta) p^m, \quad \theta(\eta, p) = \theta_0(\eta) + \sum_{m=1}^{\infty} \theta_m(\eta) p^m, \quad (8.29)$$

$$f_m(\eta) = \frac{1}{m!} \left. \frac{\partial^m f(\eta; p)}{\partial \eta^m} \right|_{p=0}, \quad \theta_m(\eta) = \frac{1}{m!} \left. \frac{\partial^m \theta(\eta; p)}{\partial \eta^m} \right|_{p=0} \quad (8.30)$$

The convergence of above series strongly depends upon auxiliary parameters h_f and h_θ . The values of h_f and h_θ are preferred in such way so that Eqs. (8.23) and (8.24) converge at $p = 1$ and finally

$$f(\eta) = f_0(\eta) + \sum_{m=1}^{\infty} f_m(\eta), \quad \theta(\eta) = \theta_0(\eta) + \sum_{m=1}^{\infty} \theta_m(\eta). \quad (8.31)$$

The problems at m^{th} -order are

$$L_f [f_m(\eta) - \chi_m f_{m-1}(\eta)] = h_f R_f^m(\eta), \quad L_\theta [\theta_m(\eta) - \chi_m \theta_{m-1}(\eta)] = h_\theta R_\theta^m(\eta), \quad (8.32)$$

$$f_m(0) = f'_m(0) = f'_m(\infty) = 0, \quad \theta'_m(0) = \theta'_m(\infty) = 0, \quad (8.33)$$

$$\begin{aligned} R_f^m(\eta) &= f_{m-1}'''(\eta) + \sum_{k=0}^{m-1} [f_{m-1-k} f_k'' - f'_{m-1-k} f_k'''] + \epsilon^2 (1 - \chi_m) \\ &+ \beta_1 \left[\sum_{k=0}^{m-1} f_{m-1-k} \sum_{l=0}^k 2f'_{k-l} f_l'' - f_{k-l} f_l''' \right] \\ &+ \beta_2 \sum_{k=0}^{m-1} [f_{m-1-k}'' f_k'' - f_{m-1-k} f_k'''], \end{aligned} \quad (8.34)$$

$$\begin{aligned} R_\theta^m(\eta) &= \left(1 + \frac{4}{3} R_d\right) \theta_{m-1}'' + \epsilon_0 \sum_{k=0}^{m-1} \theta_{m-1-k} \theta_k'' + \epsilon_0 \sum_{k=0}^{m-1} \theta'_{m-1-k} \theta'_k \\ &- \alpha \text{Pr} \sum_{k=0}^{m-1} \theta_{m-1-k} f'_k + \text{Pr} \sum_{k=0}^{m-1} \theta'_{m-1-k} f_k, \end{aligned} \quad (8.35)$$

$$\chi_m = \begin{cases} 0, & m \leq 1, \\ 1, & m > 1. \end{cases} \quad (8.36)$$

The general solutions with the contribution of special solutions can be written in the following forms

$$f_m(\eta) = f_m^*(\eta) + C_1 + C_2 e^\eta + C_3 e^{-\eta}, \quad \theta_m(\eta) = \theta_m^*(\eta) + C_4 e^\eta + C_5 e^{-\eta}. \quad (8.37)$$

8.3 Convergence of homotopy solutions

As we know that the auxiliary parameters \hbar_f and \hbar_θ play a vital role to adjust and control the convergence of the homotopy solutions (see Liao [67]). For the range of admissible values of \hbar_f and \hbar_θ , the \hbar -curves have been plotted at 15th-order of approximations. Figs. 8.1 and 8.2 indicate that the range of admissible values of \hbar_f and \hbar_θ are $-1.4 \leq \hbar_f \leq -0.2$ and $-0.8 \leq \hbar_\theta \leq -0.5$ respectively. The series solutions converge in the whole region of η when $\hbar_f = -0.8$ and $\hbar_\theta = -0.7$.

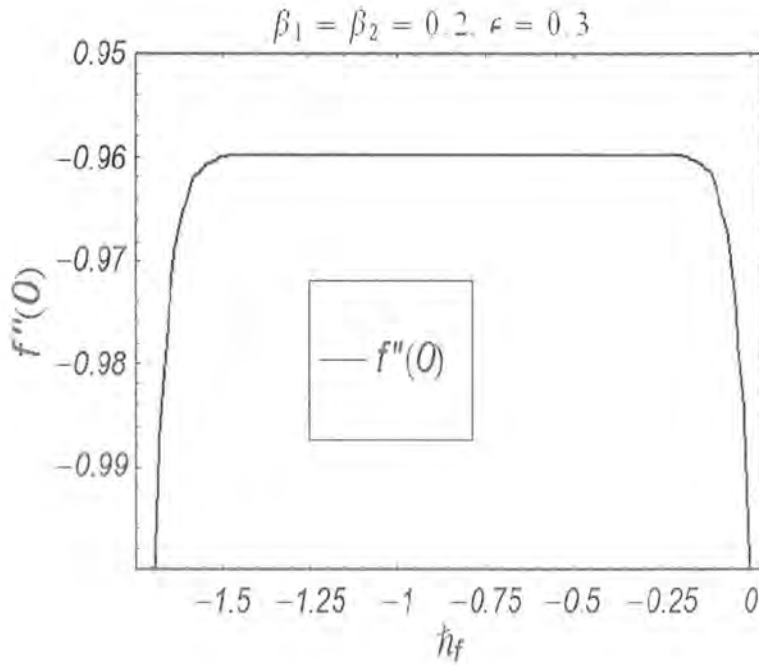


Fig. 8.1. \hbar -curve for the function f .

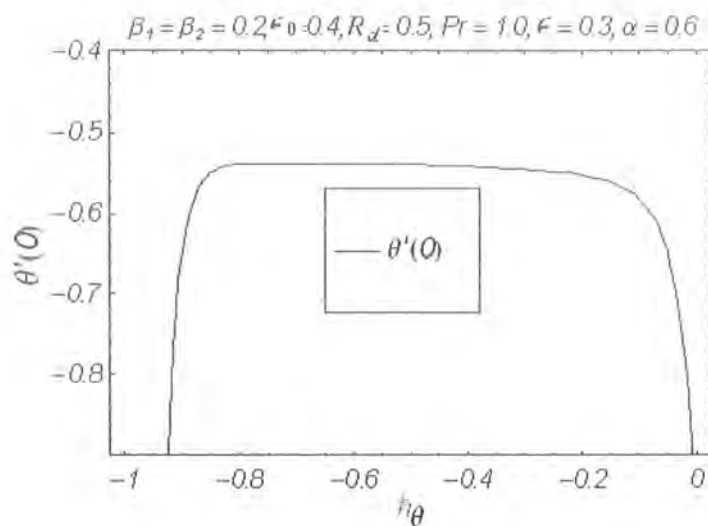


Fig. 8.2. h -curve for the function θ .

Table: 8.1. Convergence of homotopy solution for different order of approximations

when $\beta_1 = 0.1$, $\beta_2 = 0.2 = \epsilon_0$, $R_d = 0.3 = \epsilon$, $\alpha = 0.5$, $h_f = -0.8$ and $h_\theta = -0.6$.

Order of approximation	$-f''(0)$	$-\theta'(0)$
1	0.786485	0.6850
5	0.805344	0.659984
10	0.805412	0.659871
15	0.805435	0.659872
20	0.805751	0.659811
30	0.805751	0.659811

Table 8.2: Numerical values of local Nusselt number $-\theta'(0)$ for different values of

ϵ_0 , Pr , α and R_d when $\beta_1 = 0.1$, $\beta_2 = 0.2$ and $\epsilon = 0.3$.

ϵ_0	Pr	α	R_d	$-\theta'(0)$
0.0	0.7	0.5	0.3	0.56045
0.3				0.48757
0.7				0.42024
0.2	0.3			0.30872
	0.8			0.55063
	1.0			0.62742
		0.0		0.39071
		0.4		0.50911
		1.0		0.65845
			0.0	0.63003
			0.5	0.49053
			0.8	0.43879

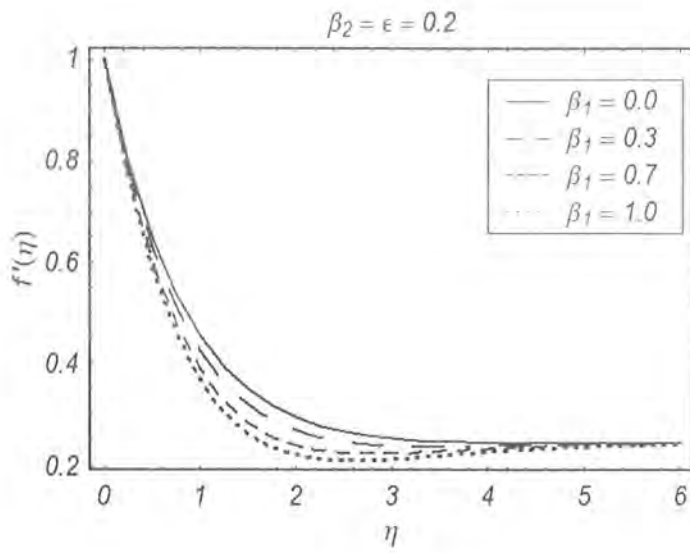


Fig. 8.3. Influence of β_1 on velocity profile $f'(\eta)$.

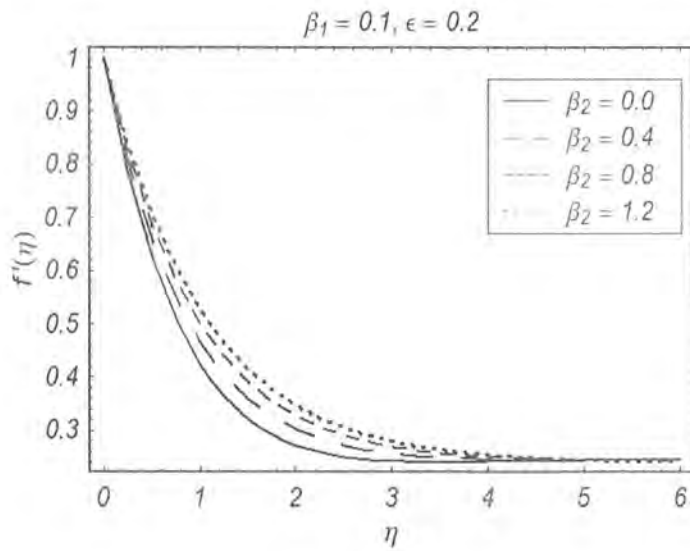


Fig. 8.4. Influence of β_2 on velocity profile $f'(\eta)$.

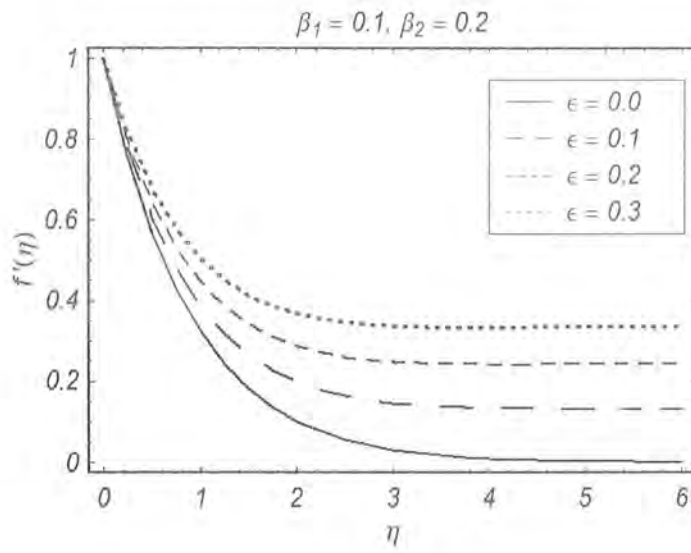


Fig. 8.5. Influence of ϵ on velocity profile $f'(\eta)$.

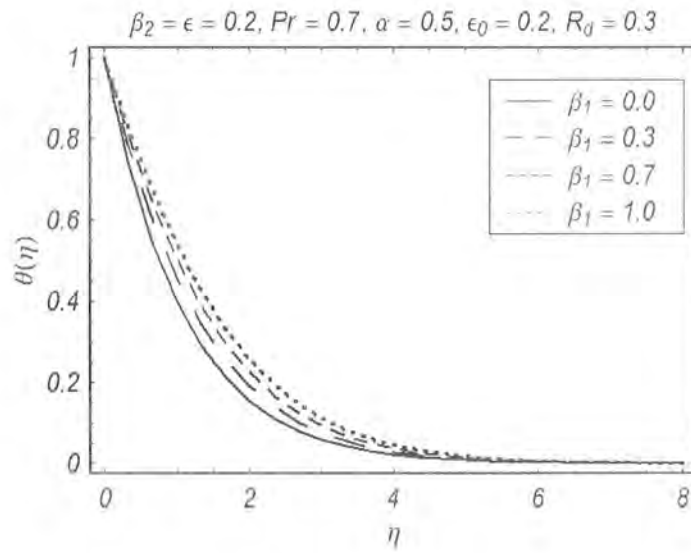


Fig. 8.6. Influence of β_1 on temperature field.

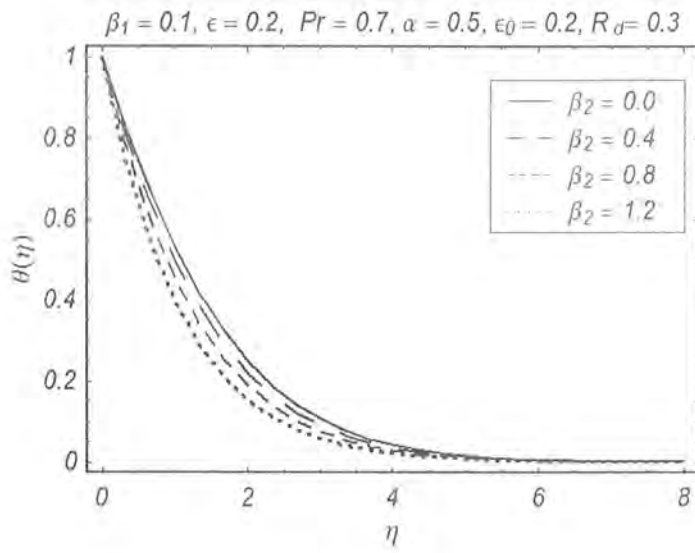


Fig. 8.7. Influence of β_2 on temperature field.

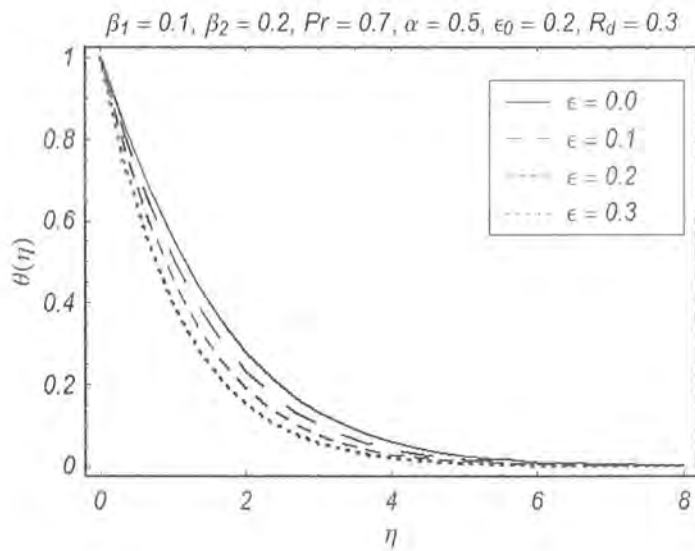


Fig. 8.8. Influence of ϵ on temperature field.

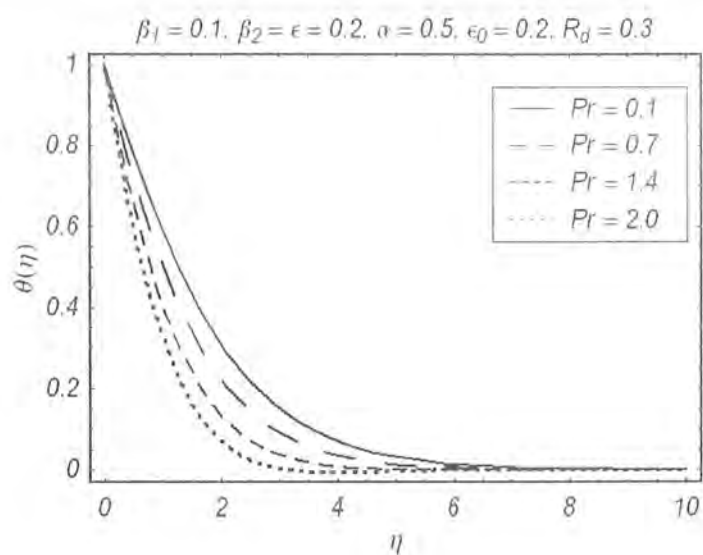


Fig. 8.9. Influence of Pr on temperature field.

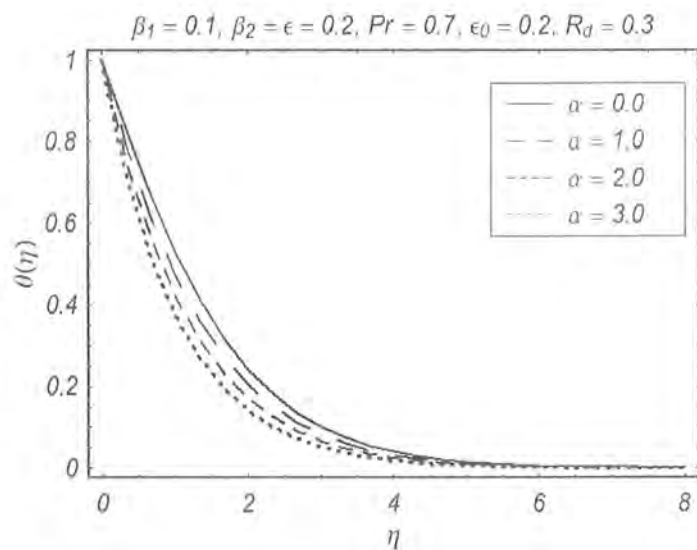


Fig. 8.10. Influence of α on temperature field.

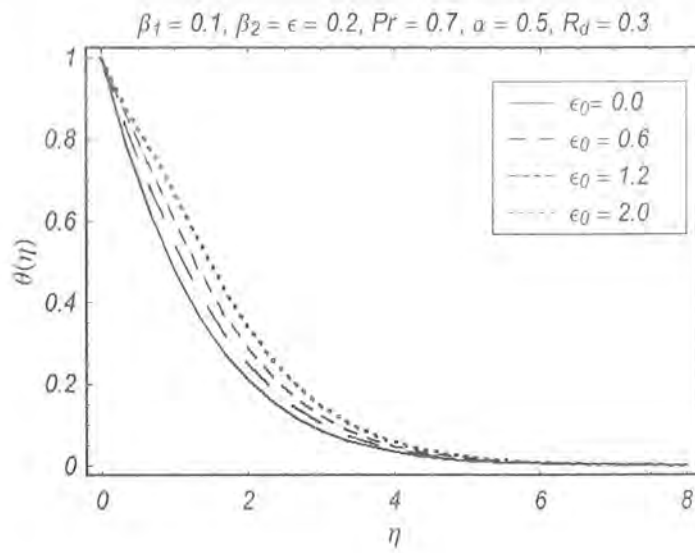


Fig. 8.11. Influence of ϵ_0 on temperature field.

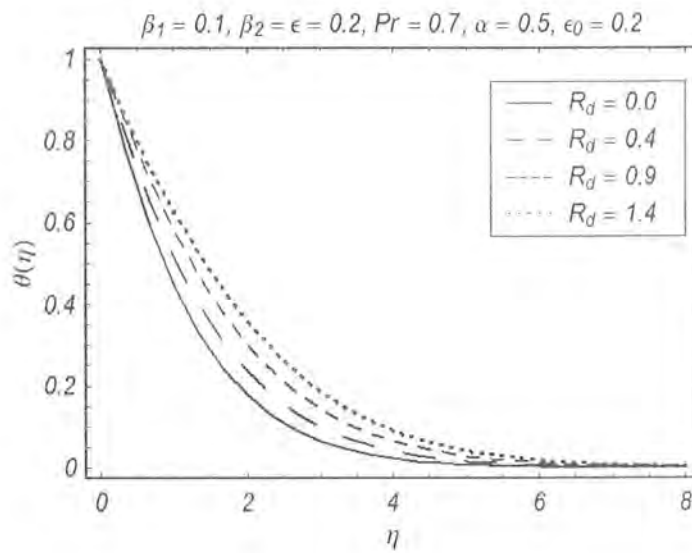


Fig. 8.12. Influence of R_d on temperature field.

8.4 Graphical results and discussion

In this section the representative results for velocity, temperature and local Nusselt number have been provided (see Figs. 8.3 – 8.12 and Tables 8.1, 8.2). Table 8.1 shows that the series solutions converge at only 15th order of approximations. The effects for different values of ϵ_0 , Pr , α and R_d when $\beta_1 = 0.1$, $\beta_2 = 0.2$ and $\epsilon = 0.3$ on local Nusselt number $-\theta'(0)$ have been presented through Table 8.2. From this table, we analyze that local Nusselt number increases due to increase in Pr and α and decreases by increasing radiation parameter R_d and ϵ_0 . In other words as the radiation process intensifies, the heat transfer rate at the sheet decreases which corresponds to a thicker thermal boundary layer.

Fig. 8.3 shows that velocity and boundary layer thickness are decreasing function of fluid parameter (Deborah number) β_1 . The behavior of fluid parameter β_2 on the velocity field f' is opposite to that accounted for β_1 (see Fig. 8.4). It is noticeable that small Deborah number ($\beta_{1,2} \ll 1$) represents the liquid-like behavior. However large Deborah number ($\beta_{1,2} > 1$) indicates the solid-like behavior. Keeping this fact in mind the graphical results are only provided for small values of β_1 and β_2 . It is clear that velocity decreases monotonically from $\eta = 0$ to ∞ for all the values of parameters. Fig. 8.5 elucidates the influence of velocity ratio parameter ϵ on the velocity field f' . The velocity field f' being a strong function of ϵ appreciably increases with an increase in ϵ . The boundary layer thickness increases with an increase in ϵ when the free stream velocity is less than the velocity of the stretching sheet. However the boundary layer thickness is a decreasing function of ϵ when the free stream velocity exceeds the stretching sheet velocity.

Fig. 8.6 indicates that temperature and the thermal boundary layer thickness increase with an increase in β_1 . However both temperature and thermal boundary layer thickness are decreasing functions of β_2 (see Fig. 8.7). From here we expect that a decrease in the thermal boundary layer thickness will be compensated with the higher rate of heat transfer at the stretching sheet. Fig. 8.8 shows that a larger free stream velocity decays the thermal boundary layer thickness rapidly. The

influence of Prandtl number Pr on the temperature is seen in Fig. 8.9. The temperature decreases as Pr increases. The smaller values of Pr ($\ll 1$) represents liquid-like materials having low viscosity and high thermal conductivity. However high viscosity oils are associated with larger values of Pr (> 1). Therefore as Pr increases this corresponds to a thinner thermal boundary layer and larger rate of heat transfer at the stretching sheet (as observed earlier in discussing the numerical data of Table 8.2). Fig. 8.10 characterizes the effects of α on the temperature. An increase in the values of α results in the increment of surface heat transfer which thins the thermal boundary layer. The occurrence of ϵ_0 in the energy equation is due to the variable thermal conductivity. It is clear from Fig. 8.11 that temperature θ is an increasing function of ϵ_0 . From the physical point of view, the larger the dependence of thermal conductivity on the temperature, the greater the temperature and the thermal boundary layer thickness. The dimensionless parameter R_d characterizes the effect of thermal radiation. It is obvious from Fig. 8.12 that an increase in the radiation effect greatly increases the temperature and thicker the thermal boundary layer.

Chapter 9

Effect of heat transfer on stagnation point flow of micropolar fluid with variable thermal conductivity and heat source/sink

This chapter addressed with the magnetohydrodynamic (MHD) flow of micropolar fluid near the stagnation-point towards a stretching sheet. The characteristics of heat transfer with variable thermal conductivity and heat source/sink are also addressed. Analytic expressions for velocity, microrotation and temperature are computed by applying homotopy analysis method (HAM). Attention has been given to the behaviors of key parameters which include the micropolar parameter (K), the Hartman number (M), the Prandtl number (Pr) and the heat source/sink parameter. The dimensionless expression of skin friction coefficient and local Nusselt number are evaluated and discussed. We observed that the velocity and microrotation fields are increasing functions of (K). Moreover there is a decrease in the thermal boundary layer thickness when the microrotation effects are increased. The present results are found in an excellent agreement with the numerical solutions

in the limiting cases.

9.1 Mathematical model

Consider the steady incompressible flow of micropolar fluid near stagnation-point towards a stretching sheet. The fluid is electrically conducting in the presence of applied magnetic field of uniform strength B_0 . The induced magnetic field is neglected for the small magnetic Reynolds consideration. Heat transfer analysis is carried out in the presence of variable thermal conductivity and heat source/sink. The velocity of the stretching sheet is $U_w(x) = cx$ (where $c > 0$ is a positive constant) while the velocity of external flow is given by $U_\infty(x) = bx$. T_w is the constant wall temperature and T_∞ is assumed to be ambient temperature. Thus the governing equations are

$$\frac{\partial u}{\partial x} + \frac{\partial v}{\partial y} = 0, \quad (9.1)$$

$$u \frac{\partial u}{\partial x} + v \frac{\partial u}{\partial y} = U_\infty \frac{dU_\infty}{dx} + \left(\nu + \frac{\kappa}{\rho} \right) \frac{\partial^2 u}{\partial y^2} + \frac{\kappa}{\rho} \frac{\partial N^*}{\partial y} - \frac{\sigma B_0^2}{\rho} u, \quad (9.2)$$

$$u \frac{\partial N^*}{\partial x} + v \frac{\partial N^*}{\partial y} = \frac{\gamma^*}{\rho j} \frac{\partial^2 N^*}{\partial y^2} - \frac{\kappa}{\rho j} \left(2N^* + \frac{\partial u}{\partial y} \right), \quad (9.3)$$

$$\rho c_p \left(u \frac{\partial T}{\partial x} + v \frac{\partial T}{\partial y} \right) = \frac{\partial}{\partial y} \left(\xi^* \frac{\partial T}{\partial y} \right) + Q(T - T_\infty), \quad (9.4)$$

By substituting $\kappa = 0$, the results for viscous fluid can also be obtained.

The relevant boundary conditions are described by

$$u = U_w(x) = cx, \quad v = 0, \quad N^* = -n_0 \frac{\partial u}{\partial y}, \quad T = T_w(x) \text{ at } y = 0, \quad (9.5)$$

$$u \longrightarrow U_\infty(x) = bx, \quad N^* \longrightarrow 0, \quad T \longrightarrow T_\infty \quad \text{as } y \longrightarrow \infty. \quad (9.6)$$

Here ν , ρ , $j = (\nu/c)$, $\gamma^* = (\mu + k/2)j$, N^* , λ , T , c_p , $\xi^* = \xi(1 + \epsilon T)$ and Q represents the kinematic viscosity, the fluid density, microinertia density, the spin gradient viscosity, the microrotation or angular velocity, the fluid temperature, the specific heat at constant pressure, the temperature

dependent thermal conductivity and the volumetric rate of heat. The boundary parameter $n_0 \in [0, 1]$. However turbulent flows is taken into account for the case $n_0 = 1$ but here the cases $n_0 = 0$ and $n_0 = 1/2$ are considered. Further $n_0 = 0$ or evenly $N^* = 0$ at the wall proceeds that the concentrated particle flows in which the microelements near to the wall surface are not able to rotate. This is also known as strong concentration of microelements. The case $n_0 = 1/2$ corresponds to vanishing of antisymmetric part of shear stress and known as weak concentration of microelements [52].

The proceeding solution is obtained as a result of the following dimensionless quantities

$$\eta = \left(\frac{c}{\nu}\right)^{1/2} y, \quad \psi(x, y) = (c\nu)^{1/2} x f(\eta), \quad N^* = (c/\nu)^{1/2} c x g(\eta), \quad \theta(\eta) = \frac{T - T_\infty}{T_w - T_\infty}. \quad (9.7)$$

The following relation is satisfied by stream function

$$u = \frac{\partial \psi}{\partial y}, \quad v = -\frac{\partial \psi}{\partial x}. \quad (9.8)$$

Now Eq. (9.1) is usually satisfied while the resultant transformed ordinary differential equations with allied boundary conditions are

$$(1 + K)f''' - f'^2 + f f'' - M f' + (\epsilon^2 + M\epsilon) + K g' = 0, \quad (9.9)$$

$$\left(1 + \frac{K}{2}\right) g'' + f g' - f' g - 2K g - K f'' = 0, \quad (9.10)$$

$$(1 + \epsilon_T \theta) \theta'' + \epsilon_T \theta'^2 + \text{Pr} \theta' f + \text{Pr} S \theta = 0, \quad (9.11)$$

$$f(0) = 0, \quad f'(0) = 1, \quad g(0) = -n_0 f''(0), \quad \theta(0) = 1, \quad (9.12)$$

$$f'(\eta) \rightarrow \epsilon, \quad \theta(\eta) \rightarrow 0, \quad g(\eta) = 0 \quad \text{as } \eta \rightarrow \infty. \quad (9.13)$$

In above expressions prime denotes the derivative with respect to η , the Hartman number $M =$

$\sigma B_0^2/\rho a$, the ratio parameter $\epsilon = b/c$, the Prandtl number $\text{Pr} = \alpha/\mu c_p$, heat source/sink parameter $S = Q/c\rho c_p$ and $K = \kappa/\mu$ the material fluid parameter.

The expression of skin friction coefficient C_{fx} and local Nusselt number Nu_x are

$$C_{fx} = \frac{\left[(\mu + \kappa) \frac{\partial u}{\partial y} + \kappa N^* \right]_{y=0}}{\rho u_w^2}, \quad Nu_x = \frac{x \left(\frac{\partial T}{\partial y} \right)_{y=0}}{(T_w - T_\infty)}, \quad (9.14)$$

which after using Eq. (9.7) are reduced as

$$\text{Re}_x^{1/2} C_{fx} = [1 + (1 - n_0)K] f''(0), \quad (9.15)$$

$$Nu \text{Re}_x^{-1/2} = -\theta'(0), \quad (9.16)$$

where $\text{Re}_x = ax^2/\nu$ is the local Reynolds number.

Statute of solution expressions with concerned boundary conditions inform us to go for the initial guesses and auxiliary linear operators which are given below

$$f_0(\eta) = \epsilon\eta + (1 - \epsilon)(1 - \exp(-\eta)), \quad g_0(\eta) = n_0(1 - \epsilon) \exp(-\eta), \quad \theta_0(\eta) = \exp(-\eta), \quad (9.17)$$

$$L_f = \frac{d^3 f}{d\eta^3} - \frac{df}{d\eta}, \quad L_g = \frac{d^2 g}{d\eta^2} - g, \quad L_\theta = \frac{d^2 \theta}{d\eta^2} - \theta. \quad (9.18)$$

The close interval from 0 to 1 is the range of embedding parameter p with the contribution of auxiliary parameters h_f , h_g and h_θ . The generalized homotopic equations analogous to Eqs. (9.9) to (9.13) are

$$(1 - p)L_f \left[\hat{f}(\eta; p) - f_0(\eta) \right] = p h_f N_f \left[\hat{f}(\eta; p) \right], \quad (9.19)$$

$$(1 - p)L_g \left[\hat{g}(\eta; p) - g_0(\eta) \right] = p h_g N_g \left[\hat{f}(\eta; p), \hat{g}(\eta; p) \right], \quad (9.20)$$

$$(1 - p)L_\theta \left[\hat{\theta}(\eta; p) - \theta_0(\eta) \right] = p h_\theta N_\theta \left[\hat{f}(\eta; p), \hat{\theta}(\eta; p) \right], \quad (9.21)$$

$$\hat{f}(0; p) = 0, \quad \frac{\partial \hat{f}}{\partial \eta}(0; p) = 1, \quad \hat{g}(0; p) = -u_0 \frac{\partial^2 \hat{f}}{\partial \eta^2}(0; p), \quad \hat{\theta}(0; p) = 1, \quad \eta = 0. \quad (9.22)$$

$$\frac{\partial \hat{f}}{\partial \eta} \longrightarrow \epsilon, \quad \hat{g}(\eta; p) \longrightarrow 0, \quad \hat{\theta}(\eta; p) \longrightarrow 0 \quad \text{when} \quad \eta \longrightarrow \infty, \quad (9.23)$$

$$\begin{aligned} N_f [\hat{f}(\eta, p), \hat{g}(\eta, p)] &= (1 + K) \frac{\partial^3 \hat{f}}{\partial \eta^3} - \left(\frac{\partial \hat{f}}{\partial \eta} \right)^2 + \hat{f} \frac{\partial^2 \hat{f}}{\partial \eta^2} - M \frac{\partial \hat{f}}{\partial \eta} + (\epsilon^2 + M\epsilon) \\ &\quad + K \frac{\partial \hat{g}}{\partial \eta}, \end{aligned} \quad (9.24)$$

$$N_g [\hat{f}(\eta, p), \hat{g}(\eta, p)] = \left(1 + \frac{K}{2} \right) \frac{\partial^2 \hat{g}}{\partial \eta^2} + \hat{f} \frac{\partial \hat{g}}{\partial \eta} - \hat{g} \frac{\partial \hat{f}}{\partial \eta} - 2K\hat{g} - K \frac{\partial^2 \hat{f}}{\partial \eta^2}, \quad (9.25)$$

$$N_\theta [\hat{f}(\eta, p), \hat{\theta}(\eta, p)] = (1 + \epsilon_T \hat{\theta}) \frac{\partial^2 \hat{\theta}}{\partial \eta^2} + \epsilon_T \left(\frac{\partial \hat{\theta}}{\partial \eta} \right)^2 + \text{Pr} \frac{\partial \hat{\theta}}{\partial \eta} \hat{f} + \text{Pr} S \hat{\theta}. \quad (9.26)$$

The expressions of \hat{f} , \hat{g} and $\hat{\theta}$ about p by means of Maclaurin's series we get

$$\hat{f}(\eta; p) = \sum_{m=0}^{\infty} f_m(\eta) p^m, \quad f_m(\eta) = \frac{1}{m!} \frac{\partial^m \hat{f}(\eta, p)}{\partial p^m} \Big|_{p=0}, \quad (9.27)$$

$$\hat{g}(\eta; p) = \sum_{m=0}^{\infty} g_m(\eta) p^m, \quad g_m(\eta) = \frac{1}{m!} \frac{\partial^m \hat{g}(\eta, p)}{\partial p^m} \Big|_{p=0}, \quad (9.28)$$

$$\hat{\theta}(\eta; p) = \sum_{m=0}^{\infty} \theta_m(\eta) p^m, \quad \theta_m(\eta) = \frac{1}{m!} \frac{\partial^m \hat{\theta}(\eta, p)}{\partial p^m} \Big|_{p=0}. \quad (9.29)$$

By taking $p = 1$, the expressions of Eqs. (9.27) to (9.29) are derived by using Eqs. (9.17) to (9.21). Explicitly m^{th} -order deformation equations corresponding to the problems (9.17) to (9.21) are

$$L_f [f_m(\eta) - \chi_m f_{m-1}(\eta)] = \hbar_f R_{f,m}(\eta), \quad (9.30)$$

$$L_g [g_m(\eta) - \chi_m g_{m-1}(\eta)] = \hbar_g R_{g,m}(\eta), \quad (9.31)$$

$$L_\theta [\theta_m(\eta) - \chi_m \theta_{m-1}(\eta)] = \hbar_\theta R_{\theta,m}(\eta), \quad (9.32)$$

$$f_m(0) = 0, \quad f'_m(0) = 0, \quad g_m(0) = 0, \quad \theta_m(0) = 0, \quad (9.33)$$

$$f'_m(\eta) \rightarrow 0, \quad g_m(\eta) \rightarrow 0, \quad \theta_m(\eta) \rightarrow 0 \quad \text{when} \quad \eta \rightarrow \infty, \quad (9.34)$$

$$\begin{aligned} R_{f,m}(\eta) = & (1 + K) \frac{\partial^3 f_{m-1}}{\partial \eta^3} - \sum_{i=0}^{m-1} \left(\frac{\partial f_{m-i-1}}{\partial \eta} \frac{\partial f_i}{\partial \eta} \right) + \sum_{i=0}^{m-1} f_i \frac{\partial^2 f_{m-i-1}}{\partial \eta^2} - M \frac{\partial f_{m-1}}{\partial \eta} \\ & + K \frac{\partial g_{m-1}}{\partial \eta} [\epsilon^2 + M\epsilon] (1 - \chi_m), \end{aligned} \quad (9.35)$$

$$R_{g,m}(\eta) = \left(1 + \frac{K}{2} \right) \frac{\partial^2 g_{m-1}}{\partial \eta^2} + \sum_{i=0}^{m-1} \left(f_i \frac{\partial g_{m-i-1}}{\partial \eta} + g_i \frac{\partial f_{m-i-1}}{\partial \eta} \right) - K \left(2 \frac{\partial^2 g_{m-1}}{\partial \eta^2} + \frac{\partial^2 f_{m-1}}{\partial \eta^2} \right), \quad (9.36)$$

$$R_{\theta,m}(\eta) = \left(\frac{\partial^2 \theta_{m-1}}{\partial \eta^2} \right) + \epsilon_T \sum_{i=0}^{m-1} \theta_i \frac{\partial^2 \theta_{m-i-1}}{\partial \eta^2} + \text{Pr} \sum_{i=0}^{m-1} \left(f_{m-i-1} \frac{\partial \theta_i}{\partial \eta} \right) + \text{Pr} S \theta_{m-1}, \quad (9.37)$$

$$\chi_m = \begin{cases} 0, & m = 1, \\ 1, & m > 1. \end{cases} \quad (9.38)$$

9.2 Analysis of solutions

Obviously, we know that the series solutions (9.27) to (9.29) contain the non-zero auxiliary parameters \hbar_f , \hbar_g and \hbar_θ . In order to see the convergence of derived solutions with the help of these non-zero auxiliary parameters, we plot the \hbar_f , \hbar_g and \hbar_θ curves at 20th order of approximations. The \hbar curves for velocity, microrotation and temperature are sketched in Fig. 9.1. This Fig. shows that the range of admissible values of \hbar_f , \hbar_g and \hbar_θ are $-1.72 \leq \hbar_f \leq -0.23$, $-1.67 \leq \hbar_g \leq -0.03$ and $-1.58 \leq \hbar_\theta \leq -0.11$. Further, the series solutions converge when we take the suitable values of \hbar_f , \hbar_g and \hbar_θ in the neighborhood of -0.8 . Table 9.1 indicates that the convergence of homotopy series solutions is achieved at 15th order of approximations.

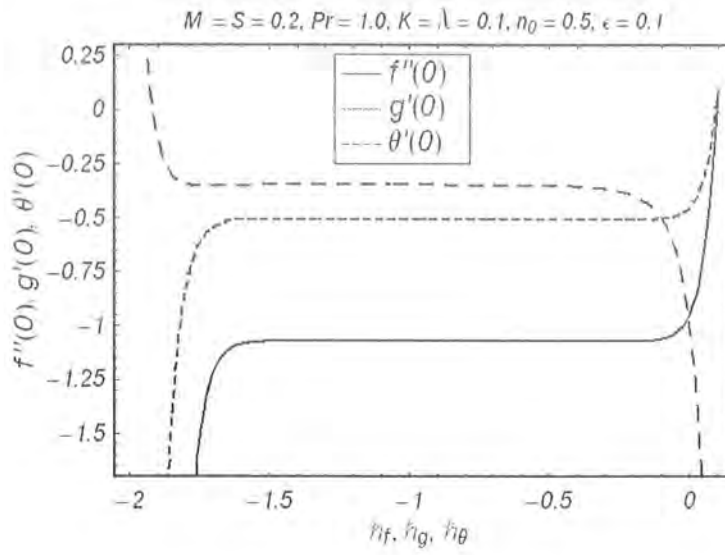


Fig. 9.1. h -curves for $f''(0)$, $g'(0)$ and $\theta'(0)$ at 20^{th} order of approximations.

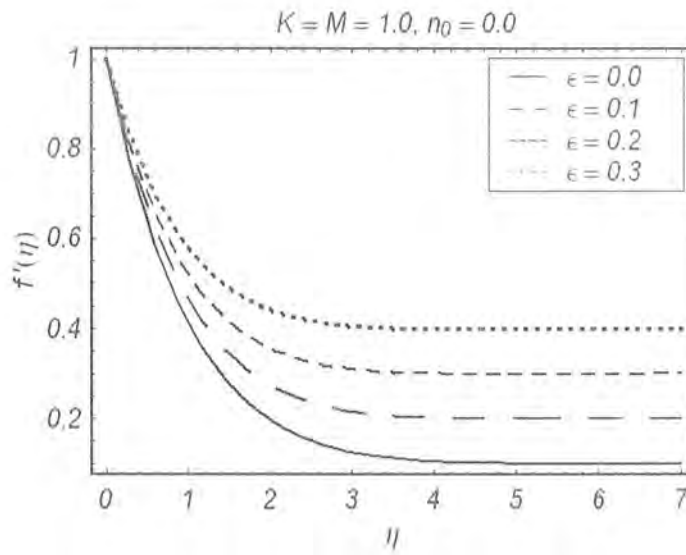


Fig. 9.2. Effect of ϵ on velocity $f'(\eta)$.

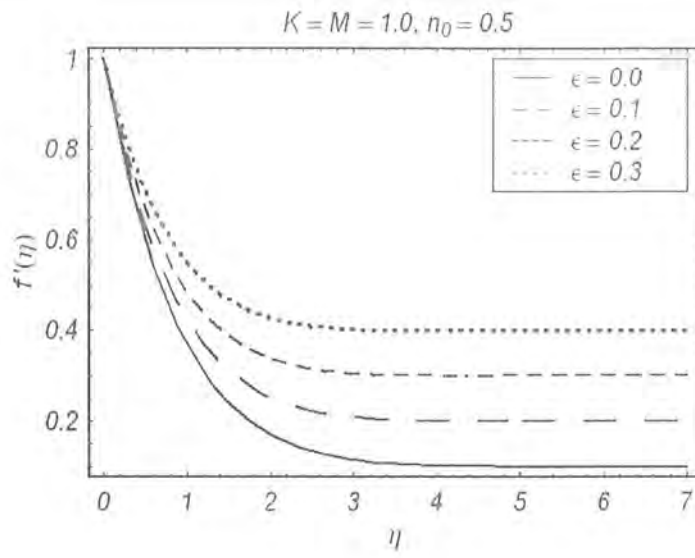


Fig. 9.3. Effect of ϵ on velocity $f'(\eta)$.

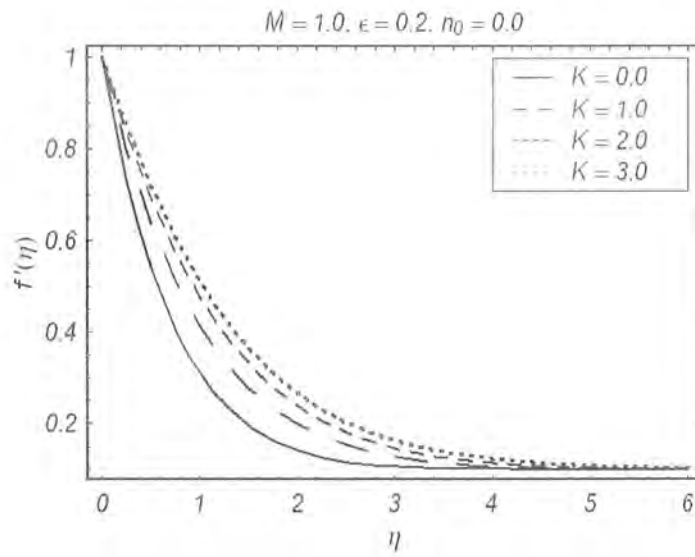


Fig. 9.4. Effect of K on velocity $f'(\eta)$.

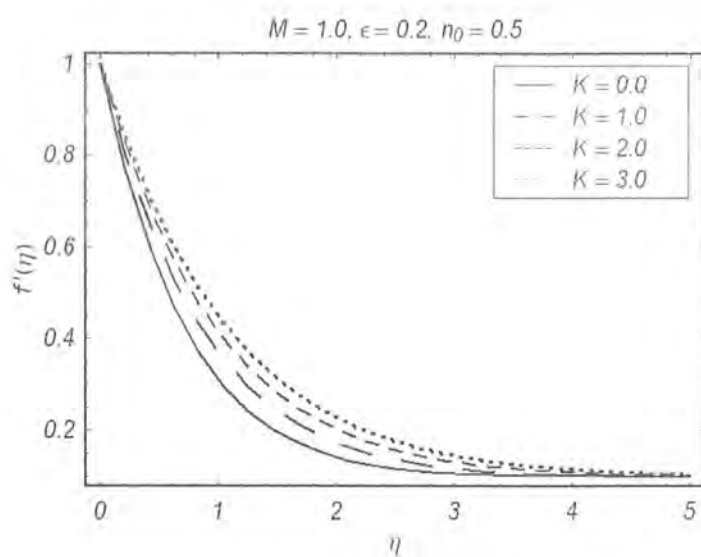


Fig. 9.5. Effect of K on velocity $f'(\eta)$.

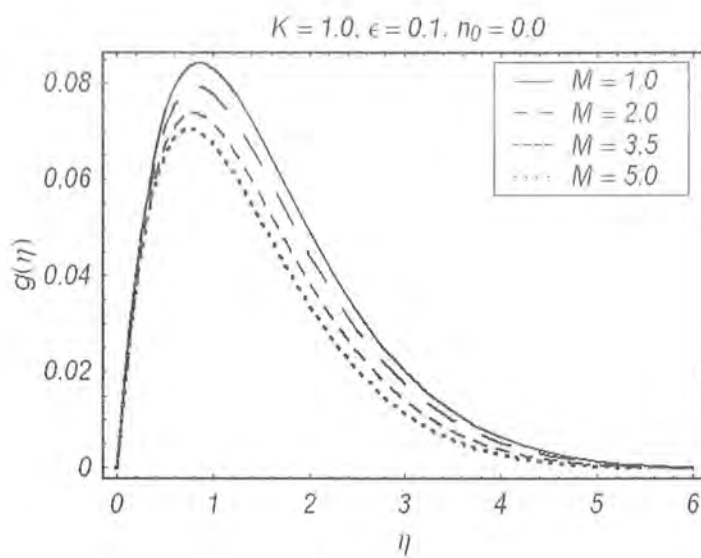


Fig. 9.6. Effect of M on microrotation $g(\eta)$.

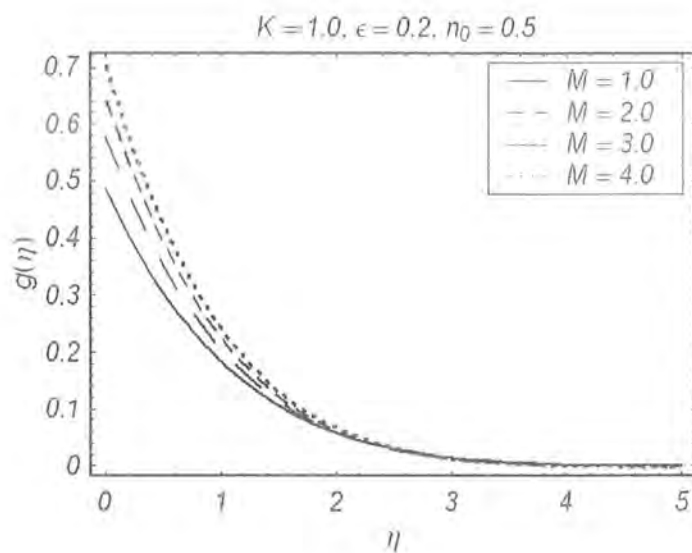


Fig. 9.7. Effect of M on microrotation $g(\eta)$.

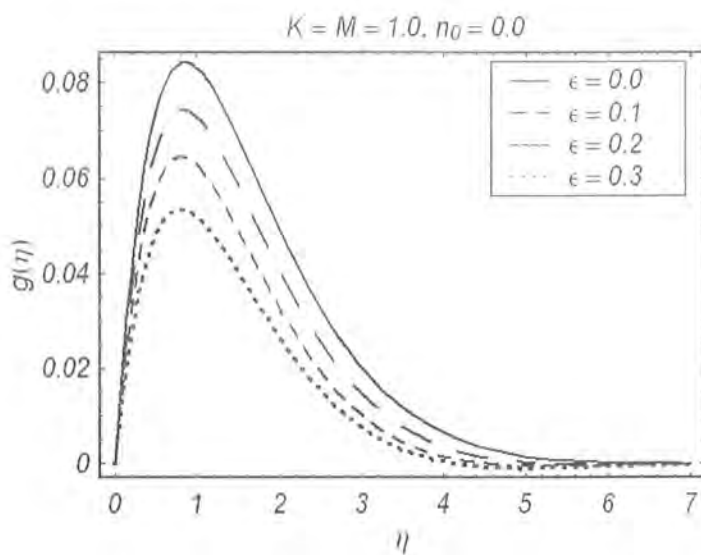


Fig. 9.8. Effect of ϵ on microrotation $g(\eta)$.

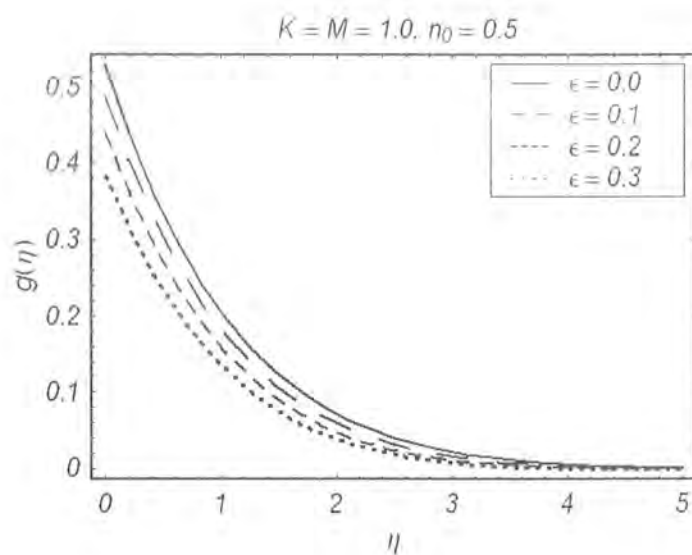


Fig. 9.9. Effect of ϵ on microrotation $g(\eta)$.

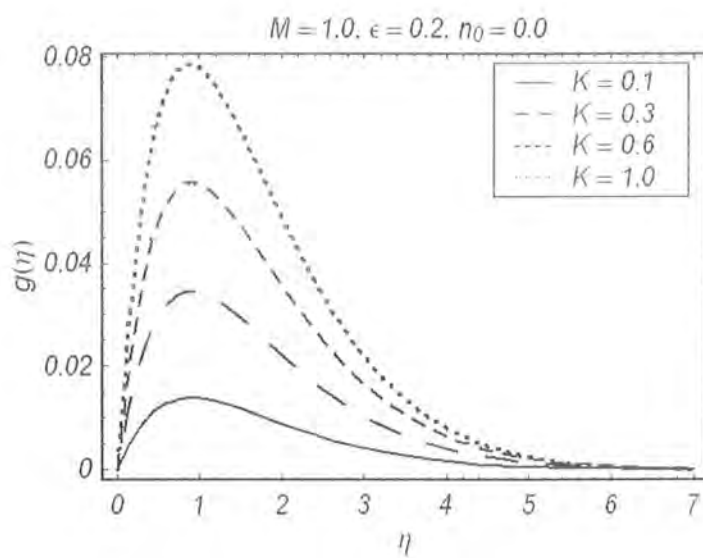


Fig. 9.10. Effect of K on microrotation $g(\eta)$.

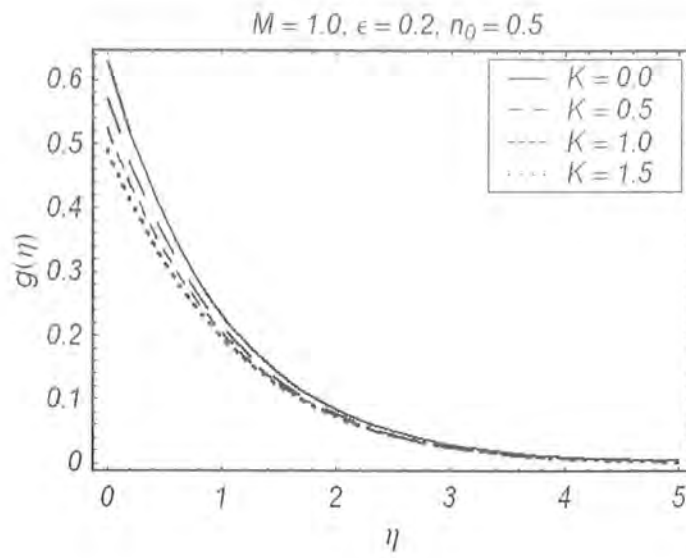


Fig. 9.11. Effect of K on microrotation $g(\eta)$.

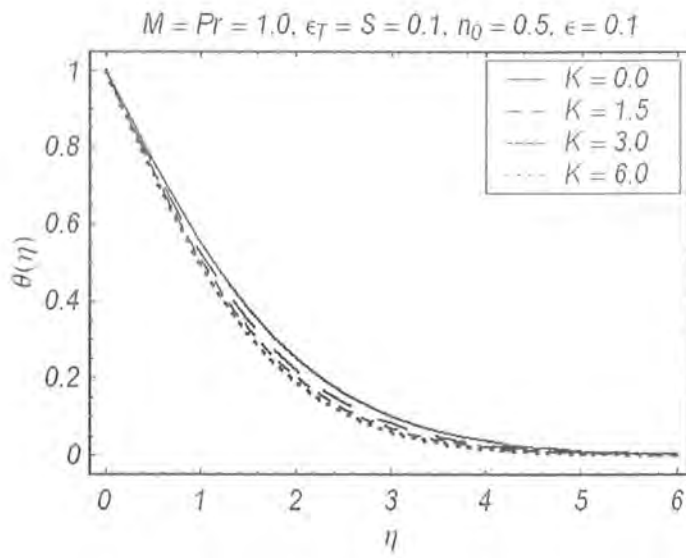


Fig. 9.12. Effect of K on temperature $\theta(\eta)$.

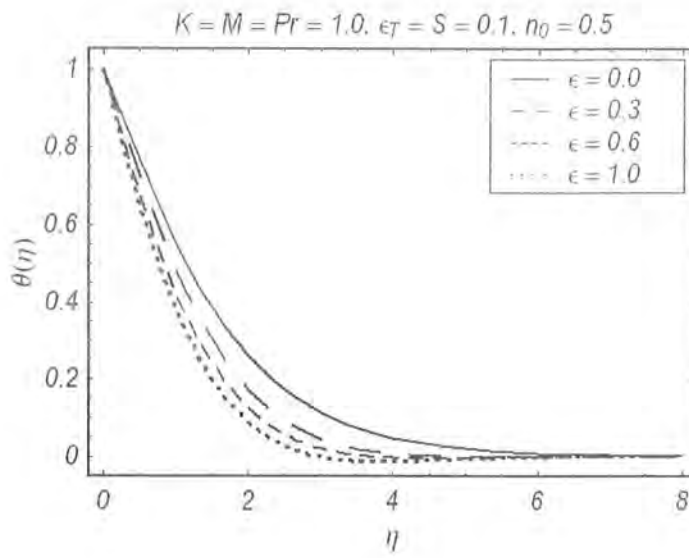


Fig. 9.13. Effect of ϵ on temperature $\theta(\eta)$.

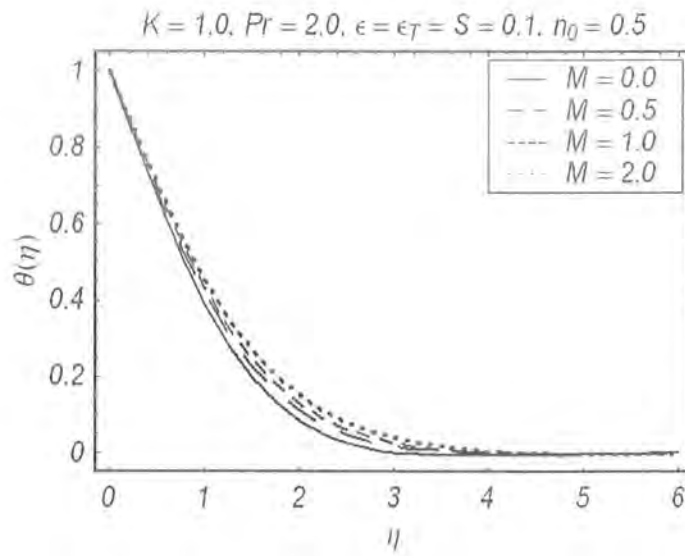


Fig. 9.14. Effect of M on temperature $\theta(\eta)$.

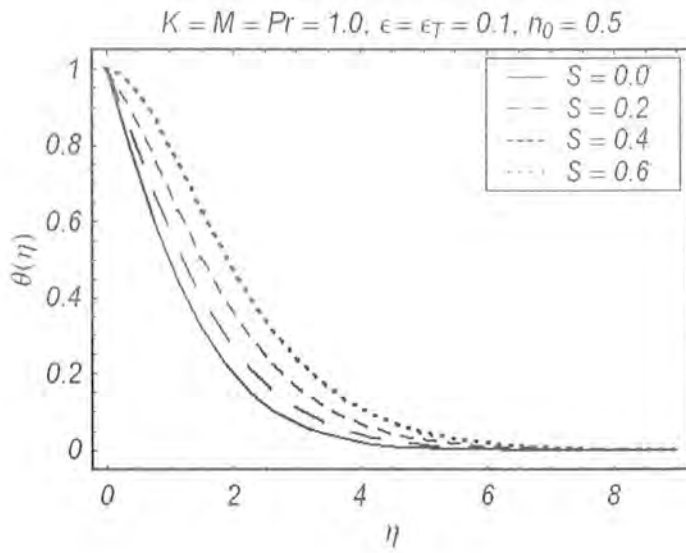


Fig. 9.15. Effect of S on temperature $\theta(\eta)$.

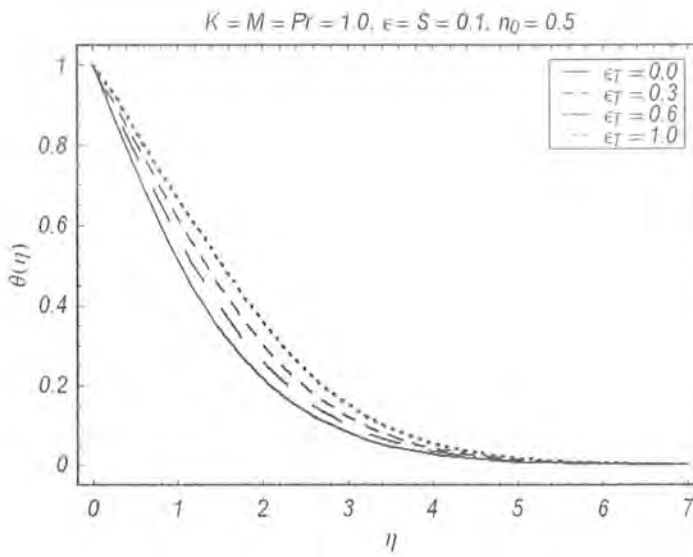


Fig. 9.16. Effect of ϵ_T on temperature $\theta(\eta)$.

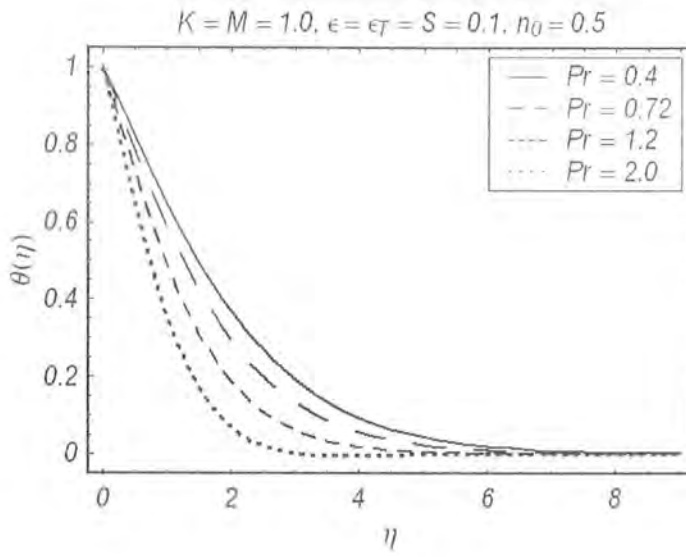


Fig. 9.17. Effect of Pr on temperature $\theta(\eta)$.

Table: 9.1. Numerical values for the convergence of HAM solutions
of $-f''(0)$, $-g'(0)$ and $-\theta'(0)$.

Order of convergence	$-f''(0)$	$-g'(0)$	$-\theta'(0)$
1	1.044	0.486	0.603333
5	1.02959	0.47741	0.463773
10	1.02959	0.477408	0.459717
15	1.02959	0.477408	0.459588
20	1.02959	0.477408	0.459581
25	1.02959	0.477408	0.459581
30	1.02959	0.477408	0.459581
35	1.02959	0.477408	0.459581

Table: 9.2. Numerical values for skin-friction coefficient $C_{fx} \text{Re}_x^{1/2}$.

ϵ	$K = 0$		$K = 1$	
	Present	Nazar et al.[59]	Present	Nazar et al.[59]
0.01	-0.998024	-0.9980	-1.365247	-1.3653
0.02	-0.995784	-0.9958	-1.362221	-1.3622
0.05	-0.987579	-0.9876	-1.351193	-1.3512
0.10	-0.969386	-0.9694	-1.326808	-1.3268
0.20	-0.918107	-0.9181	-1.257922	-1.2579
0.50	-0.667262	-0.6673	-1.917505	-1.9175

Table: 9.3. Numerical values for skin-friction coefficient $C_{f_x} \text{Re}_x^{1/2}$,

ϵ	$K = 1$		$K = 2$	
	Present	Nazar et al. [59]	Present	Nazar et al. [59]
0.01	-1.22232	-1.2224	-1.41142	-1.4116
0.02	-1.21958	-1.2196	-1.40825	-1.4084
0.05	-1.20953	-1.2095	-1.39665	-1.3967
0.10	-1.18725	-1.1872	-1.37092	-1.3709
0.20	-1.12445	-1.1244	-1.29840	-1.2984
0.50	-0.81723	-0.8172	-0.94365	-0.9437

Table: 9.4. Values of skin-friction coefficient
 $-f''(0)$ for various values of K , M and ϵ .

K	M	ϵ	$C_{fx} Re_x^{1/2}$	$C_{fx} Re_x^{1/2}$
			$n_0 = 0.0$	$n_0 = 0.5$
0.0	0.5	0.1	-1.15834	-1.15834
	0.5		-0.934076	-1.03982
	1.0		-0.794557	-0.95666
	1.2		-0.752390	-0.92932
1.0	0.0	1.0	-0.663404	-0.81091
		0.1	-0.691433	-0.84237
		0.3	-0.744626	-0.90158
		0.5	-0.794556	-0.95666
		0.7	-0.841746	-1.00831
		1.0	-0.908242	-1.08054
1.0	0.5	0.0	-0.839152	-0.99199
		0.1	-0.794556	-0.95666
		0.2	-0.739515	-0.90883
		0.3	-0.674900	-0.84960

Table: 9.5. Values of $-\theta(0)$ for different values of parameters.

K	M	ϵ	S	n_0	ϵ_T	Pr	$-\theta(0)$
0.0	0.5	0.1	0.1	0.5	0.2	1.2	0.499128
	0.5						0.523666
	1.0						0.542980
	1.2						0.484229
1.0	0.0	0.1	0.1	0.5	0.2	1.2	0.576500
		0.1					0.569229
		0.3					0.555569
		0.7					0.531295
		1.0					0.515201
		1.2					0.505440
1.0	0.5	0.1	0.0	0.5	0.2	1.0	0.530320
			0.1				0.446481
			0.2				0.343977
			0.3				0.205744
0.5	0.5	0.1	0.1	0.5	0.4	1.2	0.434250
					0.6		0.391075
					0.8		0.356597
					1.0		0.328194
0.5	0.5	0.1	0.1	0.5	0.2	0.7	0.327100
						1.0	0.428597
						1.3	0.518079
						1.5	0.509110
						1.7	0.555000

9.3 Results and discussion

Here we study the behaviors of pertinent parameters on the velocity f' , microrotation g and temperature profile θ . The velocity field f' significantly increases when there is an increase in ϵ as can be seen from Fig. 9.2. We understand that increase in ϵ accompanies with the larger free stream velocity which tends to increase the fluid velocity. The boundary layer thickness is also an increasing function of ϵ for $\epsilon < 1$. However when $\epsilon > 1$, the boundary layer thins as we increase the values of ϵ . The behavior of ϵ on f' is similar in the case of strong concentration of microelements ($n_0 = 0$) when compared with their weak concentration ($n_0 = 0.5$) (see Fig. 9.3). The variation of velocity field f' with K can be visualized from Figs. 9.4 and 9.5. There is an increase in the velocity and the boundary layer thickness with an increase in K . This increase is prominent in the case of $n_0 = 0$ when compared with $n_0 = 0.5$. Figs 9.6 – 9.11 show the effects of parameters on the microrotaion field $g(\eta)$. We observed that microrotation effects decrease with an increase in M and ϵ . However $g(\eta)$ is an increasing function of K . Moreover the microrotation profiles show a parabolic distribution for the case $n_0 = 0$. Further it can be seen that the microrotation effects are dominant near the stretching boundary.

Figs. 9.12 – 9.17 are plotted to see the variations of θ with the embedding parameters. There is a slight decrease in the temperature θ when the microrotation effects are increased (see Fig. 9.12). However the decrease in the temperature is more pronounced when the velocity ratio ϵ is increased as can be seen from Fig. 9.13. Thus it is inferred from this observation that thermal boundary layer thins as the free stream velocity is increased. Fig. 9.14 indicates that there is a minor increase in the temperature field as the magnetic field effect intensifies. Moreover the temperature profiles are negligibly affected for large values of Hartman number. The behavior of heat source/sink parameter S on the temperature can be depicted from Fig. 9.15. As expected the temperature θ appreciably rises and thermal boundary layer thickness increases with a gradual increase in S . It is quite obvious that an increase in ϵ_T corresponds to increase in the thermal

conductivity which is, therefore, associated with the larger temperature and the thermal boundary layer thickness. This fact can be visualized from Fig. 9.16. Fig. 9.17 shows that temperature θ is a decreasing function of Pr . This is because of the fact that a higher Prandtl number fluid has a relatively lower thermal conductivity which reduces conduction and thereby increases the variations of thermal characteristics. This results in the reduction of the thermal boundary layer thickness and increase in the heat transfer at the stretching surface.

Table 9.4 shows the behavior of parameters on the skin friction coefficient when the magnetic field effects are present. In accordance with the observations noted in [59] the wall shear stress uniformly decreases with an increase in K and ϵ . However skin friction coefficient is an increasing function of the Hartman number. The values of local Nusselt number corresponding to various values of the parameters are given in Table 9.5. There is an increase in the rate of heat transfer at the sheet when the microrotation effects are increased. As seen earlier in Fig. 9.15, the increasing values of S moves the profiles away from the boundary causing an enhancement in the thermal boundary layer thickness. This results in the smaller rate of heat transfer at the stretching sheet surface.

9.4 Conclusions

Here the stagnation point flow of micropolar fluid is developed. Series solutions are obtained and the main results are

- The results in limiting case are presented in excellent agreement.
- With the increasing microrotation parameter both the effects of velocity and boundary layer thickness increases.
- The convergence of velocity, microrotation and temperature profile by HAM are obtained at 15^{th} order of approximations.

- Another fact is found that for high volumetric rate of heat transfer the thermal boundary layer thickness increases.
- The temperature profile causes the reduction for positive values of Pr , K and ϵ .
- The microrotation profile $g(\eta)$ contains the opposite effect for both case (i) strong concentration (ii) weak concentration.

Bibliography

- [1] K. Hiemenz, Die Grenzschicht an einem in den gleichförmigen Flüssigkeitsstrom eingetauchten geraden Kreiszyylinder, *Dinglers Polytech. J.* 326 (1911) 321 – 324.
- [2] T. C. Chiam, Stagnation point flow towards a stretching plate, *J. Physical Society of Japan* 63 (1994) 2443 – 2444.
- [3] T. R. Mahapatra and A. S. Gupta, Magnetohydrodynamic stagnation-point flow towards a stretching sheet, *Acta Mech.* 152 (2001) 191 – 196.
- [4] Y. Y. Lok, N. Amin and I. Pop, Non-orthogonal stagnation point flow towards a stretching sheet, *Int. J. Non-Linear Mechanics* 41 (2006) 622 – 627.
- [5] A. Ishak, K. Jafar, R. Nazar and I. Pop, MHD stagnation-point flow towards a stretching sheet, *Physica. A.* 388 (2009) 3377 – 3383.
- [6] S. Nadeem, A. Hussain and M. Khan, HAM solutions for boundary layer flow in the region of the stagnation point towards a stretching sheet, *Comm. Nonlinear Sci. Numer. Simulation* 15 (2010) 475 – 481.
- [7] N. Bachok, A. Ishak and Ioan Pop, On the stagnation-point flow towards a stretching sheet with homogeneous–heterogeneous reactions effects, *Commun Nonlinear Sci. Numer. Simulat.* 16 (2011) 4296 – 4302.

- [8] T. C. Chiam, Heat transfer in a fluid with variable conductivity in a stagnation-point flow towards a stretching sheet, *Int. Commun. Heat Mass Transfer* 32 (1996) 239 – 248.
- [9] T. R. Mahapatra and A. S. Gupta, Heat transfer in stagnation-point flow towards a stretching sheet, *Heat and Mass Transfer* 38 (2002) 517 – 521.
- [10] S. R. Pop, T. Gorsan and I. Pop, Radiation effects on the flow near the stagnation point of a stretching sheet, 29 (2004) 100 – 106.
- [11] P. R. Sharma and G. Singh, Unsteady flow about a stagnation point on a stretching sheet in the presence of variable free stream, *Thammasat Int. J. Sc. Tech.* 13 (2008) 11 – 16.
- [12] Z. Abbas and T. Hayat, Stagnation slip flow and heat transfer over a nonlinear stretching sheet, *Numerical Method for partial differential equations* 27 (2009) 302 – 314.
- [13] N. Bachok, A. Ishak and I. Pop, Melting heat transfer in boundary layer stagnation-point flow towards a stretching/shrinking sheet, *Phys. Lett. A* 374 (2010) 4075 – 4079.
- [14] K. Bhattacharyya and G. C Layek, Effects of suction/blowing on steady boundary layer stagnation-point flow and heat transfer towards a shrinking sheet with thermal radiation, *Int. J. Heat and Mass Transfer* 54 (2011) 302 – 307.
- [15] T. Fang, C. F. Lee and J. Zhang, The boundary layers of an unsteady incompressible stagnation point flow with mass transfer, *Int. J. Nonlinear Mech.* 46 (2011) 942 – 948.
- [16] K. Bhattacharyya, Dual solutions in boundary layer stagnation-point flow and mass transfer with chemical reaction past a stretching/shrinking sheet, *Comm. Nonlinear Sci. Numer. Simul.* 38 (2011) 917 – 922.
- [17] A. Ishak, R. Nazar, N. Amin, D. Filip and I. Pop, Mixed convection of the stagnation point flow towards a stretching vertical permeable sheet, *Malaysian Journal of Mathematical Sciences* 2 (2007) 217 – 226.

- [18] S. Mukhopadhyay, Effects of thermal radiation on unsteady mixed convection flow and heat transfer over a stretching surface in porous medium, *Int. J. Heat and Mass Transfer* 25 (2009) 3261 – 3265.
- [19] A. Ishak, R. Nazar, N. Bachok and I. Pop, MHD mixed convection flow near the stagnation-point on a vertical permeable surface, *Physica. A.* 389 (2010) 40 – 46.
- [20] T. Hayat, Z. Abbas, I. Pop and S. Asghar, Effects of radiation and magnetic field on mixed convection stagnation-point flow over a vertical stretching sheet in a porous medium, *Int. J. Heat and Mass Transfer* 53 (2010) 466 – 474.
- [21] T. R. Mahapatra and A. S. Gupta, Stagnation-point flow of a viscoelastic fluid towards a stretching surface, *Int. J. Nonlinear Mech.* 39 (2004) 811 – 820.
- [22] F. Labropulu and D. Li, Stagnation point flow of a second grade fluid with slip, *Int. J. Nonlinear Mech.* 43 (2008) 941 – 947.
- [23] M. Mustafa, T. Hayat, I. Pop, S. Asghar and S. Obaidat, Stagnation-point flow of a nanofluid towards a stretching sheet, *Int. J. Heat and Mass Transfer* 54 (2011) 5588 – 5594.
- [24] A. Robert, V. Gorder and K. Vajravelu, Hydromagnetic stagnation point flow of a second grade fluid over a stretching sheet, *Mech. Research Communication* 37 (2010) 113 – 118.
- [25] R. A. V. Gorder and K. Vajravelu, Hydromagnetic stagnation point flow of a second grade fluid over a stretching sheet, *Mech. Research Communication* 37 (2010) 113 – 118.
- [26] T. R. Mahapatra, S. K. Nandy and A. S. Gupta, Magnetohydrodynamic stagnation point flow of a power law fluid towards a stretching surface, *Int. J. Nonlinear Mech.* 44 (2009) 124 – 129.
- [27] T. Hayat and M. Qasim, Radiation and magnetic field effects on the unsteady mixed convection flow of second grade fluid over a vertical stretching sheet. *Int. J. Numer. Meth. Fluids* 66 (2011) 466 – 474.

- [28] S. Wang and W. C. Tan, Stability analysis of double-diffusive convection of Maxwell fluid in a porous medium heated from below, *Phys. Lett. A* 372 (2008) 3046 – 3050.
- [29] S. Wang and W. Tan, Stability analysis of solet-driven double-diffusive convection of Maxwell fluid in a porous medium, *Int. J. Heat and Fluid Flow* 32 (2011) 88 – 94.
- [30] Y. Yin and k. Q. Zhu, Oscillating flow of a viscoelastic fluid in a pipe with the fractional Maxwell model, *Appl. Math. Comput.* 173 (2006) 231 – 242.
- [31] C. Fetecau, M. Jamil, C. Fetecau and I. Siddique, A note on the second problem of Stokes for Maxwell fluids, *Int. J. Non-Linear Mech.* 44 (2009) 1085 – 1090.
- [32] C. Fetecau, D. Vieru, A. Mahmood and C. Fetecau, On the energetic balance for the flow of a Maxwell fluid due to a constantly accelerating plate, *Acta Mech.* 203 (2009) 89 – 96.
- [33] C. Fetecau, A. Mahmood and M. Jamil, Exact solutions for the flow of a viscoelastic fluid induced by a circular cylinder subject to a time dependent shear stress, *Commun. Nonlinear Sci. Numer. Simulat.* 15 (2010) 3931 – 3938.
- [34] T. Hayat, C. Fetecau and M. Sajid, On MHD transient flow of Maxwell fluid in a porous medium and rotating frame, *Phys. Lett. A* 372 (2008) 1639 – 1644.
- [35] T. Hayat, Z. Abbas and M. Sajid, MHD stagnation-point flow of an upper-convected Maxwell fluid over a stretching surface, *Chaos, Solitons and Fractals* 39 (2009) 840 – 848.
- [36] T. Hayat, R. Sajjad, Z. Abbas, M. Sajid and Awatif A. Hendi, Radiation effects on MHD flow of Maxwell fluid in a channel with porous medium, *Int. J. Heat and Mass Transfer* 54 (2011) 854 – 862.
- [37] T. Hayat, M. Awais, M. Qasim and Awatif A. Hendi, Effects of mass transfer on the stagnation point flow of an upper-convected Maxwell (UCM) fluid, *Int. J. Heat and Mass Transfer* 54 (2011) 3777 – 3782.

- [38] T. Hayat and M. Awais, Three-dimensional flow of upper-convected Maxwell (UCM) fluid. *Int. J. Numer. Meth. Fluids* 66 (2011) 875 – 884.
- [39] T. Hayat and M. Qasim, Influence of thermal radiation and joule heating on MHD flow of a Maxwell fluid in the presence of thermophoresis, *Int. J. Heat Mass Transfer* 53 (2010) 4780 – 4788.
- [40] Y. J. Jian, Q. S. Liu and L. G. Yang, Ac electroosmotic flow of generalized Maxwell fluids in a rectangular microchannel, *J. Non-Newtonian Fluid Mech.* doi:10.1016/j.jnnfm.2011.08.009.
- [41] Q. S. Liu, Y. J. Jian and L. G. Yang, Time periodic electroosmotic flow of generalized Maxwell fluids between two micro-parallel plates, *J. Non-Newtonian Fluid Mech.* 166 (2011) 478 – 486.
- [42] L. C. Zheng, K. N. Wang and Y. T. Gao, Unsteady flow and heat transfer of a generalized Maxwell fluid due to a hyperbolic sine accelerating plate, *Comp. Math. Application* 61 (2011) 2209 – 2212.
- [43] R. K. Bhatnagar, G. Gupta and K. R. Rajagopal, Flow of an Oldroyd-B fluid due to a stretching sheet in the presence of a free stream velocity, *Int. J. Nonlinear. Mech.* 30 (1995) 391 – 405.
- [44] T. Hayat, A. M. Siddiqui and S. Asghar, Some simple flows on Oldroyd-B fluid, *Int. J. Eng. Sci.* 39 (2001) 135 – 147.
- [45] T. Hayat, S. Nadeem and S. Asghar, Hydromagnetic Couette flow of an Oldroyd-B fluid in a rotating system, *Int. J. Eng. Sci.* 42 (2004) 6578.
- [46] W. C. Tan and T. Masuoka, Stoke first problem for an Oldroyd-B fluid in a porous half space, *Phys. Fluids* 17 (2005) 023101 – 023107.
- [47] M. Husain, T. Hayat, C. Fetecau and S. Asghar, On accelerated flows of an Oldroyd-B fluid in a porous medium, *Nonlinear Analysis, Real world Applications* 9 (2008) 1394 – 1408.

- [48] M. Sajid, Z. Abbas, T. Javed and N. Ali, Boundary layer flow of an Oldroyd-B fluid in the region of a stagnation point over a stretching sheet, *Can. J. Phys.* 88 (2010) 635 – 640.
- [49] C. Fetecau and C. Fetecau, The first problem of Stokes for an Oldroyd-B fluid, *Int. J. Nonlinear Mech.* 38 (2003) 1539 – 1544.
- [50] D. Vieru, C. Fetecau and C. Fetecau, Exact solutions for the flow of an Oldroyd-B fluid due to an infinite plate, *Z. Angew. Mech.* 59 (2008) 834 – 847.
- [51] C. Fetecau, A. U. Awan and C. Fetecau, Taylor-Couette flow of an Oldroyd-B fluid in a circular cylinder subject to a time-dependent rotation, *Bull. Math. Soc. Sci Math. Roumanie. Tome 52* (2009) 117 – 128.
- [52] A. C. Eringen, Theory of micropolar fluids, *J. Math. Mech.* 16 (1966) 1 – 18.
- [53] T. Ariman, M. A. Turk and N. D. Sylvester, Microcontinuum fluid mechanics — a review, *Int. J. Eng. Sci.* 11 (1973) 905 – 930.
- [54] T. Ariman, M. A. Turk and N. D. Sylvester, Application of microcontinuum fluid mechanics, *Int. J. Eng. Sci.* 12 (1974) 273 – 293.
- [55] G. Lukaszewicz, *Micropolar Fluids: Theory and Application* Birkhäuser, Basel, 1999.
- [56] A. C. Eringen, *Microcontinuum field theories II: Fluent Media*, Springer, Newyork, 2001.
- [57] N. A. Kelson and T. W. Farrel, Micropolar flow over a porous stretching sheet with strong suction or injection. *Int. Comm. Heat Mass Transfer* 28 (2001) 1881 – 1897.
- [58] A. A. Mohammadein and R. S. R. Gorla, Heat transfer in a micropolar fluid over a stretching sheet with viscous dissipation and internal heat generation, *Int. J. Num. Meth. Heat & Fluid Flow* 11 (2001) 50 – 58.
- [59] R. Nazar, N. Amin, D. Filip and Ioan Pop, Stagnation point flow of a micropolar fluid towards a stretching sheet, *Int. J. Non-Linear Mec.* 39 (2004) 1227 – 1235.

- [60] T. Hayat, T. Javed and Z. Abbas, MHD flow of a micropolar fluid near a stagnation-point towards a non-linear stretching surface. *Nonlinear Anal: RWA* 10 (2009) 1514 – 1526.
- [61] N. A. Yacob and A. Ishak, Stagnation point flow towards a stretching/shrinking sheet in a micropolar fluid with a convective surface boundary condition, *Can. J. Chem. Eng.* 90 (2012) 621 – 626.
- [62] N. A. Yacob, A. Ishak and Ioan Pop, Melting heat transfer in boundary layer stagnation-point flow towards a stretching/shrinking sheet in a micropolar fluid, *Computers & Fluids* 47 (2011) 16 – 21.
- [63] T. Hayat, S. A. Shehzad and M. Qasim, Mixed convection flow of a micropolar fluid with radiation and chemical reaction, *Int. J. Numer. Meth. Fluids.* 67 (2011) 1418 – 1436.
- [64] M. M. Rashidi, S. A. Mohimani Pour and S. Abbasbanday, Analytic approximate solutions for heat transfer of a micropolar fluid through a porous medium with radiation, *Commun. Nonlinear Sci. Numer. Simulat.* 16 (2011) 1874 – 1889.
- [65] S. J. Liao, *Beyond perturbation: Introduction to homotopy analysis method*, Chapman and Hall, CRC Press, Boca Reton 2003.
- [66] S. J. Liao and Y. Tan, A general approach to obtain series solutions of nonlinear differential equations, *Stud. Appl. Math.* 119 (2007) 297 – 354.
- [67] S. J. Liao, Notes on the homotopy analysis method: Some definitions and theorems, *Comm. Non-linear Sci. Num. Simul.* 14 (2009) 983 – 997.
- [68] S. J. Liao, A general approach to get series solution of non-similarity boundary layer flows, *Commun Nonlinear Sci. Numer. Simul.* 14 (2009) 2144 – 2159.
- [69] S. J. Liao, On the relationship between the homotopy analysis method and Euler transform, *Comm. Nonlinear Sci. Numer. Simul.* 15 (2010) 1421 – 1431.

- [70] S. Abbasbandy, E. Shivanian and K. Vajravelu, Mathematical properties of h -curve in the frame work of the homotopy analysis method, *Comm. Nonlinear Sci. Numer. Simul.* 16 (2011) 4268 – 4275.
- [71] S. Abbasbandy, Homotopy analysis method for generalized Benjamin- Bona-Mahony equation, *ZAMP* 59 (2008) 51 – 62.
- [72] S. Abbasbandy and E. Shivanian, Prediction of multiplicity of solutions of nonlinear boundary value problem: Novel application of homotopy analysis method, *Comm. Nonlinear Sci. Num. Simul.* 15 (2010) 3830 – 3846.
- [73] S. Abbasbandy, Homotopy analysis method for the Kawahara equation, *Nonlinear Anal.: Real World Applications (RWA)* 11 (2010) 307 – 312.
- [74] S. Abbasbandy and A. Shirzadi, A new application of the homotopy analysis method: Solving the Sturm–Liouville problems, *Commun. Nonlinear Sci. Numer. Simulat* 16 (2011)112 – 126.
- [75] S. Abbasbandy, Approximate analytical solutions to thermo-poroelastic equations by means of the iterated homotopy analysis method, *Int. J. Comp. Math.* 88 (2011) 1763 – 1775.
- [76] I. Hashim, O. Abdulaziz and S. Momani, Homotopy analysis method for fractional IVPs, *Commun. Nonlinear Sci. Numer. Simul.* 14 (2009) 674 – 684.
- [77] A. S. Bataineh, M. S. M. Noorani and I. Hashim. On a new reliable modification of homotopy analysis method, *Commun. Nonlinear Sci. Numer. Simul.* 14 (2009) 409 – 423.
- [78] A. S. Bataineh, M. S. M. Noorani and I. Hashim, Solutions of time-dependent Emden–Fowler type equations by homotopy analysis method, *Phy. Lett. A* 371 (2007) 72 – 82.
- [79] M. M. Rashidi, G. Domairry, S. Dinarvand, The homotopy analysis method for explicit analytical solutions of Jaulent–Miodek equations, *Numer. Methods Part. Differ. Eqs.* 25 (2009) 430 – 9.

- [80] M. M. Rashidi and E. Erafani, New analytical method for solving Burgers and nonlinear heat transfer equation and comparison with HAM, *Computer Physics Communications* 180 (2009) 1539 – 1544.
- [81] K. R. Rajagopal, On boundary conditions for fluids of the differential type, in: A. Sequeira (Ed.), *Navier–Stokes Equations and Related Nonlinear Problems*, Plenum Press, New York, 1995.
- [82] K. R. Rajagopal, A.S. Gupta, *Meccanica* 19 (1984) 1948.
- [83] K. R. Rajagopal, *Theor. Comput. Fluid Dyn.* 3 (1992) 185.
- [84] K. R. Rajagopal, P. N. Kaloni, Some remarks on boundary conditions for flows of fluids of the differential type, *Control Mechanics and its Applications*, Hemisphere Press, New York, 1989.
- [85] M. S. Abel, M. M. Nandeppanavar, S. B. Malipatil, Heat transfer in a second grade fluid through a porous medium from a permeable stretching sheet with non uniform heat source/sink, *Int. J. of Heat and Mass Transfer* 53 (2010) 1788 – 1795.
- [86] M. Jamil, A. Rauf, C. Fetecau and N. A. Khan, Helical flows of second grade fluid due to constantly accelerated shear stresses, *Commun. Nonlinear Sci. Numer. Simulat.* 16 (2011) 1959 – 1969.
- [87] T. Hayat and M. Nawaz, Hall and ion-slip effects on three-dimensional flow of a second grade fluid, *Int. J. Numer. Meth. Fluids* 66 (2011) 183 – 193.
- [88] W. C. Tan and T. Masuoka, Stokes problem for a second grade fluid in a porous half space with heated boundary, *Int. J. Non-Linear Mech.* 40 (2005) 515 – 522.

- [89] T. Hayat, S. Irum, T. Javed and S. Asghar, Shrinking flow of second grade fluid in a rotating frame: an analytic solution, *Commun. Nonlinear Sci. Numer. Numer. Simul.* 15 (2010) 2932–2941.
- [90] M. Sajid and T. Hayat, Non similar series solution for boundary layer flow of a third order fluid over a stretching sheet, *Appl. Math. Comput.* 189 (2007) 1576 – 1585.
- [91] M. Malik, A. Hussain, S. Nadeem and T. Hayat, Flow of a third grade fluid between coaxial cylinders with variable viscosity, *Z. Naturforsch.* 64a (2009) 588 – 596.
- [92] T. Hayat, M. Mustafa and S. Asghar, Unsteady flow with heat transfer and mass transfer of a third grade fluid over a stretching surface in the presence of chemical reaction, *Nonlinear Analysis: Real World Appl.* 11 (2010) 3186 – 3197.
- [93] M. Sajid, Z. Abbas, T. Javed and N. Ali, Boundary layer flow of an Oldroyd-B fluid in the region of a stagnation point over a stretching sheet, *Can. J. Phys.* 88 (2010) 635 – 640.
- [94] C. D. S. Devi, H. S. Takhar and G. Nath, Unsteady mixed convection flow in a stagnation region to adjacent to a vertical surface, *Heat Mass Transfer* 26 (1991) 71 – 79.
- [95] S. Mukhopadhyay, Effects of thermal radiation on unsteady mixed convection flow and heat transfer over a stretching surface in porous medium, *Int. J. Heat and Mass Transfer* 25 (2009) 3261 – 3265.
- [96] T. Hayat, M. Mustafa and I. Pop, Heat and mass transfer for Soret and Dufour's effect on mixed convection boundary layer flow over a stretching vertical surface in a porous medium filled with a viscoelastic fluid. *Communications in Nonlinear Science and Numerical Simulation* 15 (2010) 1183 – 1196.
- [97] T. Hayat and M. Qasim, Radiation and magnetic field effects on the unsteady mixed convection flow of second grade fluid over a vertical stretching sheet. *Int. J. Numer. Meth. fluids* 66 (2011) 820 – 832.

- [98] J. Cheng, S. J. Liao, R. N. Mohapatra and K. Vajravelu, Series solutions of nano boundary layer flows analysis by means of homotopy analysis method, *J. Math. Anal. Appl.* 343 (2008) 233 – 245.
- [99] B. Yao and J. Chen, Series solution to the Falkner-Skan equation with stretching boundary, *Appl. Math. Comp.* 208 (2009) 156 – 164.
- [100] T. Hayat and M. Nawaz, Unsteady stagnation-point flow of viscous fluid caused by an impulsive rotating disk, *J. Taiwan Institute of Chem. Eng.* 42 (2011) 41 – 49.
- [101] J. Harris, *Rheology and non-Newtonian flow*, Longman, (1977).
- [102] G. S. Guram and A. C. Smith, Stagnation flows of micropolar fluids with strong and weak interactions, *Comput. Math. Appl.* 6 (1980) 213 – 233.
- [103] T. Hayat, Z. Abbas and T. Javed, Mixed convection flow of a micropolar fluid over a nonlinearly stretching sheet, *Physics Letters A* 372 (2008) 637 – 647.
- [104] S. K. Jena and M. N. Matur, Similarity solutions for laminar free convection flow of a thermo-micropolar fluid past a nano isothermal flat plate, *Int. J. Eng. Sci.* 19 (1981) 1431.
- [105] M. A. A. MAHMOUD and S. E. WAHEED, Variable fluid properties and thermal radiation effects on flow and heat transfer in micropolar fluid film past moving permeable infinite flat plate with slip velocity, *Appl. Math. Mech. -Engl. Ed.* 33 (2012) 663 – 678.